AEROELASTIC CHARACTERISTICS OF A CIRCULATION CONTROL WING

DAVID W. TAYLOR NAVAL SHIP RESEARCH AND DEVELOPMENT CENTER, BETHESDA, MARYLAND

SEPTEMBER 1976

DAVID W. TAYLOR NAVAL SHIP RESEARCH AND DEVELOPMENT CENTER

Bethesda, Md. 20084

AEROELASTIC CHARACTERISTICS OF A CIRCULATION CONTROL WING

by

Joseph B. Wilkerson

AVIATION AND SURFACE EFFECTS DEPARTMENT
RESEARCH AND DEVELOPMENT REPORT

September 1976

Report 76-0115

MAJOR DTNSRDC ORGANIZATIONAL COMPONENTS

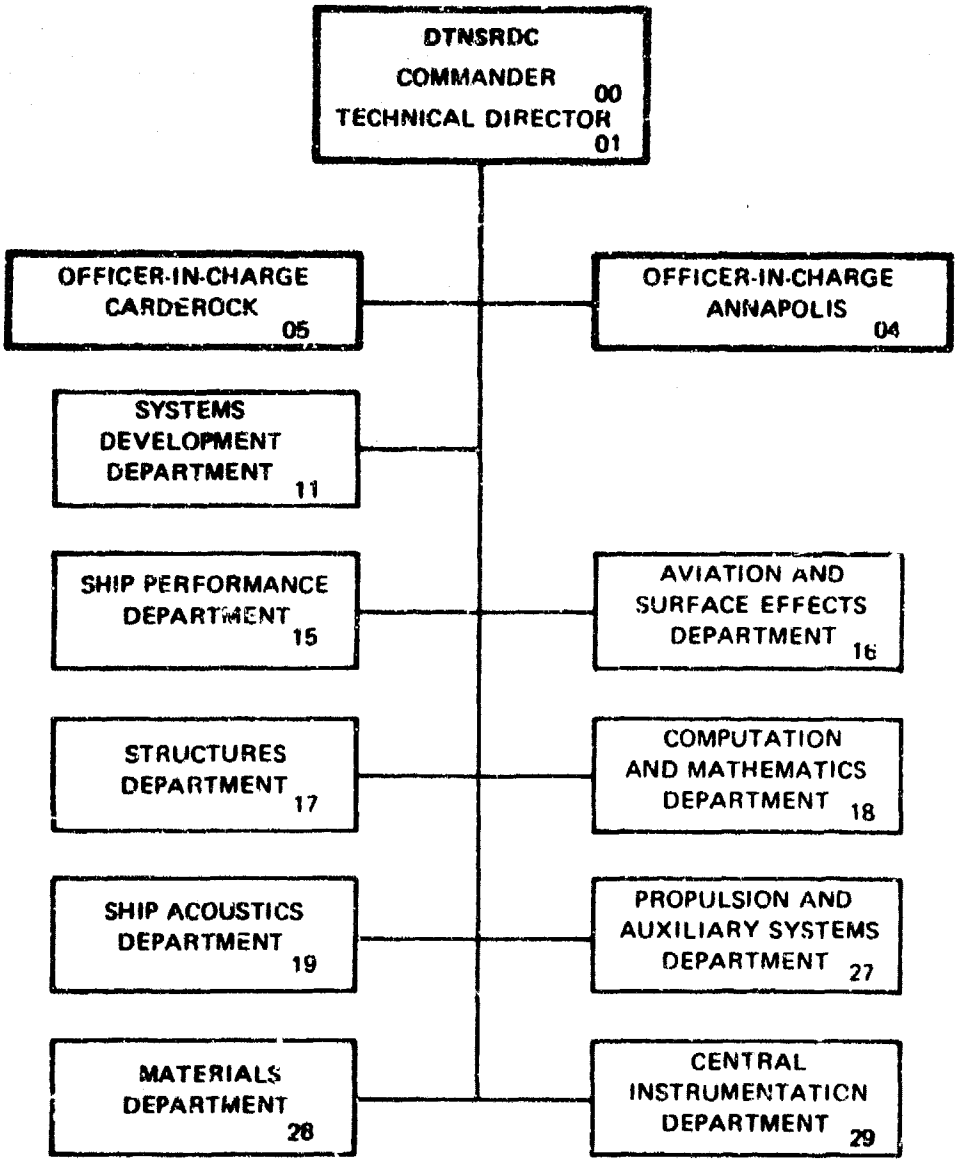

GPO 906-670

NDW-DTNSRDC 3960/43b (Rev. 11-7
GPO 928

UNCLASSIFIED

SECURITY CLASSIFICATION OF THIS PAGE (When Data Entered)

REPORT DOCUMENTATION PAGE		READ INSTRUCTIONS BEFORE COMPLETING FORM
1. REPORT NUMBER 76-0115	2. GOVT ACCESSION NO.	3. RECIPIENT'S CATALOG NUMBER
4. TITLE (and Subtitle) AEROELASTIC CHARACTERISTICS OF A CIRCULATION CONTROL WING		5. TYPE OF REPORT & PERIOD COVERED Final January 1974 - July 1975
		6. PERFORMING ORG. REPORT NUMBER ASED Report 1219
7. AUTHOR(s) Joseph B. Wilkerson		8. CONTRACT OR GRANT NUMBER(s)
9. PERFORMING ORGANIZATION NAME AND ADDRESS David W. Taylor Naval Ship Research and Development Center Bethesda, Maryland 20084		10. PROGRAM ELEMENT, PROJECT, TASK AREA & WORK UNIT NUMBERS (See reverse side)
11. CONTROLLING OFFICE NAME AND ADDRESS Naval Air Systems Command Aerodynamics Technology Administrator (AIR-320) Washington, D.C. 20361		12. REPORT DATE September 1976 13. NUMBER OF PAGES 136
14. MONITORING AGENCY NAME & ADDRESS(if different from Controlling Office)		15. SECURITY CLASS. (of this report) UNCLASSIFIED 15a. DECLASSIFICATION/DOWNGRADING SCHEDULE

16. DISTRIBUTION STATEMENT (of this Report)

APPROVED FOR PUBLIC RELEASE: DISTRIBUTION UNLIMITED

17. DISTRIBUTION STATEMENT (of the abstract entered in Block 20, if different from Report)

18. SUPPLEMENTARY NOTES

Thesis topic for Master of Science Degree submitted to the Graduate School of the University of Maryland

19. KEY WORDS (Continue on reverse side if necessary and identify by block number)

Aerodynamics, Aeroelasticity, Two-dimensional airfoils, Three-dimensional wings, Divergence, Reversal, Circulation control wing, Stall flutter, Wind tunnel, Circulation control airfoils, Boundary layer control

20. ABSTRACT (Continue on reverse side if necessary and identify by block number)

Static aeroelasticity is examined for a wing with circulation control (CC) airfoils. The airfoils use tangential blowing over a rounded trailing edge to provide a lift augmentation proportional to the jet momentum of the blown air. Airfoil lift and pitching moment magnitudes are dependent on both angle of attack and jet momentum. In combination with an elastic structure, this double dependence of lift and moment lead to a CC reversal condition,

(Continued on reverse side)

DD FORM 1 JAN 73 1473 EDITION OF 1 NOV 65 IS OBSOLETE
S/N 0102-014-6601

UNCLASSIFIED

SECURITY CLASSIFICATION OF THIS PAGE (When Data Entered)

(Block 10)

Project Element 63203N
Project No. WSL06 (1423)
Work Unit 1-1619-200

(Block 20 continued)

which is analogous to aileron reversal. Increases in jet momentum beyond the reversal point result in lift decreases. Boundaries for torsional divergence and CC reversal are theoretically examined for the simple two-dimensional case and then for a three-dimensional wing. The wing analysis uses a modified lifting line theory and two-dimensional CC airfoil data to evaluate the behavior of a circulation control wing (CCW). Two parameters, lift effectiveness and control effectiveness, define the behavior of an elastic CCW relative to that of a rigid CCW. A modified version of the wing analysis is used for comparison to wind tunnel data from a CCW model. The model had a root attachment device which allowed rigid body wing torsional deflections in response to the aerodynamic pitching moments.

Stall flutter conditions were encountered which involved only the wing bending mode oscillating at the first cantilevered natural frequency. A first order explanation of the flutter is provided by two-dimensional considerations. It is shown that the wing stall flutter boundaries may be established from the two-dimensional analysis by proper scaling and by establishing an aerodynamic equivalence.

The theory was in good agreement with wind tunnel evaluations on a model CC wing. Because of the large geometric twist in the available model, portions of the wing were at or near angle-of-attack stall conditions even though blowing maintained significant levels of lift coefficient. Such conditions are unique to CC airfoils. This caused some difficulty in obtaining a solution with the lifting line theory which would provide a numerically stable and convergent iteration. The approach used in conjunction with the modified lifting line theory and two-dimensional airfoil data is believed to be the first such analysis, notwithstanding the establishment of divergence and reversal boundaries.

PREFACE

Application of circulation control (CC) airfoil technology to both rotary wing and fixed wing aircraft is currently being pursued by the Department of the Navy and industrial contractors. Although the advantage of direct high lift control has been well established for this type of airfoil, relatively large pitching moments have not been analyzed in terms of their effect on aeroelastic limits. The purpose of this study is to establish a means of evaluating safe flight boundaries for a fixed wing application through analysis of the problems of circulation control torsional divergence, control reversal, and control effectiveness. A CC stall flutter condition is also analyzed and is shown to occur even with the wing in pure bending.

The dependence of airfoil force and moment coefficients on both angle of attack and blowing rate required modified analytical procedures. The three-dimensional analysis uses a modified lifting line theory in matrix formulation which allows nonlinear spanwise aeroelastic variations as well as partial span CC airfoils. Two-dimensional airfoil characteristics which are nonlinear with blowing rate required an iterative approach to establish a reference spanwise distribution of variables. Airfoil derivatives were then taken at this reference condition. Divergence and reversal boundaries were established by a linear analysis along with variations in lift and control effectiveness with speed.

The author is grateful for the overall guidance provided by Dr. Jewel Barlow and for his assistance in establishing the parameters of significance. The author also extends thanks to Miss Rose McCrossin and Miss Kathleen Henderson for typing and assistance in preparing this report.

The wind tunnel evaluation was performed in the DTNSRDC 8- x 10-ft subsonic wind tunnel in January 1974, and the analytical study was performed over the period April-July 1975.

TABLE OF CONTENTS

LIST OF FIGURES

Page

Page

NOTATION

Symbol	Definition	Dimension
a	Airfoil lift curve slope	
C_L	Wing lift coefficient	
C_ℓ	Section lift coefficient	
$C_{M_{50}}$	Wing pitching moment coefficient	
$C_{m_{50}}$	Section pitching moment coefficient, resolved about 50-percent chord	
C_{m_α}	Pitching moment derivative with respect to angle of attack	
C_{m_μ}	Pitching moment derivative with respect to C_μ	
C_μ	Section jet momentum coefficient, $\dot{m}_j V_j / q_\infty c$	
C_{μ_w}	Wing jet momentum coefficient, $\dot{m}_j V_j / q_\infty S$	
C.E.	Control effectiveness	
c	Chord	Feet
EA	Elastic axis location relative to airfoil leading edge	Feet
i	Induced angle	Radians
K	Torsional spring constant	Foot-pounds per radian
k	Linear spring constant	Pounds per foot
L	Wing segment lift	Pounds
L_w	Three-dimensional wing lift	
L.E.	Lift effectiveness	
r	Wing semi-span	Feet
M	Pitching moment, positive nose up	Foot-pounds

Symbol	Definition	Dimension
$\dot{m}$	Slot jet mass flow per unit length	slugs per second per feet
$\dot{m}_w$	Wing total mass flow	slugs per second
$\{m\}$	Normalized distribution of wing jet momentum	
q	Free-stream dynamic pressure	pound per feet squared
q_D	Dynamic pressure at divergence	pound per feet squared
q_R	Dynamic pressure at CC reversal	pound per feet squared
S	Reference area	feet squared
V	Free-stream velocity	feet per second
V_j	Jet velocity	feet per second
y	Wing station	feet
Δy	Wing element length	feet
α_g	Geometric angle of attack	degree
α_{TIP}	Wing tip geometric angle of attach	degree
ε	Dimensionless EA offset from michord, (= 0.50 - EA/c)	
θ	Matrix of wing torsional influence coefficients	
ϕ	Torsional deflection angle	radian
ζ	Dimensionless torsional stiffness, k/qsc	
μ	Derivative of lift coefficient with respect to C_μ	
τ	Dimensionless circulation parameter	

ABSTRACT

Static aeroelasticity is examined for a wing with circulation control (CC) airfoils. The airfoils use tangential blowing over a rounded trailing edge to provide a lift augmentation proportional to the jet momentum of the blown air. Airfoil lift and pitching moment magnitudes are dependent on both angle of attack and jet momentum. In combination with an elastic structure, this double dependence of lift and moment can lead to a CC reversal condition which is analogous to aileron reversal. Increases in jet momentum beyond the reversal point result in lift decreases. Boundaries for torsional divergence and CC reversal are theoretically examined for the simple two-dimensional case and then for a three-dimensional wing. The wing analysis uses a modified lifting line theory and two-dimensional CC airfoil data to evaluate the behavior of a circulation control wing (CCW). Two parameters, lift effectiveness and control effectiveness, define the behavior of an elastic CCW relative to that of a rigid CCW. A modified version of the wing analysis is used for comparison to wind tunnel data from a CCW model. The model had a root attachment device which allowed rigid body wing torsional deflections in response to the aerodynamic pitching moments.

Stall flutter conditions were encountered which involved only the wing bending mode oscillating at the first cantilevered natural frequency. A first order explanation of the flutter is provided by two-dimensional considerations. It is shown that the wing stall flutter boundaries may be established from the two-dimensional analysis by proper scaling and by establishing an aerodynamic equivalence.

The theory was in good agreement with wind tunnel evaluations on a model CC wing. Because of the large geometric twist in the available model, portions of the wing were at or near angle-of-attack stall conditions even though blowing maintained significant levels of lift coefficient. Such conditions are unique to CC airfoils. This caused some difficulty in obtaining a soluton with the lifting line theory which would provide a numerically stable and convergent iteration. The approach used in conjunction with the modified lifting line theory and two-dimensional airfoil data is believed to be the first such analysis, notwithstanding the establishment of divergence and reversal boundaries.

ADMINISTRATIVE INFORMATION

The work presented herein was conducted for the Naval Air Systems Command (AIR-320) under Project Element 63203N and was accomplished in the

time period January 1974 to July 1975. Preparation of this report was funded under Work Unit 4-1600-001.

The material was previously submitted to the University of Maryland in partial fulfillment of requirements for the degree of Master of Science, Aerospace Engineering. Format of the figures is that of the University of Maryland.

INTRODUCTION

Circulation control (CC) airfoil technology is currently being pursued by the David W. Taylor Naval Ship Research and Development Center (DTNSRDC), Carderock, Maryland, for application to rotary wing and fixed wing aircraft. The basic advantage of this new technology is that a high lift potential with direct lift control is attainable by controlling the jet momentum issuing from a thin spanwise slot along the rounded trailing edge of the airfoil. This means of control also produces airfoil pitching moments which are on the order of magnitude of flapped high lift airfoils, and it also offers the potential for operation at moderate to high subsonic flight speeds. Relatively large pitching moment coefficients at significant levels of dynamic pressure require that the boundaries of torsional divergence be established for safety of flight. Similar boundaries for the condition of CC reversal must also be examined to ensure satisfactory vehicle control and performance.

BACKGROUND

The CC airfoil is a boundary layer control type of airfoil which employs a thin slot on the upper trailing-edge surface. Air blown from this slot remains attached to the airfoil rounded trailing edge by the Coanda principle and establishes the airfoil stagnation points according to the combination of angle of attack and blowing magnitude. Initial experimental investigations with circulation control by tangential blowing were conducted on circular cylinders by Dunham.[1] These investigations proved the high

---

[1] Dunham, J., "Circulation Control Applied to a Circular Cylinder," Nat. Gas Turbine Est. (England) Report R. 287 (Jul 1967).

lift capability of the concept, but the geometry was complicated by multiple slots and lacked the potential of higher speed operation. Nevertheless, the results of application studies by Cheeseman[2,3] and others showed that the concept had promise. Subsequent studies at DTNSRDC have concentrated on quasi-elliptical airfoil shapes employing circular arc camber and modified trailing edge contours. This series of airfoils has provided both the high lift capability and the low profile drag characteristics demanded of practical airfoils. Stone and Englar[4] have provided a comprehensive bibliography of reports on CC airfoils and their applications.

A considerable bank of two-dimensional data has been compiled at DTNSRDC on the CC airfoil for various gemetry combinations of airfoil thickness ratio, camber, and trailing-edge design. Most of these results are covered in the aforementioned bibliography.[4] Figure 1 illustrates typical CC airfoil geometry for two-dimensional models. Some transonic data are available, but presently there is no information on the unsteady characteristics of the CC airfoil. Consequently, those problems which require this type of data, such as classical flutter, cannot be theoretically examined with any degree of confidence. The ensuing analysis therefore includes only steady-state airfoil data and addresses only the divergence, CC reversal, lift effectiveness, and stall flutter problems which are amendable to steady or quasi-steady assumptions.

The characteristics of CC airfoils depend on the two independent variables of angle of attack α and jet momentum coefficient C_μ. The dependence of lift on two independent variables gives a wide range of α and C_μ which

---

[2]Cheeseman, I. C. and A. R. Seed, "The Application of Circulation Control by Blowing to Helicopter Rotors," J.R.Ae.S., Vol. 71, No. 848 (Jul 1966).

[3]Cheeseman, I. C., "Circulation Control and Its Application to Stopped Rotor Aircraft," AIAA Paper 67-747 (Apr 1967).

[4]Stone, M. B , and R. J. Englar, "Circulation Control - A Bibliography of NSRDC Research and Selected Outside References," NSRDC Report 4108 (Jan 1974).

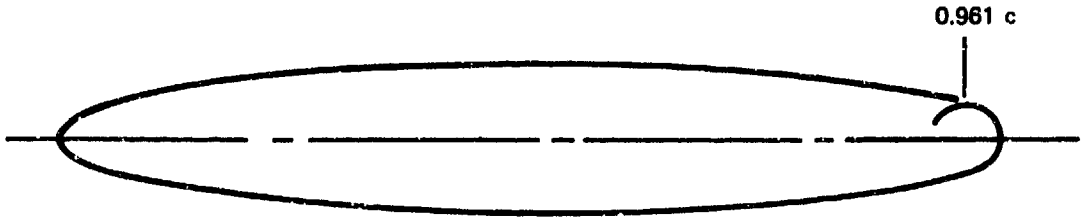

Figure 1a - 15-Percent Uncambered Ellipse

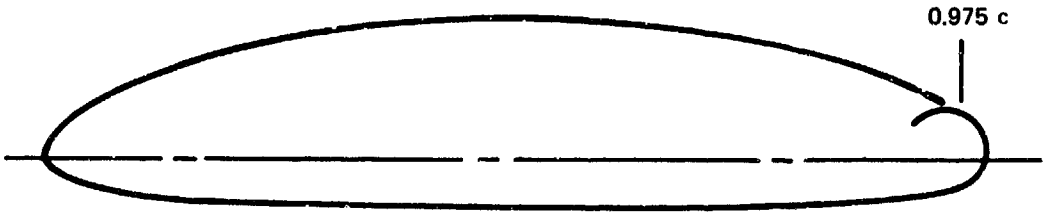

Figure 1b - 20-Percent Ellipse with 5-Percent Camber

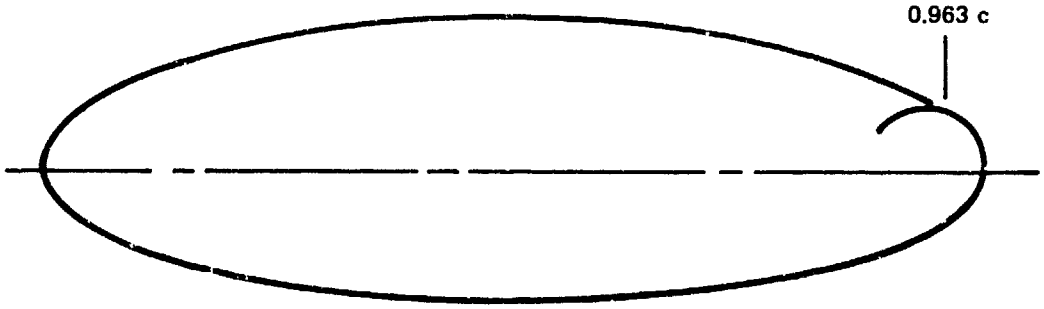

Figure 1c - 30-Percent Ellipse with 1.5-Percent Camber

Figure 1 - Typical Circulation Control Airfoil Geometry for Two-Dimensional Models

develop the same lift. Figure 2 is typical of a CC airfoil which shows both the powerful dependence on C_μ and an unusual angle-of-attack stall behavior. However, the α, C_μ combination used to develop a given C_ℓ greatly affects the aerodynamic efficiency and the drag and pitching moment coefficients. Figure 3 presents typical pitching moment coefficient data resolved to the half-chord position. Note that the magnitude and range of pitching moment coefficient are considerably larger than those of a conventional airfoil. The fact that the airfoil center of pressure varies greatly for different combinations of α and C_μ has thwarted attempts to define a conventional aerodynamic center for CC airfoils. It has therefore been customary to resolve the pitching moments about the half-chord position.

The behavior of interest in this report is the increasing magnitude of negative airfoil pitching moments as jet momentum is increased. At a given flight speed, jet momentum would be increased to provide increased C_ℓ and increased lift. However this same control also produces larger magnitudes of negative pitching moments. In the case of an elastic wing, this would result in reduced angle of attack, tending to reduce the lift. So there is a possibility that the reduction in lift due to this decrease in angle could be more powerful than the increase in lift due to increased jet momentum. The net effect would be a decrease in lift for an increase in jet momentum, or an apparent reversal of the circulation control. This condition is denoted as CC reversal.

The CC reversal condition is somewhat analogous to aileron reversal, hence the name. As is well known, aileron reversal is defined as that point where rolling moment becomes zero because of aileron-induced antisymmetric lift distribution. This occurs because of wing torsional deflections brought about by the aileron-induced pitch moments, and so it is a reversal of the net effect of the control input. Circulation control is being considered as a direct means of controlling total wing lift (and possibly rolling moment also). Therefore, the reversal condition of interest is not when rolling moment goes to zero or even when lift goes to zero; it is when the rate of change of lift due to blowing goes to

Figure 2 - Typical Lift Coefficient Characteristics of Two-Dimensional CC Airfoils

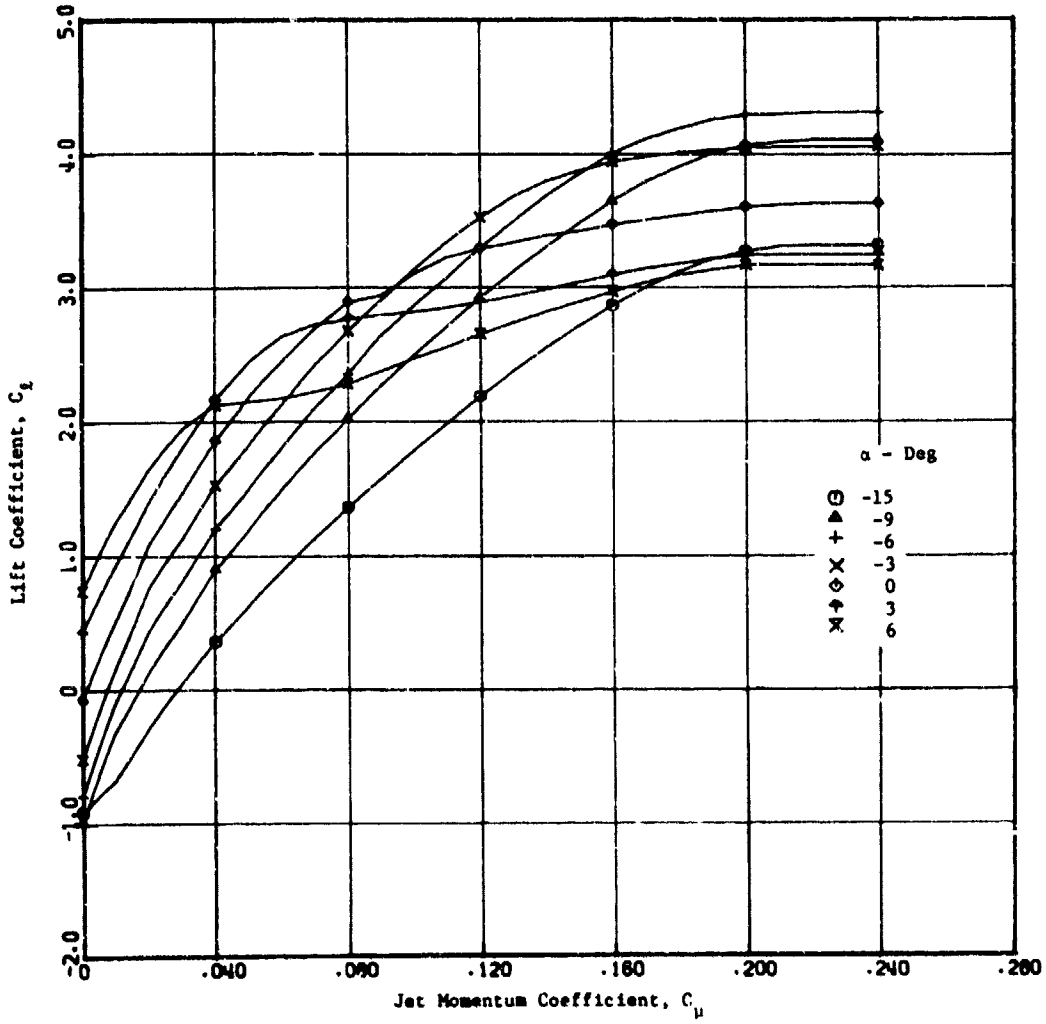

Figure 2a - 15-Percent Ellipse, C_ℓ versus C_μ

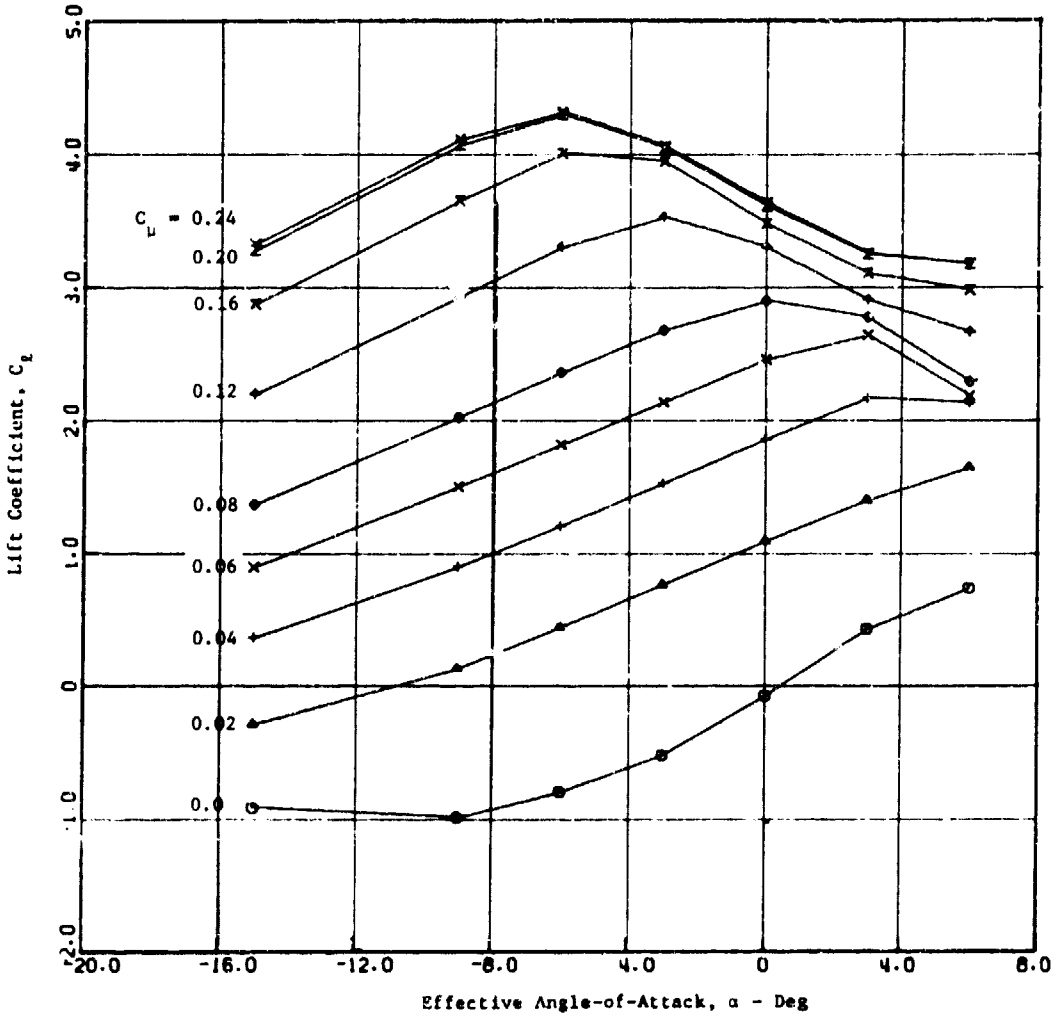

Figure 2b - 15-Percent Ellipse, C_ℓ versus α

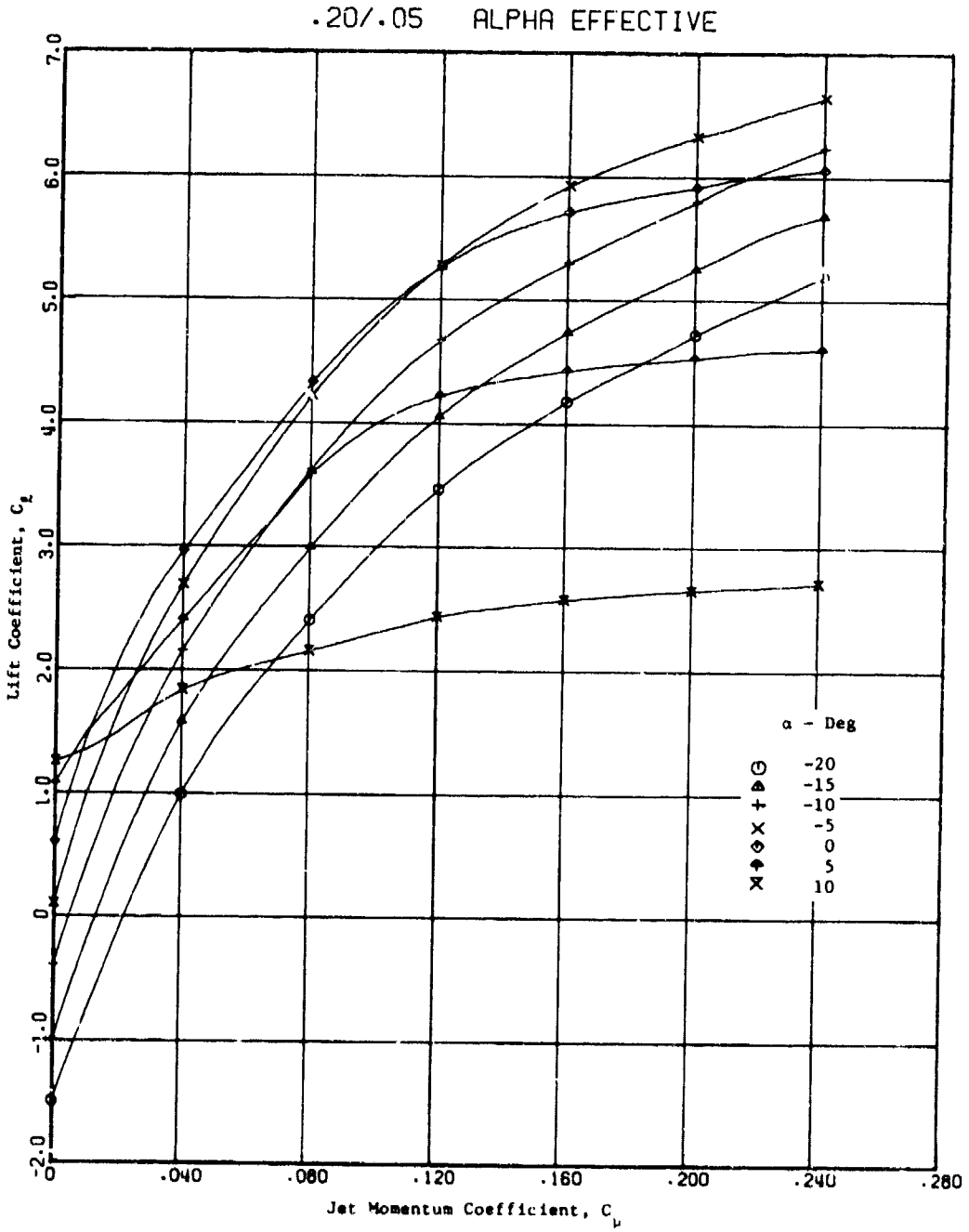

Figure 2c - 20-Percent Cambered Ellipse, C_ℓ versus C_μ

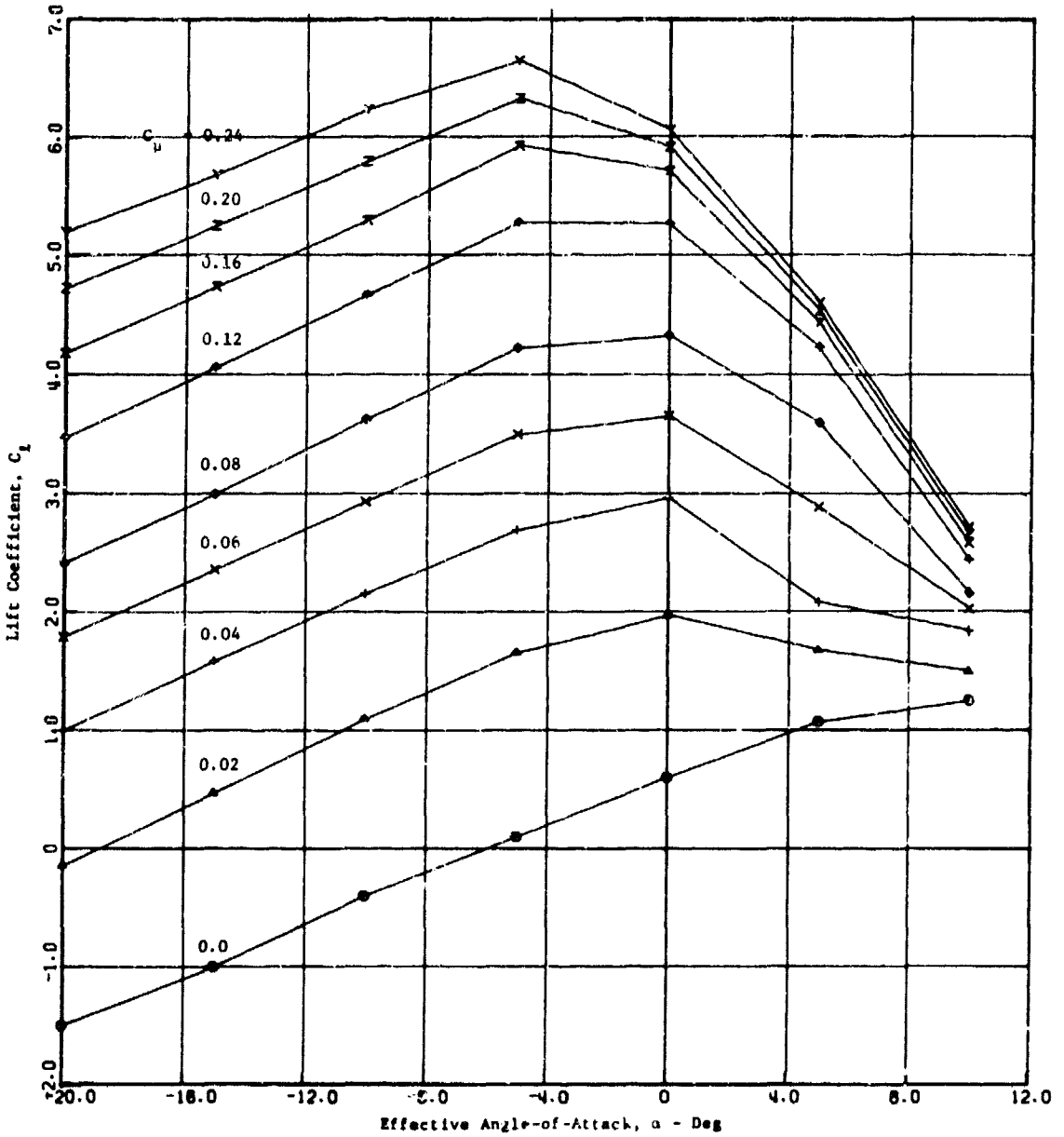

Figure 2d - 20-Percent Cambered Ellipse, C_ℓ versus α

Figure 3 - Typical Pitching Moment Coefficient Characteristics of Two-Dimensional CC Airfoils

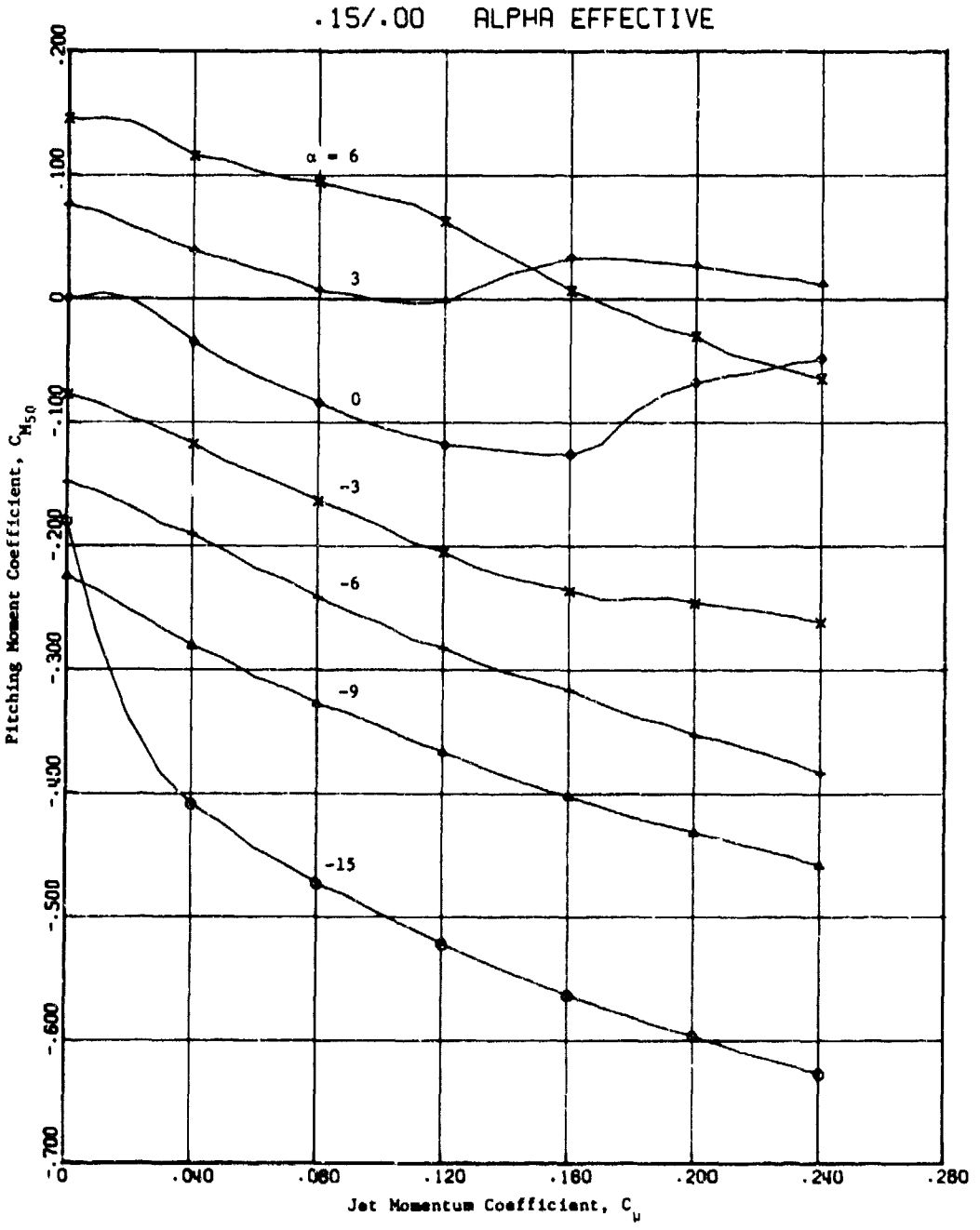

Figure 3a - 15-Percent Ellipse, $C_{m_{50}}$ versus C_μ

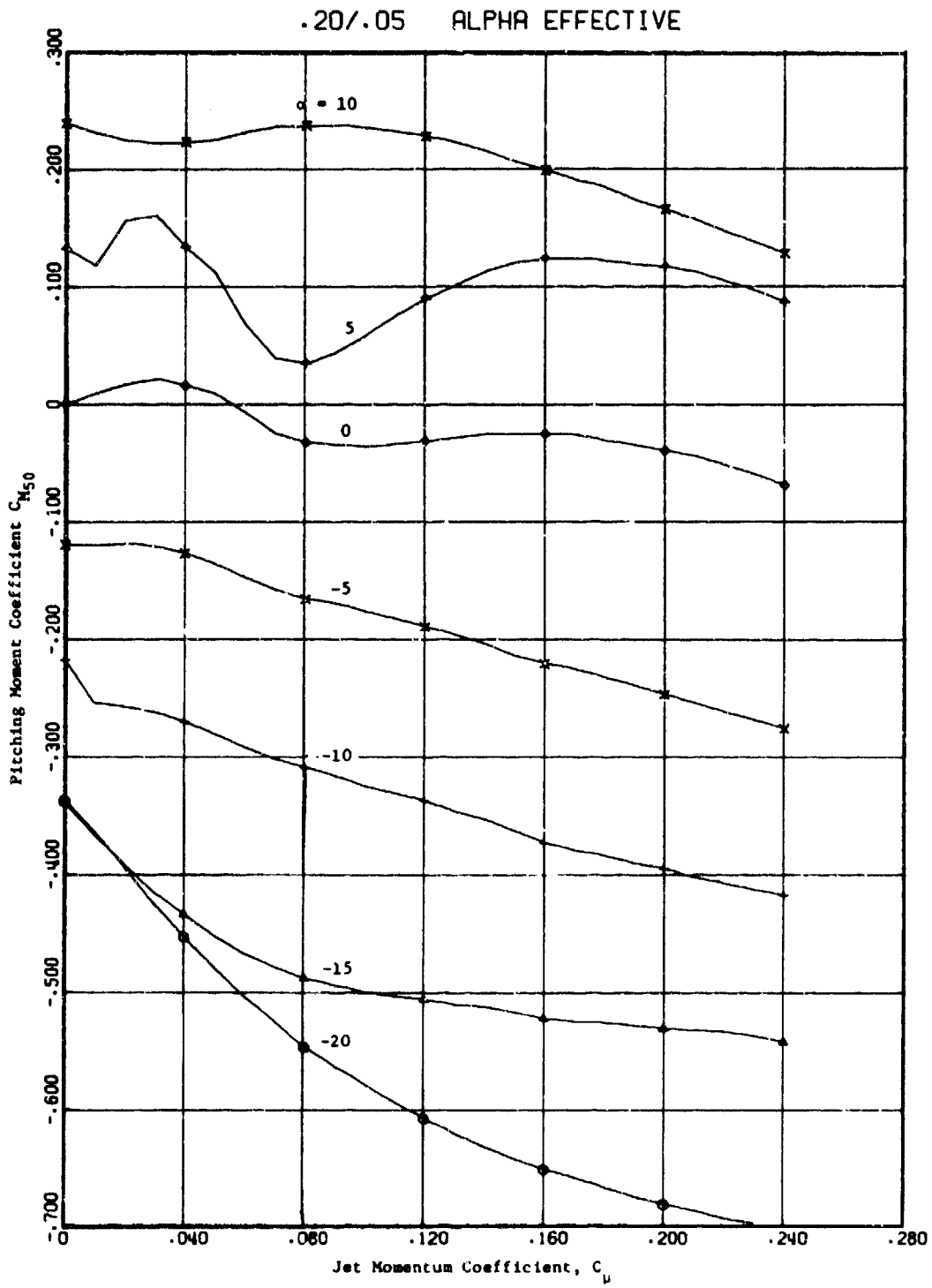

Figure 3b - 20-Percent Cambered Ellipse, $C_{m_{50}}$ versus C_μ

zero ($\partial L/\partial \dot{m}V_j = 0$). Thus CC reversal is also a reversal of the net effect of a control input. Basically the phenomenon is produced by the increasing nose-down pitching moments with increasing lift due to blowing. The mechanism is also seen to be similar to aileron reversal.

A limit-cycle stall flutter condition was experienced during wind tunnel evaluation of a CC model wing. There were no torsional deflections during this phenomenon, but the wing oscillated at its first cantilevered bending frequency and at a magnitude proportional to the blowing rate. Analysis of that condition indicates that it occurred as a result of the very gradual stall pattern of CC airfoils. The particular family of CC airfoils on the model wing have pure elliptic leading edges and encounter angle-of-attack stall at high blowing rates and low positive effective angles. It must be noted that the family of airfoils presently intended for fixed wing application do not stall until conventional stall angles are reached. However the model results used herein are sufficient for defining and examining the potential boundaries, and the analysis may be applied by using the appropriate set of two-dimensional airfoil data.

AIRFOIL DATA REPRESENTATION

The nonlinear behavior of CC airfoils with C_μ (and α) has prevented any meaningful simplified or close-form type of analysis which employs a linear approximation over the normal range of α and C_μ. However, the method used here does utilize a linear representation for analysis of the two-dimensional wing problems of divergence, CC reversal, and lift effectiveness. The section C_ℓ and $C_{m_{50}}$ may be approximated over a limited range by

$$C_\ell = C_{\ell_o} + \mu C_\mu + a\alpha \tag{1}$$

and

$$C_{m_{50}} = C_{m_o} + C_{m_\mu} C_\mu + C_{m_\alpha} \alpha$$

where

$$\mu = \partial C_\ell / \partial C_\mu$$

$$a = \partial C_\ell / \partial \alpha$$

$$C_{m_\mu} = \partial C_{m_{50}} / \partial C_\mu$$

$$C_{m_\alpha} = \partial C_{m_{50}} / \partial \alpha$$

$$C_{\ell_o} = C_\ell (\alpha = C_\mu = 0)$$

$$C_{m_o} = C_{m_{50}} \quad (\alpha = C_\mu = 0)$$

This holds only for a limited α range and for relatively low C_μ, but it is consistent with the needs of a two-dimensional analysis whose only purpose is to show behavioral trends and to aid in problem definition.

Three-dimensional CC wing divergence, reversal, and effectiveness studies also require a compact representation of section characteristics. The need for greater accuracy requires that the correct magnitudes of C_ℓ and $C_{m_{50}}$ be represented and that the "local" aerodynamic derivatives be used here to reflect differences in behavior at different combinations of α, C_μ. Application studies have resulted in computer-tabulated data decks and standard interpolation and correction computer programs which facilitate handling of the two-dimensional data. The analysis and two-dimensional representation which follow have used these data decks and programs where practical. The interpolation program also corrects the data values for slot height-to-chord ratios and Reynolds numbers which are slightly different from the basic tabulated data. This interpolation utilizes three sets of tabulated airfoil data for different combinations of thickness and camber. Each set includes two-dimensional C_ℓ, C_d, and $C_{m_{50}}$ as functions of both α and C_μ.

For a predetermined reference condition of α and C_μ, the following perturbation approach is used herein to define airfoil characteristics at any given wing section for the three-dimensional analysis:

$$C_\ell = C_\ell^* + \mu\Delta C_\mu + a\Delta\alpha$$

$$C_{m_{50}} = C_m^* + C_{m_\mu}\Delta C_\mu + C_{m_\alpha}\Delta\alpha$$

The values of C_ℓ^* and C_m^* are the section characteristics at the reference values of α^* and C_μ^*. The ΔC_μ and $\Delta\alpha$ are changes in C_μ and α from those values used in obtaining C_ℓ^* and C_m^*. The section derivatives μ, a, C_{m_μ}, and C_{m_α} are evaluated locally about the reference α^*, C_μ^* point. The change in C_μ, ΔC_μ, results from an increase in q when solving for the divergence or reversal speed while holding blowing pressure, or $\dot{m}V_j$, constant. Thus $\Delta C_\mu = C_\mu - C_\mu^*$.

The definition of $\Delta\alpha$ naturally depends on the reference angle. Two cases will be considered. The first, and more convenient, is applicable to operation where the lift curve slope is constant. Here the reference condition may be defined as that value of C_ℓ obtained at the geometric angle. All calculations for the induced angle i may then be accounted for by a closed-form solution of the lifting line theory matrix equations. The C_ℓ is then expressed as

$$C_\ell = C_\ell^*(\alpha_g, C_\mu^*) + \mu(C_\mu - C_\mu^*) + a(\phi - i) \qquad (2)$$

or

$$C_\ell = C_{\ell_o} + \mu C_\mu + a\phi - ai$$

or

$$C_\ell = \overline{C}_\ell - ai$$

Here $C_{\ell_o} = C_\ell^* - \mu C_\mu^*$, $\overline{C}_\ell = C_{\ell_o} + \mu C_\mu + a\phi$, and ϕ is the deflection angle.

The second case is applicable to wings which, at least in part, operate at or near the stall condition where the lift curve slope is not constant. The previous form is insufficient in the nonlinear range since it can yield incorrect values for a, if evaluated at the geometric angle, and considerable error is introduced if the slope is assumed to be constant over the entire corrected induced angle i. It was found during this study that numerical instabilities and even multistable conditions that yield erroneous results may be obtained if one tries to reevaluate a in an iterative manner. However, the following form provided a stable iterative solution for most of the cases tried. The reference condition is taken as that of the rigid wing in order to establish a reference distribution of induced angle. Particulars on how this reference distribution is obtained are given later in connection with the wing root elasticity case. However, once the distribution is obtained, C_ℓ may be represented by small variations about that point as

$$C_\ell = C_\ell{}^* (\alpha_g - i^*, C_\mu{}^*) + \mu(C_\mu - C_\mu{}^*) + a(\phi - \Delta i) \qquad (3)$$

or

$$C_\ell = C_{\ell_o} + \mu C_\mu + a\phi - a\Delta i$$

or

$$C_\ell = C_\ell - a\Delta i$$

where $C_{\ell_o} = C_\ell{}^*(\alpha_g - i^*, C_\mu{}^*) - \mu C_\mu{}^*$ and $\bar{C}_\ell = C_{\ell_o} + \mu C_\mu + a\phi$. The same notation and procedure are applied to the pitching moment coefficient.

Stall flutter analysis depends heavily on the airfoil nonlinear behavior with angle of attack. The above linearized approaches are therefore useless in such calculations. Appropriate representations of airfoil characteristics are described in the relevant sections.

TWO-DIMENSIONAL STATIC AEROELASTICITY

The two-dimensional case is considered here for purposes of establishing the primary relationship which governs torsional divergence, CC reversal,

and lift and control effectiveness. Consider a section of a CC wing acting in a two-dimensional flow. As shown in Figure 4, the section is torsionally

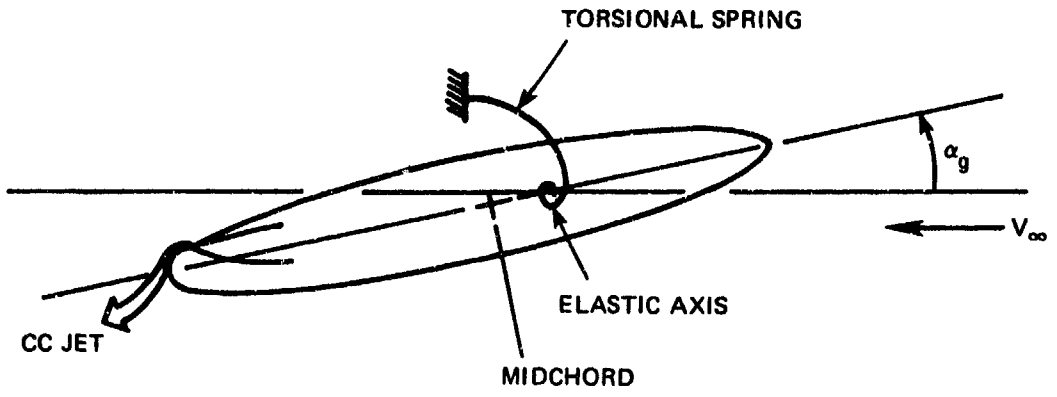

Figure 4 - Two-Dimensional Representation of Aeroelastic Wing

restrained by means of a spring mount about a position which establishes the elastic axis. The position of the elastic axis from the airfoil leading edge will be denoted by EA.

Available CC two-dimensional data have been resolved about the airfoil midchord; this, then, will be the reference point for aerodynamic forces and moments. The lift and moment about the EA are then given by:

$$L = qSC_\ell$$

$$\Sigma M_{EA} = 0 = qSc(C_{m_{50}} - \varepsilon C_\ell) - K\phi$$

where $\varepsilon = 0.50 - EA/c$ = elastic axis position relative to midchord, positive forward

ϕ = torsional deflection

K = torsional spring constant

Lift and moment coefficients are described by Equation (1); there the angle of attack is the geometric incidence plus torsional deflection about the EA, or $\alpha = \alpha_g + \phi$. Substitution into the moment equation gives the deflection angle

$$\phi = \frac{\bar{C}_{m_{50}} - \varepsilon\bar{C}_\ell}{\zeta - (C_{m_\alpha} - \varepsilon a)} = \frac{\bar{C}_{m_{50}} - \varepsilon\bar{C}_\ell}{\gamma} \qquad (4)$$

where

$$C_{m_{50}} = C_{m_o} + C_{m_\mu} C_\mu + C_{m_\alpha} \alpha_g$$

$$\bar{C}_\ell = C_{\ell_o} + \mu C_\mu + a\alpha_g$$

$$\gamma = \zeta - (C_{m_\alpha} - \varepsilon a)$$

$$\zeta = K/qSc$$

Equations (1) and (4) can then be substituted into the lift equation to yield

$$L = qS\ (\bar{C}_\ell + a\phi)$$

or

$$L = qS \left[(C_{\ell_o} + a\alpha_g)\ (1 - \frac{a\varepsilon}{\gamma}) + (C_{m_o} + C_{m_\alpha}\ \alpha_g)\ \frac{a}{\gamma}\right] + \left[\mu(1 - \frac{a\varepsilon}{\gamma}) + C_{m_\mu}\ \frac{a}{\gamma}\right] \dot{m}V_j \qquad (5)$$

TORSIONAL DIVERGENCE

It is readily apparent from Equation (4) that torsional divergence will occur when $\gamma = 0$, or at that point when the dimensionless stiffness (K/qSc) just balances the natural aerodynamic tendency in pitch. Therefore the critical value of dimensionless stiffness is given by

$$\zeta_D \equiv \frac{K}{q_D Sc} = (C_{m_\alpha} - \varepsilon a)$$

For a predesigned torsional stiffness, the divergence q is given by

$$q_D = \frac{K}{Sc\ (C_{m_\alpha} - \varepsilon a)} \tag{6}$$

The divergence equation indicates no dependence on initial settings of angle of attack or blowing. The obvious point is that a conventional wing of symmetrical section properties will theoretically diverge in a negative direction as readily as it will diverge in the positive direction. A cambered conventional section will behave similarly but relative to its zero lift angle. The lift curve slope must then be evaluated for differences in behavior at positive or negative lifts. If the CC airfoil is viewed as a variable camber section, where camber is dependent on blowing rate, it is seen that the airfoil derivatives C_{m_α} and a are themselves dependent <u>both</u> on angle of attack and on blowing rate and therefore that both affect the value of q_D.

A special case occurs for $(C_{m_\alpha} - \varepsilon a)<0$, or $\varepsilon > C_{m_\alpha}/a$, for here the denominator of Equation (4) remains positive even for zero stiffness. Consequently a torsional divergence does not exist. Physically, C_{m_α}/a denotes the instantaneous moment center due to angle of attack. Thus $\varepsilon > C_{m_\alpha}/a$ is a condition which requires that EA be placed sufficiently forward to ensure that $\partial C_{m_{EA}}/\partial\alpha$ is negative. This always produces aerodynamic restoring moments and therefore ensures a stable condition.

The dimensionless divergence stiffness ζ_D may be plotted for various operating conditions of α, C_μ in order to define the tradeoff between required stiffness and EA position. The graph shown in Figure 5 uses

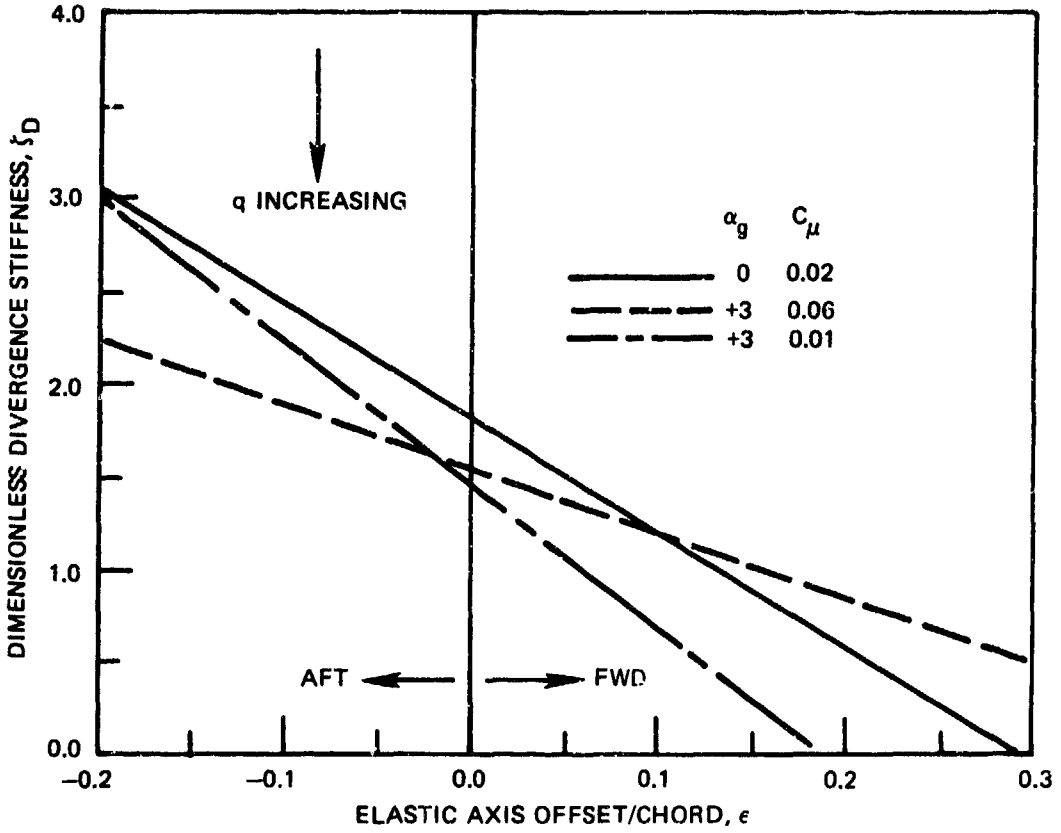

Figure 5 - Effect of Elastic Axis Position on Two-Dimensional Divergence Stiffness

two-dimensional data of a 15-percent thickness uncambered elliptical airfoil with a modified rounded trailing edge. Note that the separate lines are due to variations in the airfoil derivatives as obtained from two-dimensional data; in contrast, the assumed linearity of Equation (1) would provide only one line for a given airfoil. Values of ζ above the divergence lines correspond to $\gamma>0$ in Equation (4) and so are not divergent. As q is increased, the value of ζ decreases and approaches the divergence value ζ_D from above. Note that a "substiff" design point $\zeta<\zeta_D$ also appears feasible from the graph. However regardless of the stiffness, $\zeta = \infty$ at $q = 0$ and so the divergence condition would have to be passed through before the substiff design point is reached-an obvious impossibility.

In general the trend of Figure 5 is typical in that it shows lower stiffness requirements, or higher values of q_D, for more forward positions of the elastic axis. Also the curves indicate that an EA position of around 0.25c would minimize the problem of torsional divergence.

CIRCULATION CONTROL REVERSAL

As mentioned in the introduction, the CC reversal condition is defined as that value of q at which there is no change in lift for a change in the blowing control input, or

$$\frac{\partial L}{\partial \dot{m} V_j} = 0$$

Applying this condition to Equation (5) yields

$$\mu + \frac{a}{\gamma_R} (C_{m_\mu} - \varepsilon\mu) = 0$$

In terms of the dimensionless stiffness and reversal q, the above equation becomes

$$\zeta_R \equiv \frac{K}{q_R Sc} = C_{m_\alpha} - \frac{a}{\mu} C_{m_\mu} \qquad (7)$$

or

$$q_R = \frac{K}{Sc \left(C_{m_\alpha} - \frac{a}{\mu} C_{m_\mu}\right)}$$

The reversal stiffness ζ_R is seen to be independent of the EA position; this is in contrast to the dependence of divergence speed on this parameter. However divergence was defined as a condition of the total lift whereas reversal is a condition of only that lift due to blowing.

At this point it is appropriate to also consider the deflection angle at the reversal condition. Combining Equations (7) and (4) yields the following:

$$\phi_R = \frac{\bar{C}_{m_{50}} - \varepsilon \bar{C}_\ell}{\gamma_R}$$

where

$$\gamma_R = \zeta_R - (C_{m_\alpha} - \varepsilon a)$$

$$= \zeta_R - \zeta_D$$

The region of interest is for those conditions when the reversal speed is less than the divergence speed (or $\zeta_R > \zeta_D$, or $\gamma_R > 0$). Thus the sign of ϕ_R is determined by the numerator, which simply represents an equivalent moment coefficient resolved about the elastic axis $C_{m_{EA}} = \bar{C}_{m_{50}} - \varepsilon \bar{C}_\ell$.

Figure 6 presents two-dimensional data which have been resolved about three chord positions that represent three EA positions. As shown, the forward EA position provides negative moments almost exclusively, indicating $\phi_R < 0$. The different behavior for the aft position indicates that the sign and magnitude of ϕ_R are heavily dependent on the geometric angle of attack.

Evaluation of ϕ_R by using the linear relations of Equation (1) gives the expanded expression

$$\phi_R = \frac{(C_{m_o} - \varepsilon C_{\ell_o}) + (C_{m_\alpha} - \varepsilon a)\alpha_g + (C_{m_\mu} - \varepsilon \mu) C_\mu}{-(C_{m_\mu} - \varepsilon \mu)\ (a/\mu)}$$

The typical variations shown in Figure 7 support the conclusions reached above. More specifically, (1) EA position has considerable impact on the deflection magnitude and sign at reversal conditions even though it

Figure 6 - Pitching Moment Coefficient Resolved to Different Chord Locations

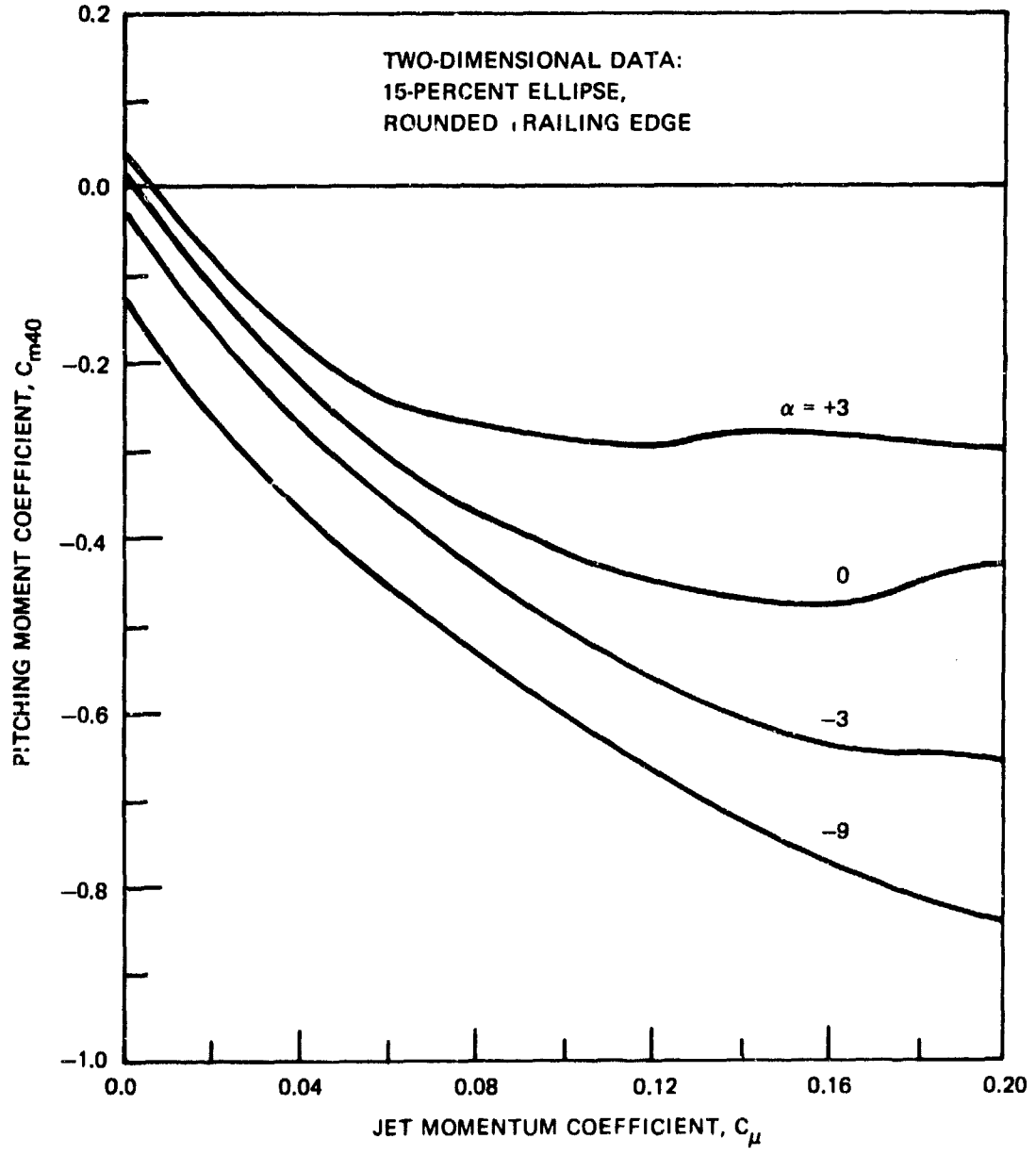

Figure 6a - Resolution to 40-Percent Chord

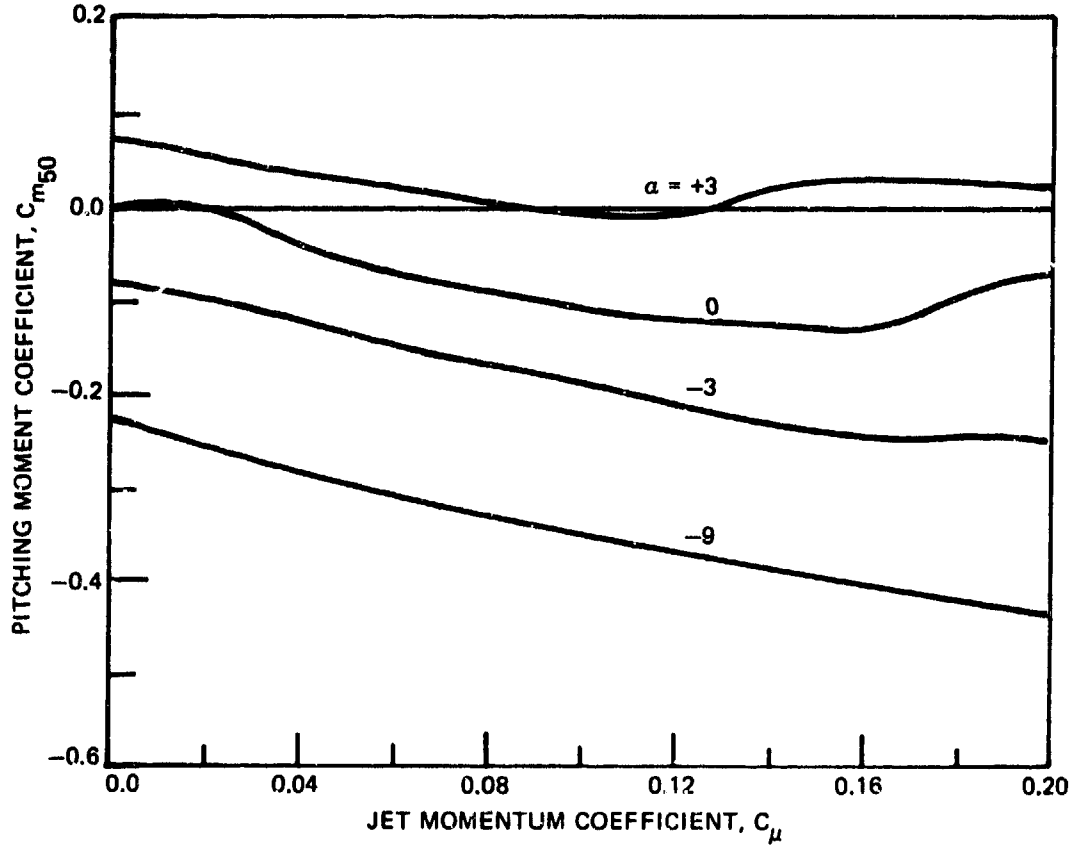

Figure 6b - Resolution to 50-Percent Chord

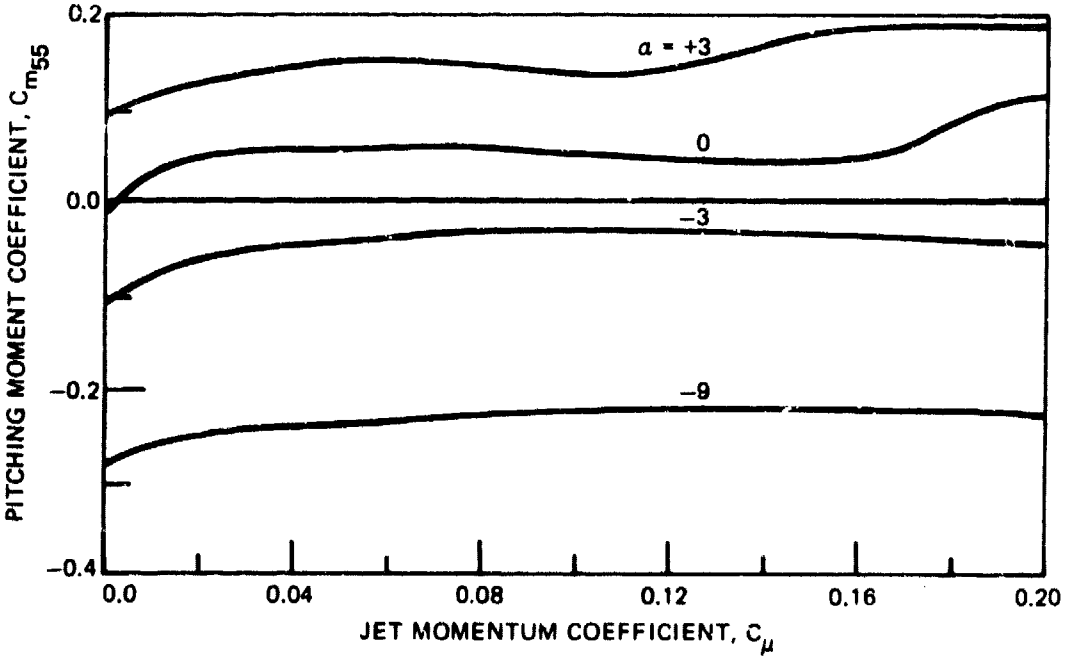

Figure 6c - Resolution to 55-Percent Chord

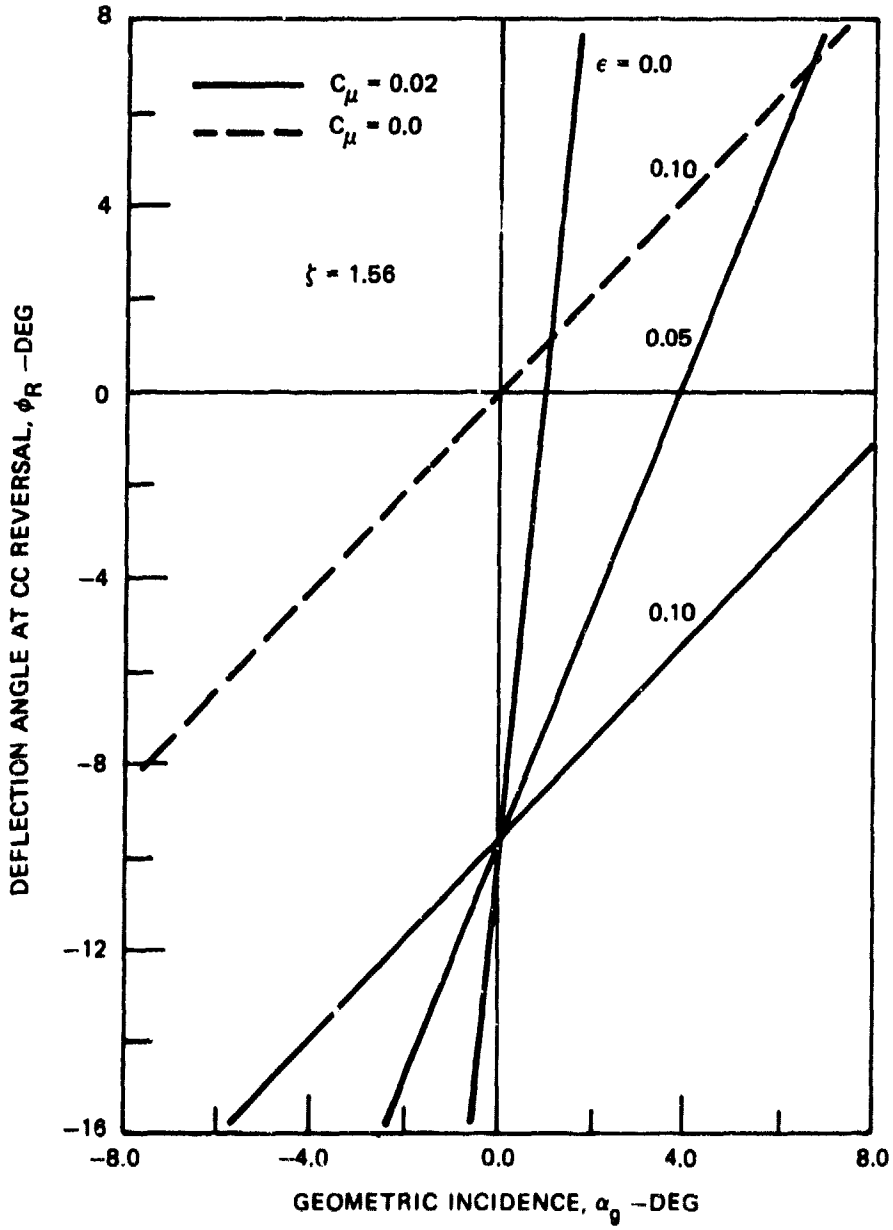

Figure 7 - Sensitivity of Reversal Speed Deflection Angle to Elastic Axis Offset

does not directly affect reversal speed and (2) slightly forward EA positions are desirable because of reduced sensitivity to angle of attack. As shown in Figure 7, ϕ_R is independent of ε at $\alpha_g = 0$. Setting $C_{m_o} = C_{\ell_o} = \alpha_g = 0$ in the above equation gives

$$\phi_R = -\frac{1}{a}\mu C_\mu, \quad (C_{m_o} = C_{\ell_o} = \alpha_g = 0)$$

This corresponds to a zero net lift since $\alpha_g = 0$ and the reversal condition is defined as zero net lift due to blowing (for the linear analysis).

Another point of interest is the variation in deflection angle as it approaches ϕ_R. The following inequality may be stated for q approaching q_R which is less than q_D:

$$\zeta > \zeta_R > \zeta_D$$

Then by using Equations (4) and (6) and the above inequality,

$$\frac{\phi}{\phi_R} = \frac{\zeta_R - \zeta_D}{\zeta - \zeta_D} \geq +0$$

First of all, this states that ϕ does not change sign as $q \to q_R$. Since the above ratio is always positive, the sign of ϕ must remain at its initial plus or minus value. Therefore those regions in Figure 7 which show $\phi_R > 0$ must correspond to inital $\phi > 0$ values also, and vice versa. Second, the above equation states that ϕ approaches ϕ_R as an inverse function of q such that the values of Figure 7 also represent maxima (or minima) values up to q_R.

To return to Equation (7), the reversal stiffness (or reversal q) does not depend either on α or on C_μ in this linear analysis. Thus the various

combinations of Figure 7 all correspond to a single reversal stiffness. However both the nonlinear behavior of pitching moment indicated in Figure 6b and that of lift coefficient derivatives shown previously suggest that ζ_R does, in fact, depend on both α and C_μ. The curves of Figure 8 were

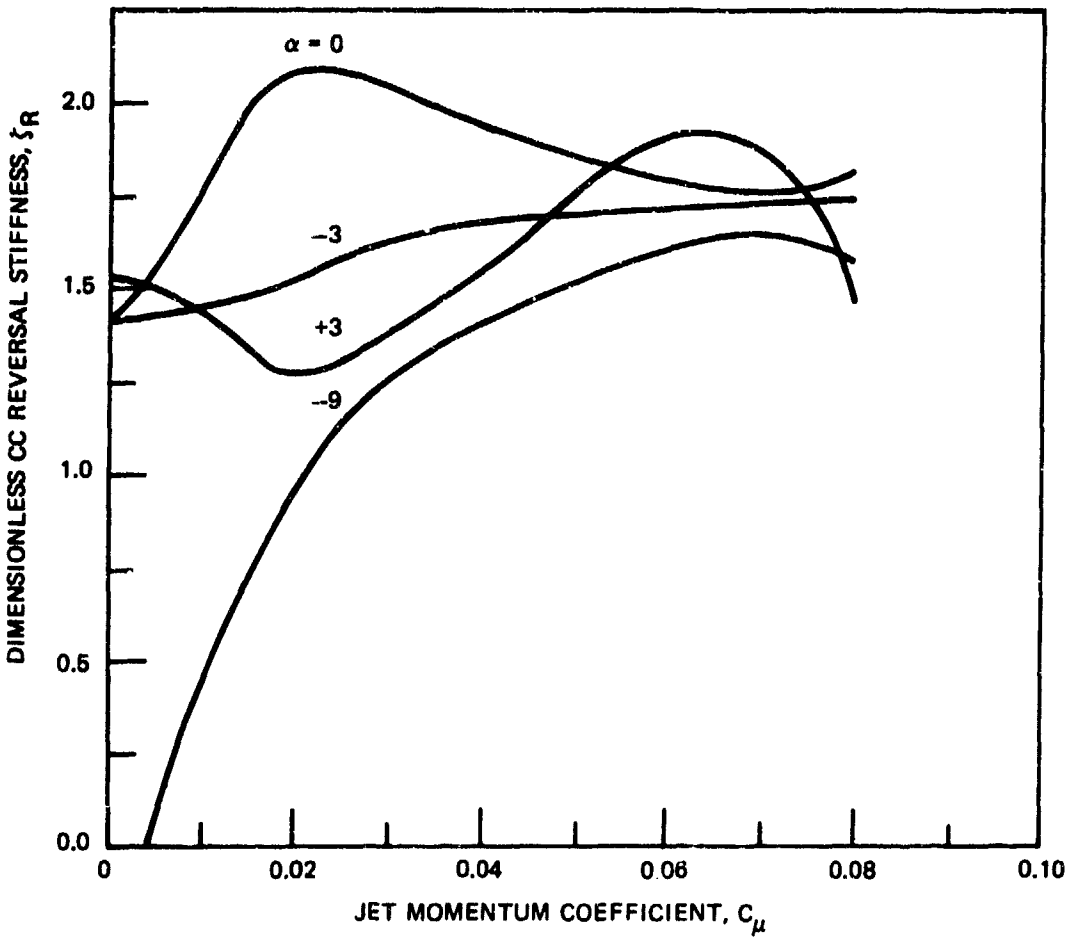

Figure 8 - Effect of Local Airfoil Derivatives on Two-Dimensional Reversal Stiffness

obtained by taking the local airfoil derivatives from two-dimensional data and applying Equation (7) to each point. Although this approach shows definite variations, it still allows for a conservative and yet representative choice of derivatives which may be used in the linear analysis to bracket the reversal speed. On the other hand, it indicates that if local

derivatives from two-dimensional data are to be used, they must be carefully selected in order to provide conservative results over a broad operating range.

LIFT AND CONTROL EFFECTIVENESS

It should be noted that because of other terms in Equation (5), the change in wing lift may be different than expected by the defined CC reversal condition. For instance, the reversal condition may not be reached and yet the lift may have diverged. Comparisons of both lift and control effectiveness are therefore required to establish the overall wing behavior. Treating these in reverse order, CC control effectiveness (C.E.) is analogous to aileron effectiveness. It is a measure of wing lift response to a change in the control input of jet momentum. Herein it is normalized relative to the control effectiveness of an idealized rigid wing response. The variation of C.E. with jet momentum and with q provides a direct measure of the available control. The definition of C.E., shown later, is such that C.E. = 0 at the point of CC reversal. This is also analogous to the definition of aileron effectiveness which goes to zero at the point of aileron reversal.

Since aileron control contributes only an antisymmetric lift distribution, it does not contribute to the net wing lift. However the circulation control contributes a symmetric lift distribution when used as a direct lift control, and so it affects the net wing lift. Hence there is also a need to define a lift effectiveness parameter L.E. This is a measure of the elastic wings net lift relative to the lift which would be available from an idealized rigid wing. Thus the two parameters L.E. and C.E. respectively measure the net lift and the available control power of the elastic wing relative to these characteristics of an idealized rigid wing.

Lift effectiveness is the ratio of elastic wing lift, from Equation (5), to the lift of a rigid wing. The rigid wing lift is also obtained from Equation (5) by setting $\gamma = \infty$ which is the zero deflection case. Lift effectiveness as a function of q for constant blowing is then

$$L.E. = \frac{qS\left[(C_{\ell_o} + a\alpha_g)\left(1 - \frac{a\varepsilon}{\gamma}\right) + (C_{m_o} + C_{m_\alpha}\alpha_g)\frac{a}{\gamma}\right] + \left[\mu\left(1 - \frac{a\varepsilon}{\gamma}\right) + C_{m_\mu}\frac{a}{\gamma}\right]\dot{m}V_j}{qS(C_{\ell_o} + a\alpha_g) + \mu\dot{m}V_j}$$

or

$$L.E. = 1 - \frac{a\varepsilon}{\gamma} + \left[\frac{qS(C_{m_o} + C_{m_\alpha}\alpha_g) + C_{m_\mu}\dot{m}V_j}{qS(C_{\ell_o} + a\alpha_g) + \mu\dot{m}V_j}\right]\frac{a}{\gamma} \qquad (8)$$

where γ is also a function of q as previously defined. Obviously Equation (8) retains the same qualities of divergence and CC reversal that have been examined for Equation (5). However, it is complicated by singularities when the rigid wing lift in the denominator goes to zero. Although this is possible for almost any $\alpha_g < 0$ with blowing, it is not an operational condition of interest and so does not limit the usefulness of the parameter as defined. The lift effectiveness at reversal is also of interest. Substituting Equation (7) and the definition of γ into Equation (8) results in

$$L.E._{REV} = 1 + \frac{1}{\varepsilon - C_{m_\mu}/\mu}\left[\frac{qS(C_{m_o} + C_{m_\alpha}\alpha_g) + C_{m_\mu}\dot{m}V_j}{qS(C_{\ell_o} + a\alpha_g) + \mu\dot{m}V_j} - \varepsilon\right]$$

Control effectiveness is defined as the elastic wing lift response to a control input, normalized by the idealized rigid wing response or

$$C.E. = \frac{\partial L/\partial \dot{m}V_j \text{ of flexible wing}}{\partial L/\partial \dot{m}V_j \text{ of rigid wing}}$$

This definition corresponds to C.E. = 0 at CC reversal. Evaluating the above parameter by using Equation (5) yields

$$C.E. = 1 + \frac{a}{\gamma}\left[\frac{C_{m_\mu}}{\mu} - \varepsilon\right] \tag{9}$$

Further substitution of Equations (6) and (7) into (9) gives the more compact form

$$C.E. = \frac{1-q/q_R}{1-q/q_D} \tag{10}$$

In the latter form, it is obvious that C.E. $\rightarrow$ 0 as $q \rightarrow q_R$ and that C.E. is undefined at the divergence singularity. This presents no real problem since at a divergence condition, C.E. is rather meaningless anyway.

Lift and control effectiveness parameters become identical in the special case of $C_{m_o} = C_{\ell_o} = \alpha_g = 0$ and take the form of Equation (9). Typical variations with speed for this case are shown in Figure 9 for different EA offsets ε. These curves are generated for fixed controls or blowing rate ($\dot{m}V_j$). Thus the magnitude of blowing coefficient C_μ decreases with increasing q. The more forward EA positions are seen to produce reduced values of both lift and control effectiveness. In contrast, negative EA offset produces augmented lift and control effectiveness but at the same time it results in a lower divergence q as was shown in Figure 5.

Reversal speed and C.E. are shown to be independent of α_g by Equations (7) and (9). Therefore Figure 9 represents C.E. for any value of α_g, but it represents L.E. only for $\alpha_g = 0$. The reversal stiffness is also shown to be independent of ε by Equation (7); this is reflected in Figure 9 by the coalesence of curves at zero effectiveness. Lift effectiveness variation with speed is shown in Figure 10 for $\alpha_g = \pm 3$ deg, again for conditions of constant blowing rate. The strong effect of angle of attack on pitching moments is very evident here, reflecting the relation of Equation (8).

The previous graphs have shown the variations of L.E. with speed for constant reference values of stiffness K and blowing rate $\dot{m}V_j$. Figure 11

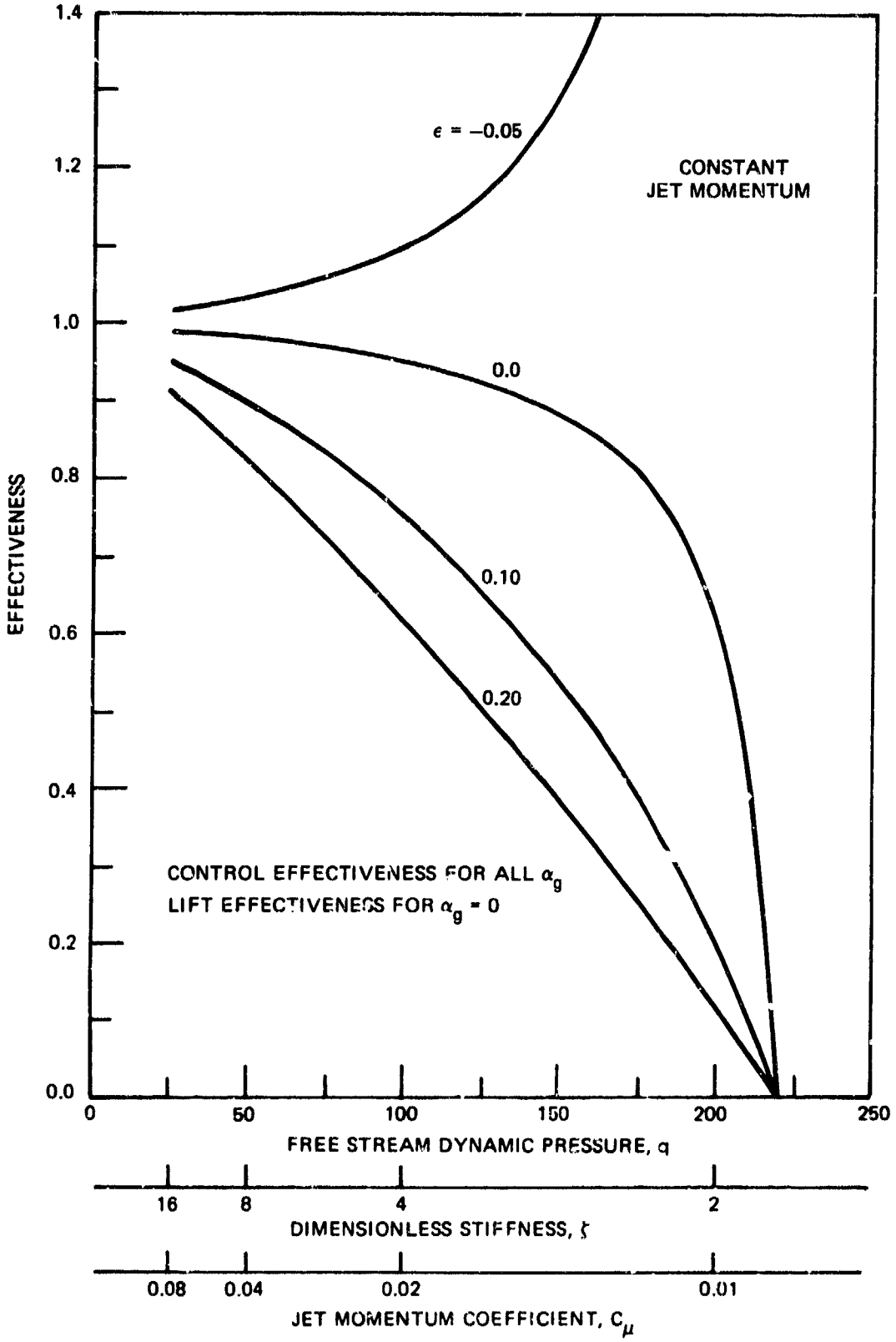

Figure 9 - Typical Variation of Two-Dimensional Lift Effectiveness and Control Effectiveness with Speed

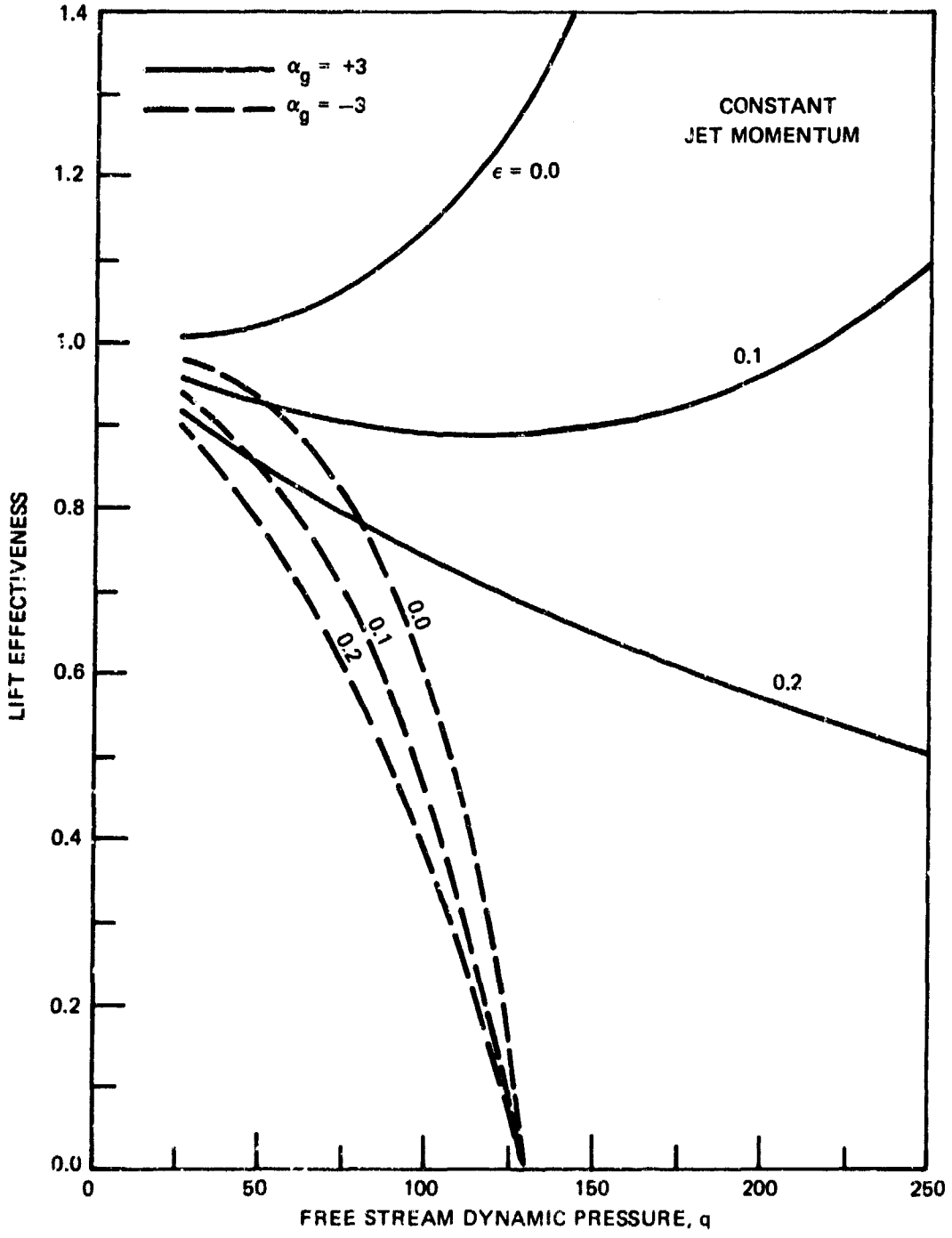

Figure 10 - Effect of Initial Incidence Angle on Two-Dimensional Lift Effectiveness

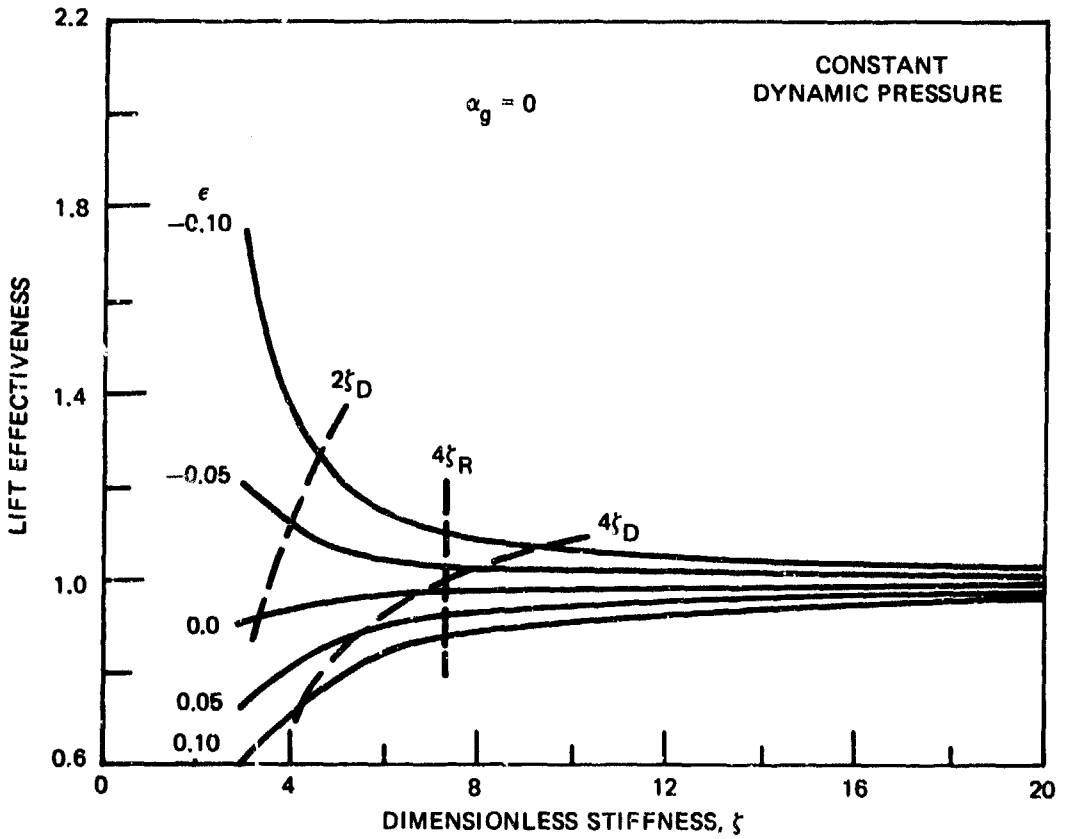

Figure 11 - Effect of Stiffness on Two-Dimensional Lift Effectiveness

evaluates the variation of L.E. with stiffness at constant q for different values of EA offset at $\alpha_g = 0$. Dashed lines show the stiffness magnitude relative to divergence and reversal stiffness. It appears from this plot that design stiffness on the order of $4\zeta_R$ would be sufficient to provide safe operation and avoid excessive structural deflection. Figure 12 presents the variation of L.E. with C_μ at constant q for two EA positions. Note that the effects of angle of attack quickly diminish as C_μ increases, approaching the L.E. value at $\alpha_g = 0$ deg.

Some understanding is attainable from the simplified preceding equations, but their application is limited to crude first order approximations of divergence and reversal. Spanwise variations in elastic bending and airfoil characteristics, as well as three-dimensional wing effects, are, of course, absent from the simple analysis. In fairness, the analysis may apply quite well to cases where three-dimensional wing aerodynamic derivatives are available, especially when only a root end restraint is to be considered (as will be done later). Nevertheless a more precise analysis is required if two-dimensional airfoil characteristics are to be generally applied to a wing.

THREE-DIMENSIONAL STATIC AEROELASTICITY

This section is concerned with spanwise variations in airfoils and torsional stiffness variations in wings. Aerodynamic theory utilizes the lifting line approach to calculate local induced angles which are dependent on the wing lift distribution. The equations are expressed in standard matrix form for both lift and pitching moment coefficients.

The wing-induced angle distribution i may be related to local values of a nondimensional circulation parameter τ by a geometrically defined matrix N. This basic relationship is explained in some detail on pages 303-307 of Scanlon and Rosenbaum.[5] Local lift is a function of both the nondimensional circulation and the characteristics of the local two-dimensional airfoil. Combining these relations then provides a matrix

---

[5]Scanlon, R. H. and R. Rosenbaum, "Introduction to the Study of Aircraft Vibration and Flutter," MacMillan, New York, (1951).

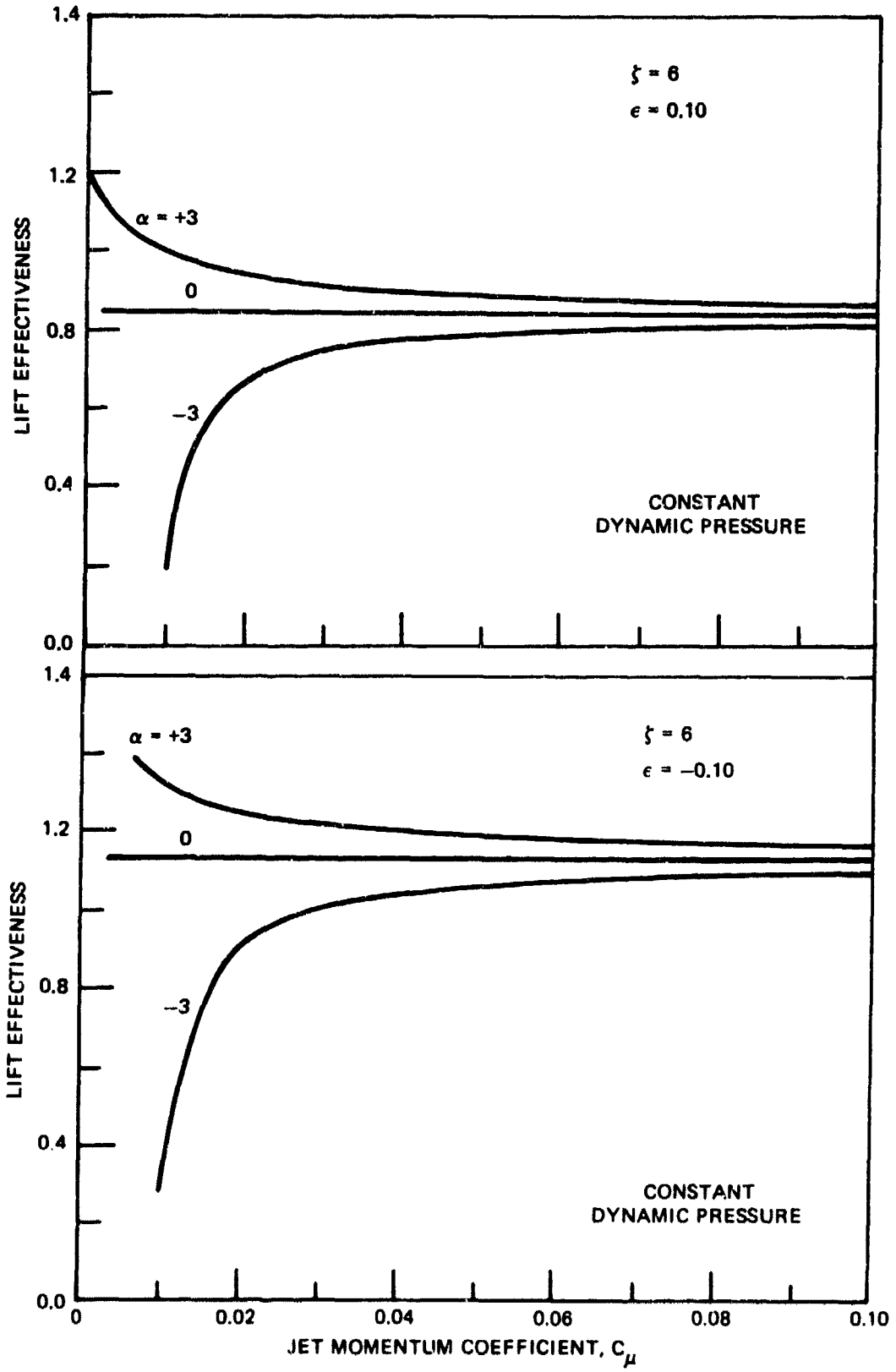

Figure 12 - Effect of Jet Momentum on Two-Dimensional Lift Effectiveness

expression for the distributed wing lift. The induced angle distribution is given by

$$\{i\} = N\{\tau\} \tag{11}$$

and the lift per unit span is related to the section circulation by

$$L' = \rho V \Gamma$$

or

$$L' = 2\ell q \tau \tag{12}$$

where $\tau \equiv \Gamma/\ell V$. The lift per unit span is also related to local airfoil properties by

$$L' = qcC_\ell \tag{13}$$

A comparison of Equations (12) and (13) then establishes the relation between τ and the local airfoil lift coefficient as

$$\tau = \frac{cC_\ell}{2\ell} \tag{14}$$

Section lift is given simply by $L = \Delta y L'$. The set of equations to be solved is then:

$$\{L\} = q[2\ell\Delta y]\ \{\tau\} \tag{15a}$$

$$\{\tau\} = \left\{\frac{cC_\ell}{2\ell}\right\} \tag{15b}$$

$$\{i\} = N\{\tau\} \tag{15c}$$

The dependence of C_ℓ on i provides the final relationship. The form of this relationship also determines the solution form for the equations. In the following, Equations (15) will be solved by using relations in Equation (2) for the case of distributed elasticity and those in Equation (3) for the case of wing root elasticity.

DISTRIBUTED ELASTICITY

This section provides an analysis of a wing having distributed torsional elasticity and resulting distributed torsional deflection. Airfoil characteristics will be represented by Equation (2) and are therefore assumed to be linear with angle of attack. Combining the last of Equation (2) with Equations (15b) and (15c) gives the following expression for the τ distribution:

$$\{\tau\} = \left[I + \left[\frac{ca}{2\ell}\right] N\right]^{-1} \left\{\frac{c\bar{C}_\ell}{2\ell}\right\}$$

Substitution into Equation (15a) then gives the lift distribution:

$$\{L\} = q(\Omega_s) \left\{\frac{c\bar{C}_\ell}{2\ell}\right\} \tag{16}$$

where $(\Omega_s) = [2\ell\Delta y] + \left[I + \left[\frac{ca}{2\ell}\right] N\right]^{-1}$. The distributed elastic twist is related to aerodynamic moments by the matrix of structural influence coefficients

$$\{\phi\} = \Theta\{M\} \tag{17}$$

Aerodynamic moments are expressed as follows where the moment coefficient has the same form as Equation (2):

$$\{M\} = q\left[\Delta y c^2\right] \{C_{m_{50}} - \varepsilon C_\ell\}$$

or

$$\{M\} = q[\Delta yc]\left\{\bar{C}_{m_{50}}\right\} - q\left[\Delta yc^2 C_{m_\alpha}\right]\{i\} - q\,[\Delta yc^2\varepsilon]\,\{C_\ell\} \qquad (18)$$

The following relations are available from Equations (15):

$$q\,[\Delta yc^2\varepsilon]\,\{C_\ell\} = [c\varepsilon]\,\{L\}$$

$$\{i\} = \frac{1}{q}\,N\left[\frac{1}{2\ell\Delta y}\right]\{L\}$$

which may be used to express the moment in terms of lift.

$$\{M\} = q\,[\Delta yc^2]\,\{\bar{C}_{m_{50}}\} - [s]\,\{L\} \qquad (19)$$

where $[s] = [\Delta yc^2 C_{m_\alpha}]\,N\left[\frac{1}{2\ell\Delta y}\right] + [c\varepsilon]$ and $\bar{C}_{m_{50}} = C_{m_o} + C_{m_\mu} C_\mu + C_{m_\alpha}\phi$.

The distributed elastic twist is obtained by substituting Equations (16) and (19) into Equation (17). Coefficients $\bar{C}_\ell$ and $C_{m_{50}}$ are expanded, and the resulting matrix equation is solved for the ϕ distribution to give

$$\{\phi\} = q\,Q^{-1}\,\theta\,[\Delta yc^2]\,\{C_{m_o} + C_{m_\mu}\,C_\mu\}$$

$$-q\,Q^{-1}\,\theta\,[s]\,(\Omega_s)\left[\frac{c}{2\ell}\right]\left\{C_{\ell_o} + \mu C_\mu\right\} \qquad (20)$$

where $Q = I - q\theta[\Delta yc^2 C_{m_\alpha}] + q\theta[s]\,(\Omega_s)\left\{\frac{ca}{2\ell}\right\}$.

The need to describe the moment coefficient in terms of both α and C_μ is unique to the family of blown airfoils and to CC airfoils in particular.

This requirement causes the above equation for elastic deflection to be more complex than its equivalent for a wing of conventional airfoils. Moment coefficient dependence on induced angle caused the more complex [s] term of Equation (19), and dependence on the elastic twist required the C_{m_α} term in the Q matrix. Although it is correct, the Q matrix is an undesirable feature of the anlysis since it contains q, and so Q^{-1} prohibits an algebraic factoring of all q terms in the final lift equation.

Lift distribution on the wing may now be obtained by expanding $\overline{C}_\ell$ in Equation (16) and substituting Equation (20) for the elastic twist. The jet momentum coefficient C_μ is expressed directly as $\dot{m}V_j$ since this is a quantity over which a pilot would have direct control. A fixed control type of analysis then maintains constant $\dot{m}V_j$; as a result, C_μ changes inversely with q. The wing lift distribution is then

$$\{L\} = q\,(\Omega_s)\left\{\frac{cC_{\ell_o}}{2\ell}\right\} + (\Omega_s)\left[\frac{\mu}{2\ell}\right]\{\dot{m}V_j\}$$

$$+ q^2\,(\Omega_s)\left[\frac{ca}{2\ell}\right] Q^{-1}\,\theta\left[\Lambda yc^2\right]\{C_{m_o}\}$$

$$+ q\,(\Omega_s)\left[\frac{ca}{2\ell}\right] Q^{-1}\,\theta\left[\Delta ycC_{m_\mu}\right]\{\dot{m}V_j\}$$

$$- q^2\,(\Omega_s)\left[\frac{ca}{2\ell}\right] Q^{-1}\,\theta[s]\,(\Omega_s)\left\{\frac{cC_{\ell_o}}{2\ell}\right\}$$

$$- q\,(\Omega_s)\left[\frac{ca}{2\ell}\right] Q^{-1}\,\theta[s]\,(\Omega_s)\left[\frac{\mu}{2\ell}\right]\{\dot{m}V_j\} \qquad (21)$$

Torsional Divergence

It is apparent from Equation (20) that Q^{-1} must exist in order for $\{\phi\}$ to be finite. The same observation may be made for the lift from Equation

(21). Therefore the divergence q is established by requiring that Q be singular, or det Q = 0. Note that $Q^{-1} = Q = I$ for q = 0 and that the lift reduces to

$$\{L\} = (\Omega_s)\left[\frac{\mu}{2\ell}\right]\{\dot{m}V_j\}$$

This is obviously not a valid condition since it corresponds to $C_\mu = \infty$ and the aerodynamics involved are not representative. However it implies that the trivial solution of q = 0 is eliminated in the above process since it does not result in det Q = 0. Therefore the desired solution is the lowest positive q which satisfies the criteria. The process also eliminates the need to evaluate the right-hand side of Equation (21) for calculations of divergence speed. It is practical because of the speed and accessibility of modern digital computers.

Basically it is seen that Q, and thus q_D, depend on the parameters a, C_{m_α}, ϵ, c, ℓ, and θ (stiffness matrix). These are the same parameters which govern the two-dimensional divergence, given by Equation (6), but they bear the more complex relations imposed by aerodynamic and elastic spanwise interactions.

Circulation Control Reversal and Effectiveness

As with the two-dimensional case, CC reversal is defined as the point where wing lift does not change with blowing. However, spanwise variations of L and $\dot{m}V_j$ require a slightly different mathematical definition. Let the total wing lift be

$$L_w \equiv [1]\{L\}$$

and define the distribution of jet momentum as

$$\{\dot{m}V_j\} = \dot{m}V_j)_r \{m\}$$

where $\dot{m}V_j)_r$ is the jet momentum at some wing reference station and {m} is then a dimensionless distribution of jet momentum normalized by the reference value. The reversal condition is then defined in scalar terms as

$$\frac{\partial L_w}{\partial \dot{m}V_j)_r} = 0$$

This condition may be evaluated from Equation (21) where the scalar quantity $\dot{m}V_j)_r$ may be taken across the matrix products:

$$\frac{\partial L_w}{\partial \dot{m}V_j)_r} = 0 = \lfloor 1 \rfloor \ (\Omega_s) \left[\frac{\mu}{2\ell}\right] \{m\} + q \ \ 1 \ \ (\Omega_s) \left[\frac{ca}{2\ell}\right] Q^{-1} \theta \left[\Delta y c C_{m_\mu}\right] \{m\}$$

$$- q \lfloor 1 \rfloor \ (\Omega_s) \left[\frac{ca}{2\ell}\right] Q^{-1} \theta \ [s] \ (\Omega_s) \left[\frac{\mu}{2\ell}\right] \{m\}$$

From this form, the reversal speed is

$$q_R = \frac{1 \ \ (\Omega_s) \left[\frac{\mu}{2\ell}\right] \{m\}}{\lfloor 1 \rfloor \ (\Omega_s) \left[\frac{ca}{2\ell}\right] Q^{-1} \theta \ \left[\left[\Delta y c C_{m_\mu}\right] - [s] \ (\Omega_s) \left[\frac{\mu}{2\ell}\right]\right] \ \{m\}} \qquad (22)$$

The solution given by Equation (22) is direct in the sense that Q^{-1} is a direct calculation which is readily attainable from several computer techniques. However it is iterative since Q itself is dependent on q. Hence it must be reevaluated by using the initially calculated $q_{R,}$ which then yields a new q_R from Equation (22). This is then a recursive-type formula, but it does not require the change in form which is necessary with some techniques for successive iterations.[5,6] For this reason, it is believed to be a more direct solution procedure for computer programming.

---

[6] Bisplinghoff, R. L. et al., "Aeroelasticity," Addison-Wesley, Massachusetts (1957).

Once the reversal q is obtained, Equation (21) may be used directly to calculate the lift distribution and, if desired, the total wing lift since Q^{-1} is then available at q_R.

As with the two-dimensional case, the equation for q_R does not appear to depend on the magnitude of blowing $\dot{m}V_j)_r$ or on any other initial conditions of angle of attack or camber. However these values do affect the local airfoil derivatives contained in Equation (22) and therefore do have an effect on q_R. Also like the two-dimensional case, Equation (18) shows that the aerodynamic moment and therefore the deflection angle are affected by the EA offset.

Lift effectiveness is again defined as elastic wing lift relative to rigid wing lift as discussed earlier. Elastic wing lift is the summation of distributed lift from Equation (21). Rigid wing lift is the same minus those terms due to elastic deflection. The lift effectiveness is then obtained from their ratio:

$$\text{Elastic Wing:} \quad L_w(E) = [1]\ \{L\}_{\text{Equation (21)}}$$

$$\text{Rigid Wing:} \quad L_w(R) = q\ [1]\ (\Omega_s) \left\{\frac{cC_{\ell_o}}{2\ell}\right\} + [1]\ (\Omega_s) \left[\frac{\mu}{2\ell}\right] \{\dot{m}V_j\}$$

$$\text{Lift Effectiveness:} \quad L.E. \equiv \frac{L_w(E)}{L_w(R)} \tag{23}$$

No simplification is possible for the general case, but the indicated calculations are direct when L.E. is generated versus q.

Circulation control effectiveness is defined as the sensitivity of the elastic wing lift to jet momentum relative to the sensitivity of the rigid wing lift to jet momentum, or

$$C.E. \equiv \frac{\partial L_w/\partial \dot{m}V_j)_r \quad \text{(elastic wing)}}{\partial L_w/\partial \dot{m}V_j)_r \quad \text{(rigid wing)}} \tag{24}$$

$$C.E. = \frac{\lfloor 1 \rfloor (\Omega_s) \left[\frac{\mu}{2\ell}\right] \{m\} + q \lfloor 1 \rfloor (\Omega_s) \left[\frac{ca}{2\ell}\right] Q^{-1} \theta \left[\left[\Delta y_{cc} C_{m_\mu}\right] - [s] (\Omega_s) \left[\frac{\mu}{2\ell}\right]\right] \{m\}}{\lfloor 1 \rfloor (\Omega_s) \left[\frac{\mu}{2\ell}\right] \{m\}} \tag{25}$$

It is seen from Equations (22) and (25) that these parameters have been consistently defined such that circulation control effectiveness is zero at the reversal speed. Neither L.E. nor C.E. is defined at the divergence speed since Q is singlular at that point but, as previously discussed, there is no need for their evaluation in this instance.

The relations presented in this section provide analytical ability for the general case of a circulation control wing. Matrix expressions have contained such terms as chord, EA offset, and lift and moment derivatives with respect to α and C_μ. Thus the analysis is applicable to the general case where chord and EA offset vary with span and where airfoil characteristics vary with span (including partial-span CC airfoils). The airfoil representation has assumed angle-of-attack linearity for variations about the geometric angle and has assumed C_μ linearity for variations about an arbitrary reference C_μ. Although this analysis has been oriented to specific static aeroelastic problems, the basic lift equations may certainly be applied to performance-oriented design goals as well.

Now consider a special case of the preceding analysis, one that allows for elastic deflection at the wing root only. However it includes an iteration procedure for obtaining the rigid-wing-induced angle distribution which eliminates an angle-of-attack linearity assumption for the rigid wing. The procedure was found necessary for the analysis of wings which while operating under partial angle-of-attack stall conditions still develop significant lift coefficients due to blowing.

WING ROOT ELASTICITY

The following analysis retains the previous lifting line theory and is for a three-dimensional wing with varying aerodynamic properties. However elastic properties allow for torsional softness only at the wing root. Thus

the deflection mode is one of a rigid body where all spanwise stations experience equal torsional deflections and all contribute equally to the pitching moment which causes that deflection.

This special case is considered for theoretical comparison to model data from just such a device. A blade from a CC rotor model was experimentally evaluated as a fixed wing, both with and without root torsional flexibility. The natural torsional stiffness of the blade was much too high to allow torsional deflections for the q range available in the DTNSRDC 8- x 10-ft subsonic wind tunnel. Accordingly, special root end fixture was designed and used to provide the blade with a rigid mode torsional response to its own aerodynamic moments. Experimental results from the model will be presented later along with an analytical comparison.

As previously described, the model blade geometry included considerable built-in twist or washout. When tested as a fixed wing, this led to an inboard angle-of-attack stall condition even though significant lift coefficients were maintained by CC blowing. The combination of negative lift curve slopes and operation in a nonlinear α range required an iterative solution to obtain induced angles. Airfoil characteristics for this analysis are represented by Equation (3), where the reference condition is the iterated solution for the rigid wing including induced angle distribution. Local airfoil derivatives are taken at this reference condition, and a linear analysis is used to establish the boundaries of torsional divergence and CC reversal. A byproduct of this approach is the solution to the rigid wing lift distribution without any restricting assumptions of airfoil linearity.

Consider first only the rigid wing; the problem is to converge on its induced angle distribution. Combining Equation (3) with Equations (15b) and (15c) gives the following expression for Δi:

$$\{\Delta i\} = P^{-1} N \left[\frac{cC_\ell}{2\ell}\right] - P^{-1}\{i\} \qquad (26)$$

where $P = I + N\left[\frac{ca}{2\ell}\right]$. Here Δi represents the difference between the

initial (or previous) induced angle and the induced angle for the next iteration. Obviously the solution criterion is for $\Delta i = 0$, where the terms on the right-hand side are in balance. At each step in the iteration, the previous angle distribution is adjusted by Δi and is then used to reevaluate the effective angle-of-attack distribution and the corresponding C_ℓ distribution. Local values of the lift curve slope are also reevaluated. This gives additional equations to be used in conjunction with Equation (26) for describing the iteration procedure:

$$\{i\} = \{i\} + \{\Delta i\}$$

$$\{\alpha\} = \{\alpha_g\} - \{i\}$$

$$\{C_\ell\} = \{C_\ell|\alpha, C_\mu\}$$

$$\{a\} = \{a|\alpha, C_\mu\}$$

Convergence to $\{\Delta i\} = 0$ yields the induced angle, lift coefficient, effective angle, and lift curve slope distributions of the rigid wing. These become the reference distributions which are denoted as $\{\ \}^*$ for the remaining analysis. At this point, the rigid wing lift is given by

$$\{L\} = q[2\ell\Delta y]\left\{\frac{cC_\ell}{2\ell}\right\}^*$$

or

$$\{L\} = q\{\Delta y c\ C_\ell{}^*\} \tag{27}$$

The elastic wing has the additional variation of torsional deflection which, in turn, changes the lift distribution and the induced angle distribution from those of the rigid wing. These are assumed to be relatively

small variations from the rigid wing and are approximated by linear relations. The induced angle distribution of the elastic wing may be related to that of the rigid wing by using Equation (15c):

$$\{i\} = \{i\}^* + \{\Delta i\} = N\{\tau\}$$

or

$$\{\Delta i\} = N\{\tau\} - \{i\}^* \tag{28}$$

Applying Equation (3) to Equation (15b) gives the following expression for dimensionless circulation:

$$\{\tau\} = \left[\frac{c}{2\ell}\right] \{C_{\ell_o} + \mu C_\mu\} + \left[\frac{ca}{2\ell}\right] \{\phi\} - \left[\frac{ca}{2\ell}\right] \{\Delta i\} \tag{29}$$

Combining Equations (28) and (29) gives the elastic wing circulation

$$\{\tau\} = R^{-1} \left[\frac{c}{2\ell}\right] \{C_{\ell_o} + \mu C_\mu\} + R^{-1} \left[\frac{ca}{2\ell}\right] \{\phi\} + R^{-1} \left[\frac{ca}{2\ell}\right] \{i\}^* \tag{30}$$

where $R = I + \left[\frac{ca}{2\ell}\right] N$.

Substitution of Equation (30) into Equation (15a) then provides the lift distribution of the elastic wing in terms of the deflection angle ϕ as

$$\{L\} = q(\Omega_s) \left\{\frac{cC_{\ell_o}}{2\ell}\right\} + (\Omega_s) \left[\frac{\mu}{2\ell}\right] \{\dot{m}V_j\} + q(\Omega_s) \left[\frac{ca}{2\ell}\right] \{i\}^*$$

$$+ q(\Omega_s) \left[\frac{ca}{2\ell}\right] \{\phi\} \tag{31}$$

where $(\Omega_s) = [2\ell\Lambda y]\, R^{-1}$.

The deflection angle ϕ must be expressed in terms of other variables in order to reduce Equation (31) to a usable form. For the case of root elasticity only, the distribution of ϕ is constant with a magnitude Φ, determined by the sum of the outboard wing moments:

$$\{\phi\} = \Phi\{1\}$$

The moment balance is then

$$K\Phi = \lfloor 1 \rfloor \{M\} \tag{32}$$

where the aerodynamic moments about the EA are expressed as follows:

$$\{M\} = q[\Delta yc^2] \{C_{m_{50}} - \varepsilon C_\ell\}$$

$$\{M\} = q[\Delta yc^2] \{C_{m_o} + C_{m_\mu} C_\mu\} + q\Phi[\Delta yc^2 C_{m_\alpha}] \{1\}$$

$$- q[\Delta yc^2 C_{m_\alpha}] \{\Delta i\} - [c\varepsilon] \{L\}$$

But $\{\Delta i\} = N\{\tau\} - \{i\}^*$ from Equation (28) and $\{\tau\} = \frac{1}{q}\left[\frac{1}{2\ell\Delta y}\right]\{L\}$ from Equation (15a); thus

$$\{\Delta i\} = \frac{1}{q} N \left[\frac{1}{2\ell\Delta y}\right] \{L\} - \{i\}^*$$

The moment equation in terms of lift is then:

$$\{M\} = q[\Delta yc^2] \{C_{m_o} + C_{m_\mu} C_\mu\} + q\Phi[\Delta yc^2 C_{m_\alpha}] \{1\}$$

$$+ q[\Delta yc^2 C_{m_\alpha}] \{i\}^* - [s] \{L\} \tag{33}$$

where $[s] = [\Delta yc^2 C_{m_\alpha}] N \left[\frac{1}{2\ell\Delta y}\right] + [c\varepsilon]$.

A solution for the deflection magnitude Φ is obtained by substituting the lift distribution, Equation (31), into the moment distribution, Equation (33). This is then applied to Equation (32) which is solved for Φ; the result is shown by Equation (34):

$$\Phi = \frac{q}{K-\lambda q} A - \frac{q}{K-\lambda q} \left(\lfloor 1 \rfloor [s] \{W\} \right) + \frac{\dot{m}V_j)_r}{K-\lambda q} B - \frac{\dot{m}V_j)_r}{K-\lambda q} \left(\lfloor 1 \rfloor [s] \{U\} \right) \qquad (34)$$

The lift distribution of the elastic wing is now obtained by direct substitution of the rigid body deflection angle Φ into Equation (31). After gathering terms, this gives the lift distribution to be

$$\{L\} = q\{W\} + \dot{m}V_j)_r \{U\} + \frac{q}{K-\lambda q} A\{V\} - \frac{q}{K-\lambda q} \left(\lfloor 1 \rfloor [s] \{W\} \right) \{V\}$$

$$+ \frac{q}{K-\lambda q} \dot{m}V_j)_r B\{V\} - \frac{q}{K-\lambda q} \dot{m}V_j)_r \left(\lfloor 1 \rfloor [s] \{U\} \right) \{V\} \qquad (35)$$

where $\{W\} = (\Omega_s) \left[\frac{c}{2\ell} \right] \{C_{\ell_o} + a i^*\}$

$\{U\} = (\Omega_s) \left[\frac{\mu}{2\ell} \right] \{m\}$

$\{V\} = (\Omega_s) \left[\frac{ca}{2\ell} \right] \{1\}$

$A = \lfloor 1 \rfloor [\Delta y c^2] \{C_{m_o} + C_{m_\alpha} i^*\}$

$B = \lfloor 1 \rfloor [\Delta y c C_{m_\mu}] \{m\}$

$[s] = [\Delta y c^2 C_{m_\alpha}] N \left[\frac{1}{2\ell \Delta y} \right] + [c\varepsilon]$

$\lambda = \lfloor 1 \rfloor [\Delta y c^2 C_{m_\alpha}] \{1\} - \lfloor 1 \rfloor [s] \{V\}.$

Note that the matrix factors in parentheses in Equations (34) and (35) and the defined terms A, B, and λ are all scalar quantities.

Torsional Divergence

It is clearly seen from Equation (34) that the deflection angle is divergent as $K-\lambda q$ approaches zero. Equation (35), which describes lift, is seen to diverge at this condition also. The divergence speed is then given by

$$q_D = K/\lambda \tag{36}$$

where q_D is seen to depend on stiffness K and the distributions of C_{m_α}, a, ε, and c. These relations are more easily seen when the terms of λ are expanded and regrouped as

$$\lambda = \lfloor 1 \rfloor \left[\Delta y c^2 C_{m_\alpha}\right] \left[I + N\left[\frac{ca}{2\ell}\right]\right]^{-1} \{1\} - \lfloor 1 \rfloor \left[c\varepsilon\right] (\Omega_s) \left[\frac{ca}{2\ell}\right] \{1\}$$

Circulation Control Reversal and Effectiveness

The definitions of circulation control reversal and of lift and control effectiveness used here are identical to those previously defined for the general case of distributed elasticity. Taking $\partial L_w / \partial \dot{m} V_j)_r$ from Equation (35) yields

$$\frac{\partial L_w}{\partial \dot{m} V_j)_r} = \lfloor 1 \rfloor \{U\} + \frac{q}{K-\lambda q} \left(B - \lfloor 1 \rfloor [s] \{U\}\right) \lfloor 1 \rfloor \{V\} \tag{37}$$

Reversal speed corresponds to that value of q at which the above partial derivative goes to zero or

$$q_R = \frac{K}{\lambda - (B - \lfloor 1 \rfloor [s] \{U\}) \frac{\lfloor 1 \rfloor \{V\}}{\lfloor 1 \rfloor \{U\}}} \tag{38}$$

Both reversal speed and divergence speed for this case (Equations (38) and (36), respectively) are seen to be less complex than their counterparts for

the case of distributed elasticity and yet more complex than those for the two-dimensional case. This simply reflects the relative complexity of the wing root elasticity problem with respect to those other two cases.

It is certainly advantageous, if not common practice, to design to the condition of $q_D > q_R$, or $q_D/q_R > 1$. This relation is obtained by combining Equations (36) and (38), and it may be used directly in lieu of individual calculations for q_D and q_R.

$$\frac{q_D}{q_R} = 1 - \frac{1}{\lambda} \left(B - \lfloor 1 \rfloor [s] \{U\}\right) \frac{\lfloor 1 \rfloor \{V\}}{\lfloor 1 \rfloor \{U\}}$$

The factors λ, $\{V\}$, and $\{U\}$ are normally positive. Thus in order for the above equation to satisfy the previous inequality ($q_D/q_R > 1$), $B - \lfloor 1 \rfloor [s] \{U\}$ must be less than zero. But B is normally negative (because C_{m_μ} is negative) and because it is dependent on airfoil characteristics, it is not readily changed. The design parameter which may be varied is seen to be the elastic axis offset ϵ that occurs in the matrix [s]. Examination then shows that to increase the ratio q_D/q_R, ϵ should be increasing positively (forward). Basically it is seen [from Equation (36)] that an increase in ϵ decreases λ and thus increases q_D. The effect on q_R is less obvious and involves canceling effects in the denominator of Equation (38). This at least indicates a smaller change in q_R, accounting for the increased q_D/q_R ratio. The reduced effect of ϵ on q_R is not surprising since the previous simplified two-dimensional analysis had predicted no effect at all.

Lift effectiveness was defined by Equation (23). Applying Equation (35), and the notation used there to the definition of L.E. gives

$$L_w(E) = \lfloor 1 \rfloor \{L\} \quad \text{Equation (35)}$$

$$L_w(R) = q \lfloor 1 \rfloor \{W\} + \dot{m}V_j)_r \lfloor 1 \rfloor \{U\}$$

$$\text{L.E.} \equiv \frac{L_w(E)}{L_w(R)}$$

So then

$$L.E. = 1 + \frac{q}{K-\lambda q}\left(\frac{q(A - \lfloor 1 \rfloor [s]\{W\}) + \dot{m}V_j)_r (B - \lfloor 1 \rfloor [s]\{U\})}{q \lfloor 1 \rfloor \{W\} + \dot{m}V_j)_r \lfloor 1 \rfloor \{U\}}\right) \lfloor 1 \rfloor \{V\}$$

This value of lift effectiveness at the reversal speed is of interest since this establishes relative importance. If the reversal speed is determined to be marginally satisfactory (does not yield broad safety margins) then it may be important to maintain high lift effectiveness at the reversal boundary. This would be a quantitative consideration beyond the normal procedure of designing $q_D > q_R > q_{max}$. Evaluating L.E. at q_R gives

$$L.E._{REV} = \frac{q_R \lfloor 1 \rfloor \{W\} - q_R\left(\frac{A - \lfloor 1 \rfloor [s] \{W\}}{B - \lfloor 1 \rfloor [s] \{U\}}\right) \lfloor 1 \rfloor \{U\}}{q_R \lfloor 1 \rfloor \{W\} + \dot{m}V_j)_r \lfloor 1 \rfloor \{U\}}$$

Circulation control effectiveness was defined by Equation (24). As previously discussed, it is a measure of elastic wing lift response to a change in the input control of jet momentum. It differs from lift effectiveness in that the latter is elastic wing total lift at a fixed control setting. Applying Equation (37) to the definition gives:

$$C.E. = \frac{\lfloor 1 \rfloor \{U\} + \frac{q}{K-\lambda q}(B - \lfloor 1 \rfloor [s] \{U\}) \lfloor 1 \rfloor \{V\}}{\lfloor 1 \rfloor \{U\}}$$

Substitution of the equations for q_D and q_R provide the following simplified form:

$$C.E. = \frac{1 - q/q_R}{1 - q/q_D} \tag{39}$$

First of all, it is noteworthy that this is the same relation obtained for the two-dimensional case despite the fact that the definitions of q_R and q_D

are quite different. Second, Equation (39) shows again that C.E. goes to zero as q approaches q_R. Finally and most significant, Equation (39) establishes the importance of the concept of circulation control reversal as defined herein. Specifically the values of q_R and q_D not only aid in defining boundaries of the flight envelope but they alone can describe the effectiveness of circulation control over the entire flight envelope.

Trim and Stability

The equations developed above for wing root elasticity may also be readily applied to such problems as aircraft trim and stability. This subject is beyond the scope of the present report, but it would be neglectful not to mention such alternative uses. The following brief treatment is intended merely to show the new interpretation of terms and their application.

Very simply, the equations for wing root elasticity may be thought of as applying to the aircraft itself where (1) the spring restoring moment stems from the horizontal tail surface, (2) the deflection angle Φ represents an aircraft attitude change, and (3) the parameter ε represents the dimensionless distance from wing midchord to aircraft center of gravity (CG). The wing aerodynamic coefficients are still referenced to the midchord position. The horizontal tail surface contributes a nose-down pitching moment to the aircraft given by:

$$M_t = - X_t \, q_t \, S_t \, (C_{L_{t_o}} + a_t \, \Phi) \qquad (40)$$

where $C_{L_{t_o}}$ is taken as positive up and accounts for the combined effects of tail incidence, downwash at the tail, elevator setting, and initial aircraft attitude. The following definitions are useful:

$$K_t = X_t \, q_t \, S_t \, a_t$$

$$\zeta_t = \frac{K_t}{q\bar{S}\bar{c}} = \frac{X_t}{\bar{c}} \frac{q_t}{q} \frac{S_t}{S} a_t$$

where $\bar{c}$ is the wing mean, or reference, chord. Note the equivalence between K_t here and K from Equation (32).

When the aircraft is in moment equilibrium, the summation of moments about the CG equals zero. This is basically a balance between wing moments, Equations (33), and tail moments, Equation (40). Equating these two to zero and solving for Φ gives the aircraft trim attitude, where Φ is the change in attitude from the initial assumed angle.

$$\Phi = \frac{1}{\zeta_t S\bar{c}-\lambda} (A - \lfloor 1 \rfloor [s] \{W\}) + \frac{1}{\zeta_t S\bar{c}-\lambda} \frac{\dot{m}V_j)_r}{q} (B - \lfloor 1 \rfloor [s] \{U\})$$

$$- \frac{\zeta_t S\bar{c}}{\zeta_t S\bar{c}-\lambda} \frac{C_{L_{t_o}}}{a_t}$$

The above value for Φ may then be used in Equation (31) to evaluate the trim-corrected wing lift distribution.

Certain static stability problems may also be analyzed. The following considers the aircraft longitudinal angle-of-attack stability. The wing moment from Equation (33) is repeated below, after Equation (31) has been substituted for lift and regathering terms.

$$M_w = q(A - \lfloor 1 \rfloor [s] \{W\}) + \dot{m}V_j)_r (B - \lfloor 1 \rfloor [s] \{U\}) + q\Phi\lambda$$

The summation of moments about the CG is simply the above wing moment and the tail moment from Equation (40). The criteria for angle-of-attack stability is then

$$\frac{\partial M_{CG}}{\partial \Phi} = q(\lambda - \zeta_t S\bar{c}) < 0$$

The advantage in using the equations of this analysis for trim and stability problems is the greater accuracy obtained through the combined use of two-dimensional airfoil data for both lift and moment coefficients and proper spanwise distributions provided by the lifting line theory. It has become increasingly apparent that pitching moments from CC airfoils have significant contributions and must be included for an accurate analysis.

CIRCULATION CONTROL WING MODEL

A semispan model of a circulation control wing (CCW) was evaluated in the DTNSRDC 8- x 10-ft subsonic wind tunnel to experimentally verify the existence of the CC reversal phenomenon and to provide data on the behavior of a torsionally soft CCW for comparison with theory. The wing model consisted of one blade from a CC helicopter rotor model and provided full-span blowing. The standard rotor model setup was used for the CCW test since data acquisition, data reduction techniques, and air supply lines were established for this configuration. Figure 13 shows the CCW model in the wind tunnel. The wing was mounted in a zero sweep position on the rotor head, which was locked for this test to prevent rotation. All force data were taken from the wind tunnel balance frame by using Toledo scales and a Beckman analog-to-digital converter. Lift scale accuracy is believed to be within $\pm$ 0.1 lb and pitching moment within $\pm$ 0.1 ft-lb. Each data point is an average of 10 to 12 records taken on the Beckman system. Wing duct pressure was measured by an internally mounted Kulite pressure transducer (type CQL-080-25, 25 psia, $\pm$ 1%). Air mass flow to the wing was measured with a venturi meter in the air supply line.

Geometry of the CCW model is given in Table 1. The semispan model measured 40 in. (1.016 m) from the head centerline to the wing tip. Circulation control airfoils extended from Station 4 (0.1016 m) to Station 39.88 (1.013 m) with a linear variation of airfoil thickness and camber in between. Root and tip airfoil geometry are shown in Figure 14. It is emphasized that

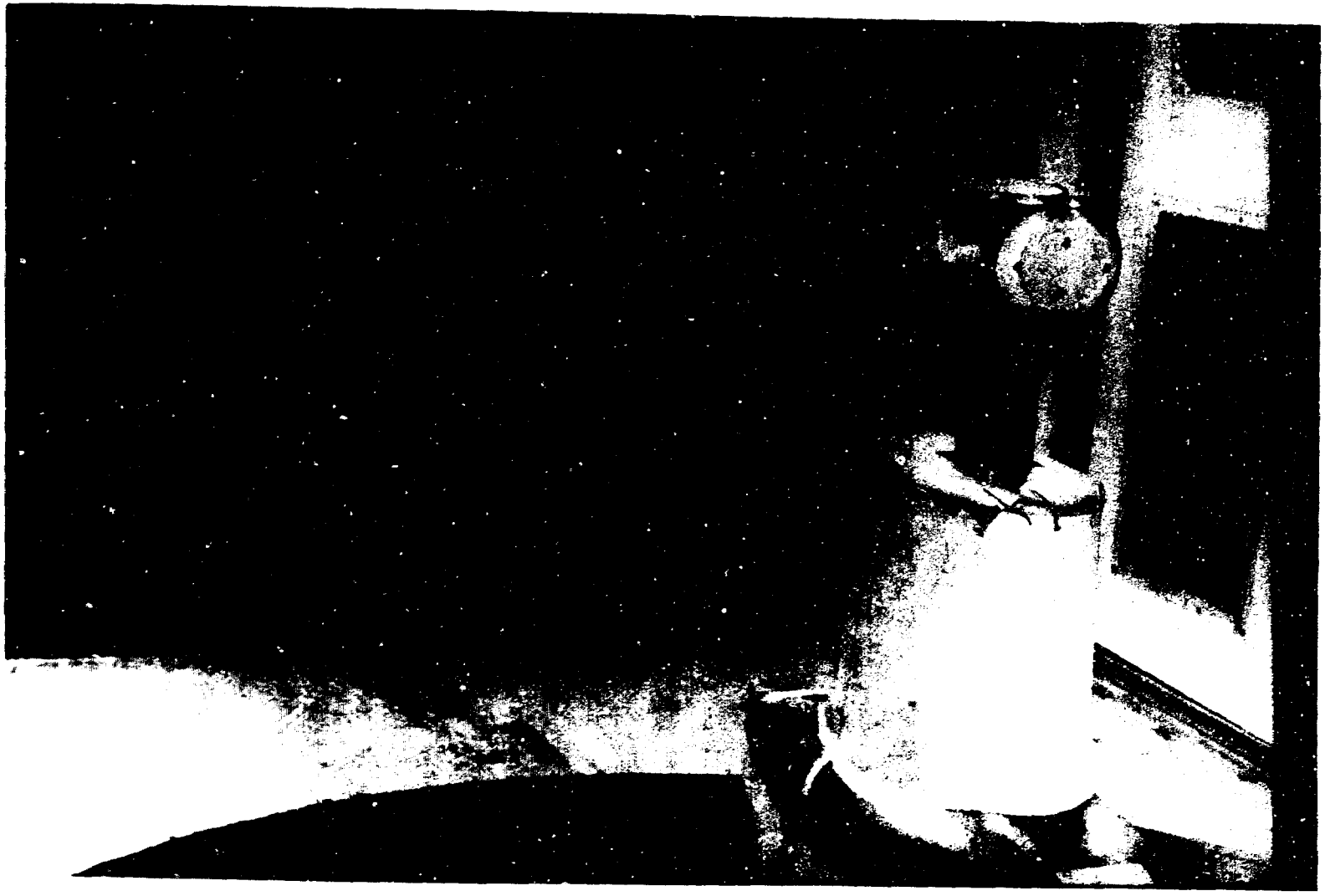

Figure 13 - Circulation Control Wing Model in Subsonic Wind Tunnel

TABLE 1 - CIRCULATION CONTROL WING MODEL GEOMETRY

Wing Parameters	
Semispan, ft/m	3.00/0.914
Chord, in/cm	3.2/8.13
Geometric Twist, deg	-8.63

Airfoil Parameters		
	Root	Tip
Thickness Ratio, t/c	0.25	0.15
Camber Ratio, δ/c	0.0625	0.0
Coanda Radius Ratio, R/c	0.0497	0.0403
Slot Height Ratio, h/c	0.0015	0.00312

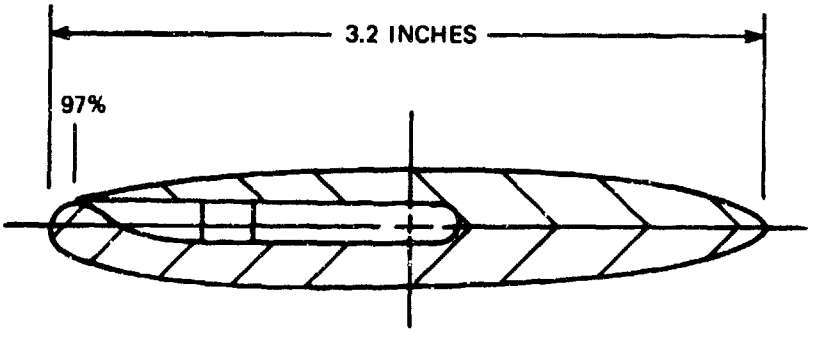

TIP SECTION

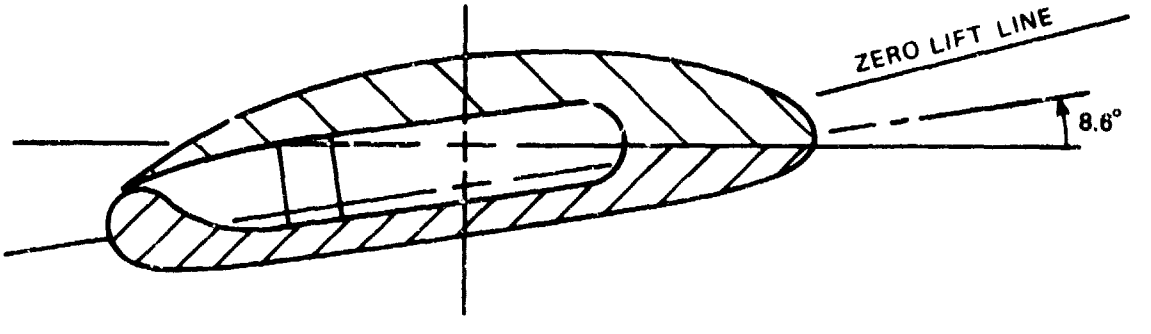

ROOT SECTION

Figure 14 - Airfoil Geometry of CCW Model

the model wing geometry was actually designed for rotary wing application and was used in this study only because of its availability. The geometry does not reflect current designs for application of CC airfoils to fixed wing aircraft. However, it does reflect characteristics which are basic to current CC airfoils, e.g., high lift augmentation and pitching moment of significant magnitude. As such, the test results are sufficient to identify the parameters of importance to this study and to serve for comparison to the theory presented later.

Two types of data were taken with the model wing. For the first set, the wing was rigidly mounted to its support, and a range of wing incidence angles and jet momentum provided a performance map for the configuration and served as a reference for the second data set. For the second set, the CCW was mounted to a torsionally soft, spring-restrained, root-end attachment which allowed a rigid body mode of response to the aerodynamic pitching moments that simulated the distributed aeroelastic response of a full-scale wing. Such a device was needed to provide a low torsion stiffness consistent with the limited dynamic pressure range of the wind tunnel. Since the results depend directly on this device, it will be described in some detail.

Figure 15 illustrates the mechanism that allows this torsional degree of freedom. Two sets of ball bearings join a fixed outer ring (attached to the rotor head) and a free inner ring to which the wing is attached. The inner ring has a through-center hole for the wing air supply. Torsional freedom is restrained by two linear springs at the top of the mechanism. One end of each spring is attached to the rigid outer ring. Stops on the arm prevent torsional deflection beyond about $\pm$ 14 deg (this also corresponds to the compressed length of the tension springs). The mechanism was designed to allow wing torsional freedom about one of three chordwise positions -0.4c, 0.5c, or 0.6c. The 0.4c position was not used since it resulted in excessive nose-down deflections for the stiffness used.

Figure 15 - Soft Torsion Root Attachment Device

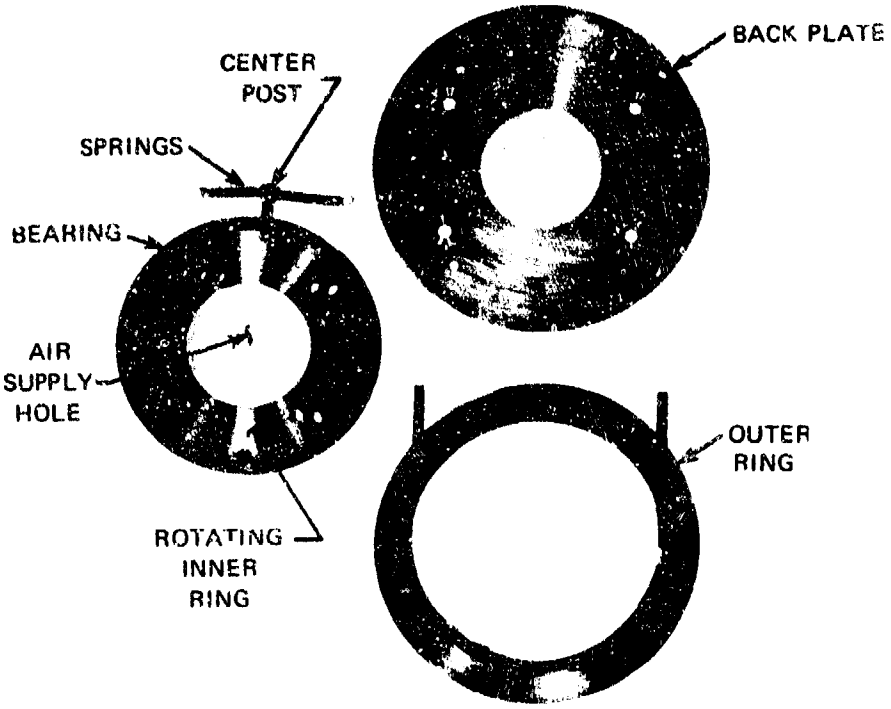

Figure 15a - Exploded View

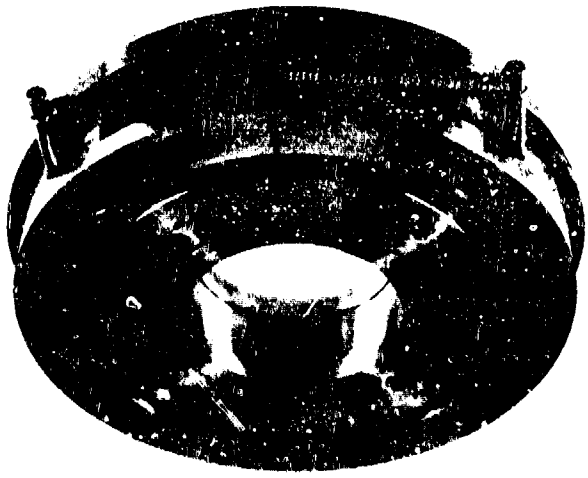

Figure 15b - Assembled View

Figure 15c - Installation for $\varepsilon = 0.0$

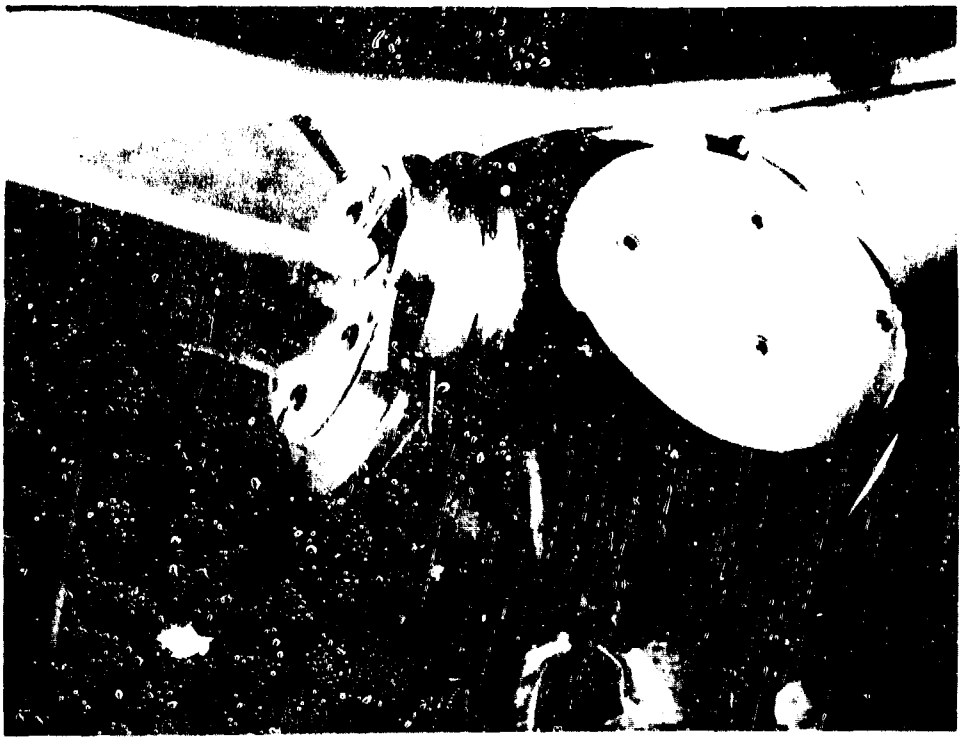

Figure 15d - Installation for $\varepsilon = -0.10$

Figure 16 indicates the arrangement of the springs relative to the

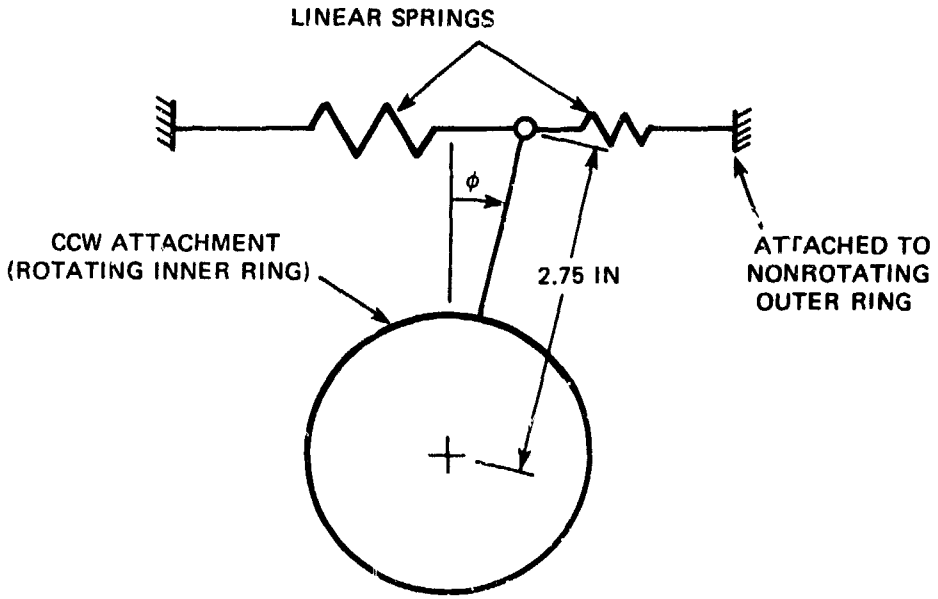

Figure 16 - Details of Wing Root Attachment Device

centerline of rotation. The equivalent rotational spring constant $K_\theta = 2Kr^2$ was calculated from the average linear spring constants to be $K_\theta = 4.7505$ ft-lb/radian. Figure 17 shows the linear calibration for each spring and the normal spring operating range. Differences in the preload values for the two springs are unimportant since they do not fall within the operating range.

Wing incidence angle was set by initially allowing the wing to come to a torsional equilibrium, where the torsional spring balanced any wing gravity moments. Torsional freedom was then locked out and the desired incidence angle was set. Thus when the lock was released, the wing was in equilibrium at the desired incidence.

The second data set was taken by using the soft torsion mechanism for several values of initial wing incidence and a range of jet momentum. Additionally, free-stream q was varied to obtain the desired results. At low q, the torsional spring restrained the deflection to small values which

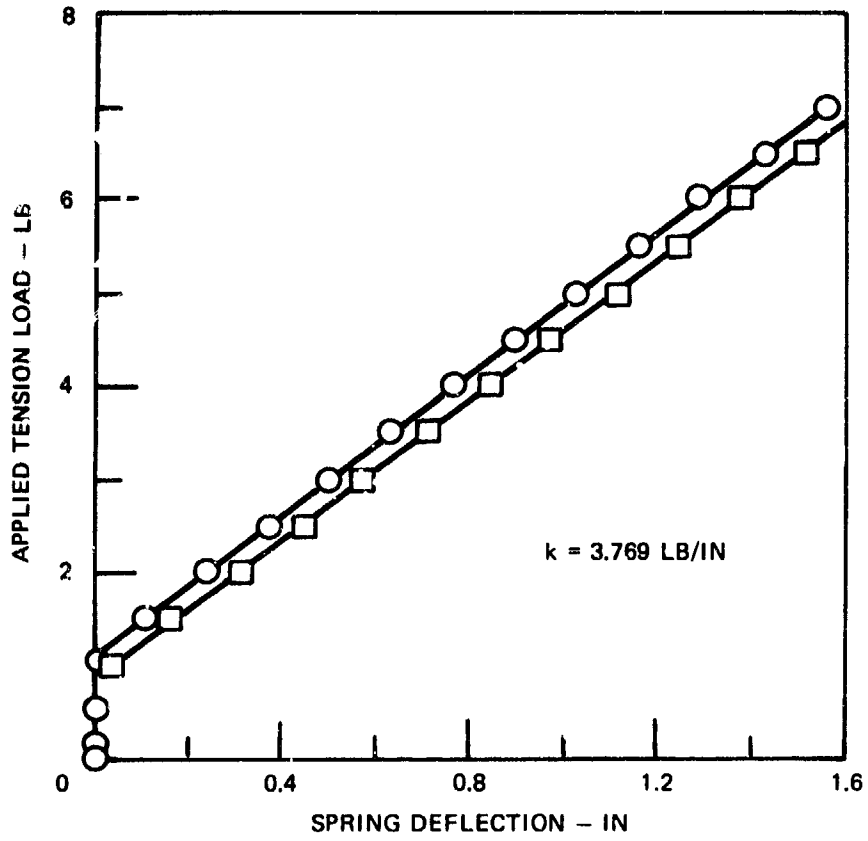

Figure 17 - Linear Calibration for the Two Springs

corresponded to a high ratio of spring stiffness to aerodynamic pitching moment. The significant deflections occurring at higher q provided experimental data in the regions of torsional divergence and CC reversal. During the entire test program, the model was visible through plexiglass panels in the wind tunnel walls and the observer recorded estimated torsional deflections when appropriate to ensure correct interpretation of the data. A particular run was terminated whenever the model wing reached full deflection limits, as noted by the observer. This data set will be presented and later compared to the theoretical analysis.

TORSIONALLY RIGID MODEL WING

The lift coefficient behavior of the torsionally rigid CCW model is shown in Figure 18 for a range of incidence angles and blowing magnitudes.

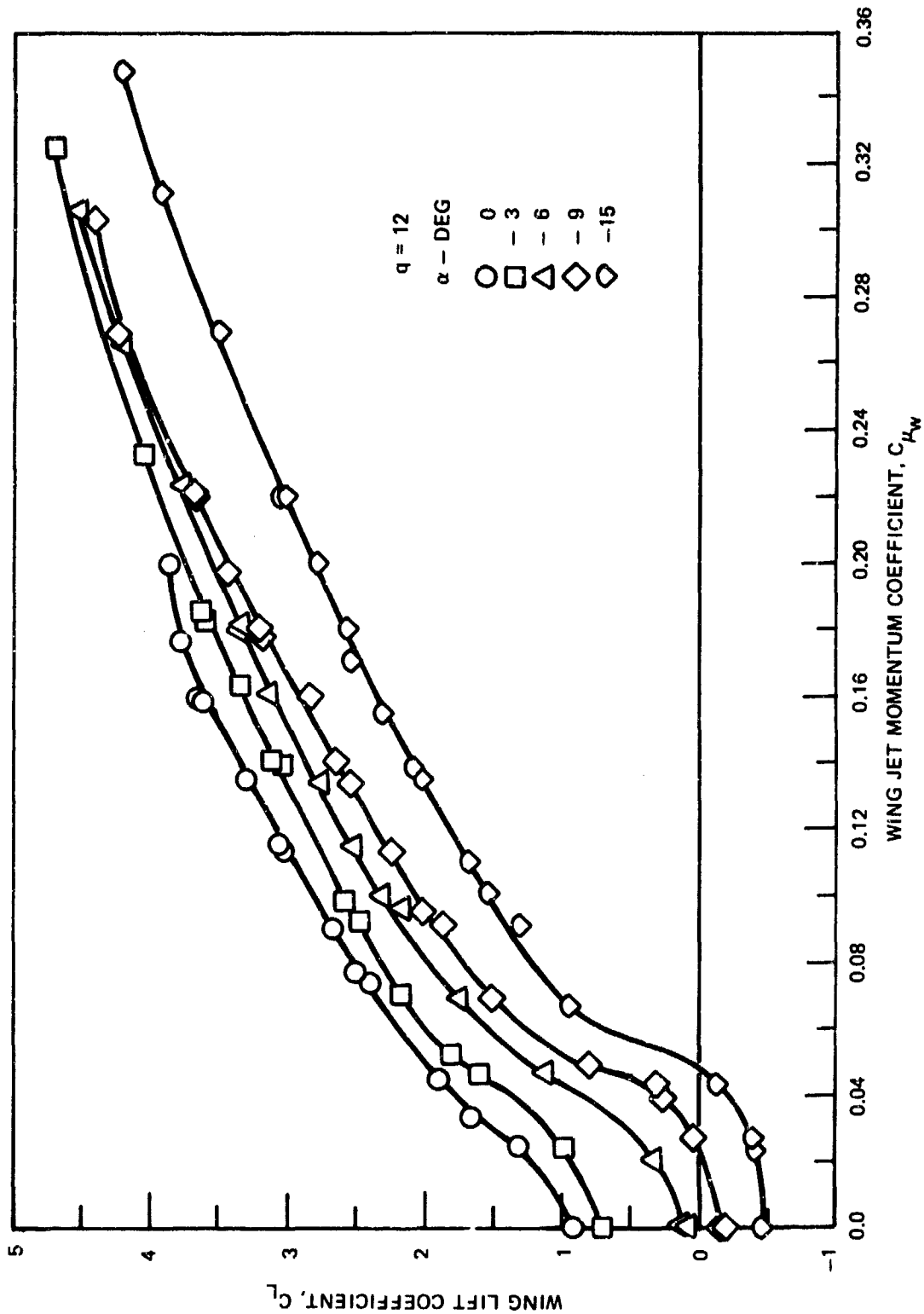

Figure 18 - Lift Coefficients for the Torsionally Rigid CCW Model

The data shown for the CCW model follow the same trends as previously shown for the basic CC airfoil, namely, increasing lift with both increasing jet momentum and increasing incidence angle. Wing root pitching moments are shown in coefficient form in Figure 19 for the same case. Root pitching moments were measured by four strain gages mounted at the wing root in a Wheatstone-bridge arrangement rather than by wind tunnel balance scales in order to provide greater accuracy for the relatively low magnitudes of wing pitching moments.

MODEL WING WITH ELASTIC AXIS AT 0.5 CHORD

Torsionally soft wing root conditions were examined over a range of q, initial incidence, jet momentum, and EA position. In general, the test procedure was to hold wind tunnel q constant and to vary wing duct pressure, or C_{μ_w}. Since the root spring constant was fixed, the dimensionless stiffness ζ was varied by changing wind tunnel q.

Figure 20 shows the elastic wing lift variation with C_{μ_w} at different q settings, or different ζ, for three initial α_{TIP} values. Rigid wing data are also shown for purposes of comparison. The powerful effect of dimensionless stiffness ζ on the wing lift is clearly evident in Figure 20a (initial α_{TIP} = - 3 deg); it resulted in a condition of CC reversal for the lower value of ζ. The reversal condition did not show up for the higher ζ even at the extreme C_{μ_w} values shown, but the reduction of lift effectiveness due to gradually decreasing angle-of-attack was quite evident. In contrast, lift effectiveness was seen to improve at low C_{μ_w} for the low ζ condition, corresponding to small positive pitching moments. But as C_{μ_w} increased, the pitching moment decreased to approach zero, causing a reduced deflection angle. The reduced angle-of-attack resulted in further reductions of pitching moment until finally the wing could no longer sustain a positive pitching moment and deflection angle. At a slightly higher C_{μ_w}, the pitching moment became negative, causing an angle-of-attack reduction which

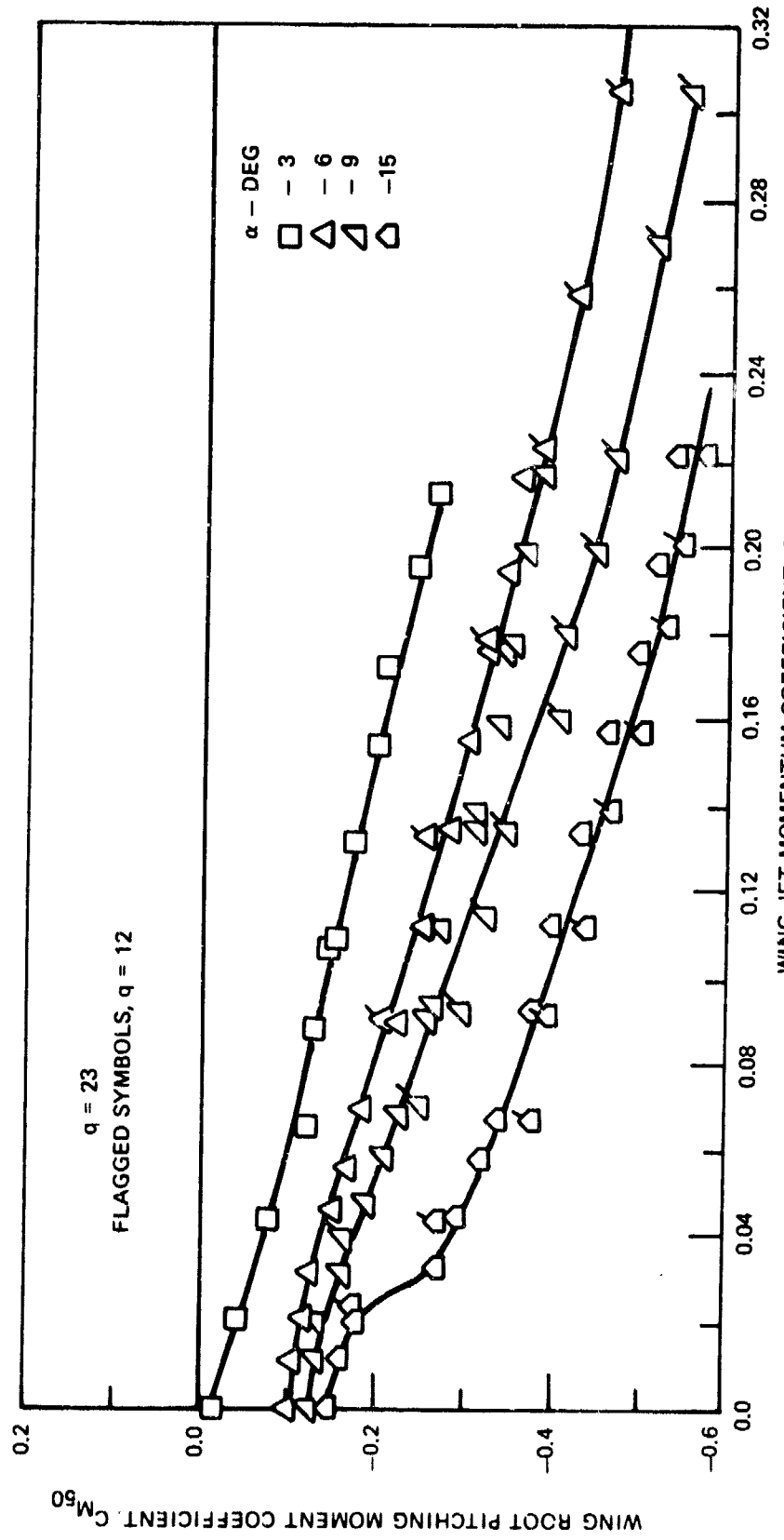

Figure 19 - Root Pitching Moment Coefficients for the Torsionally Rigid CCW Model

Figure 20 - Effect of Torsional Stiffness on the Lift Coefficient Characteristics of the Elastic CCW Model at Different Initial α_{TIP} Values

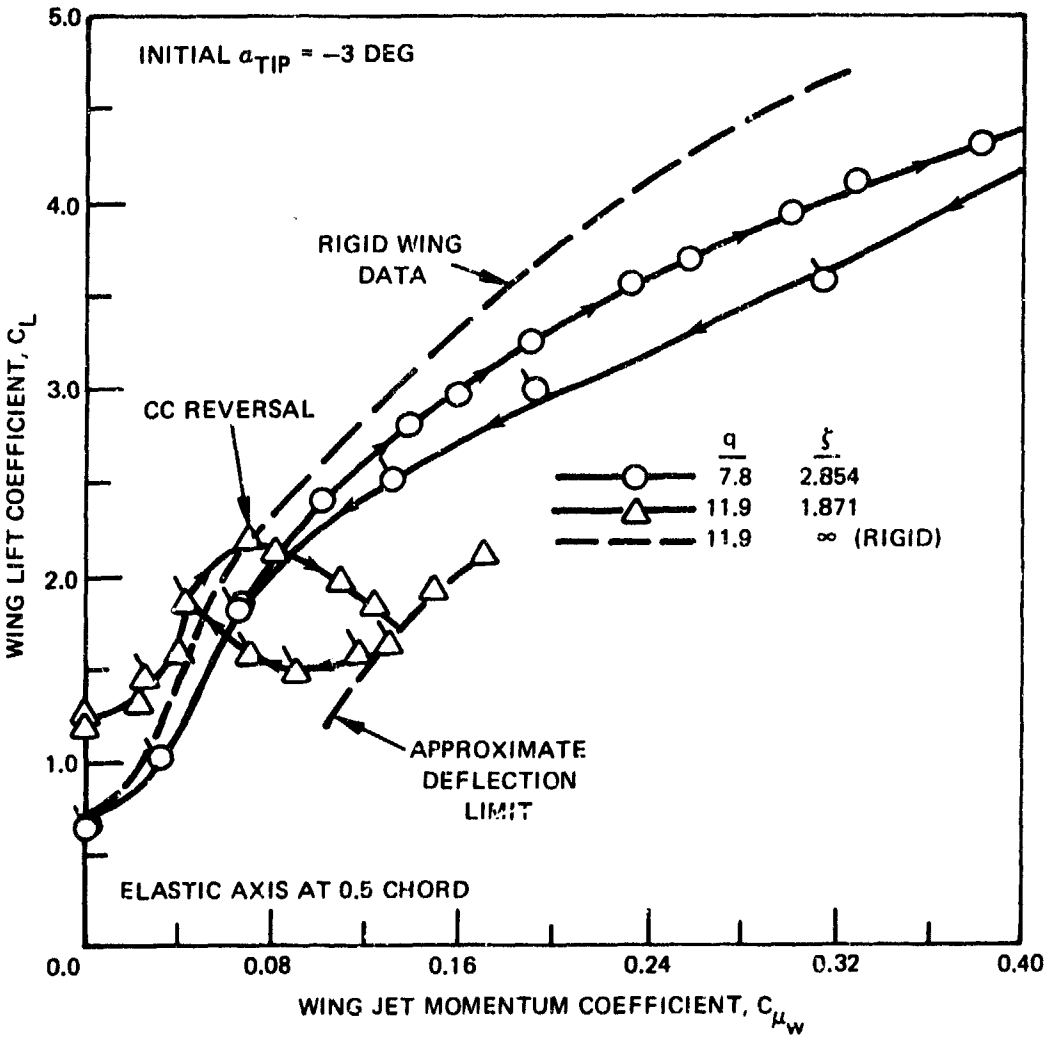

Figure 20a - Initial α_{TIP} = -3 Degrees

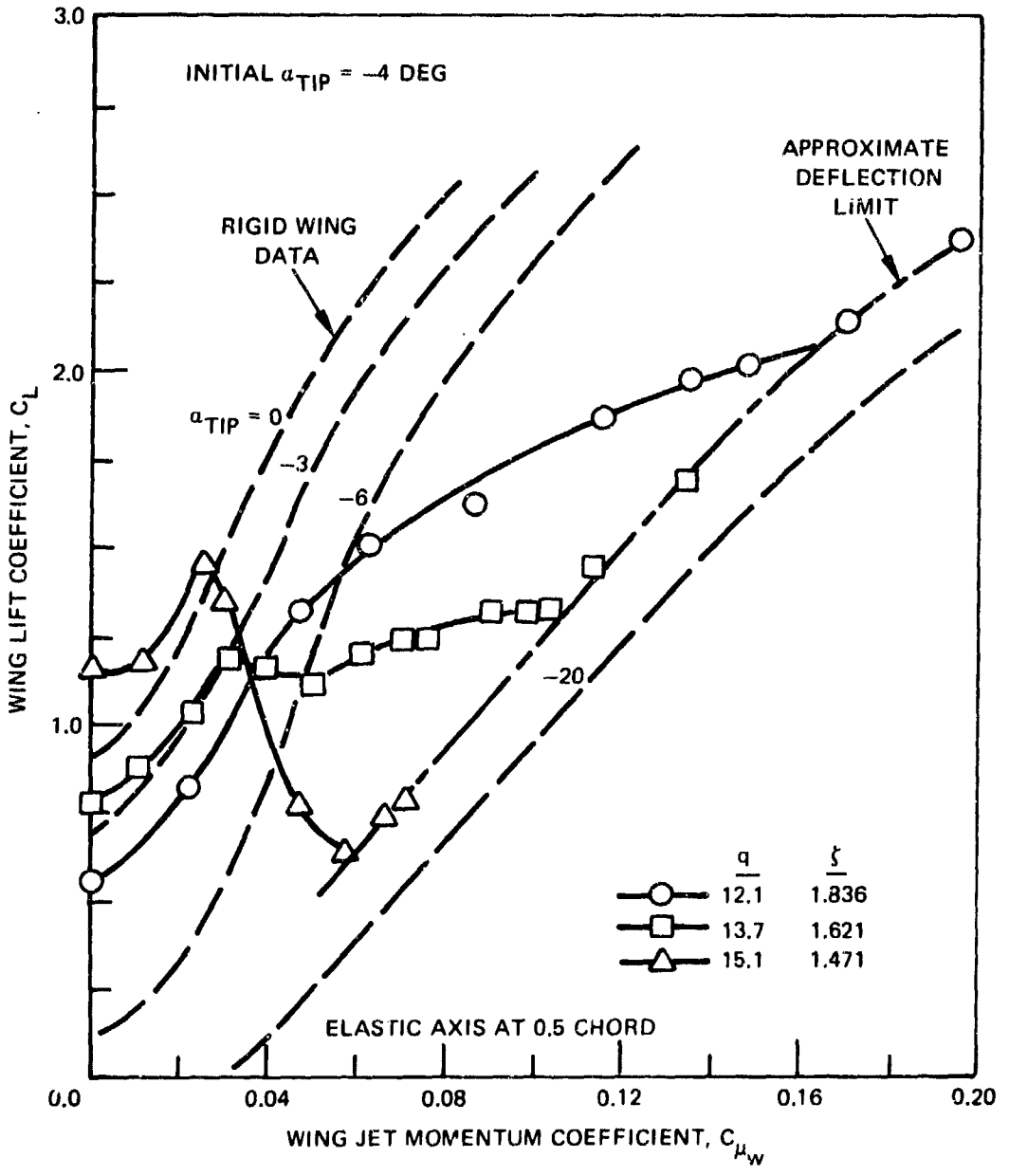

Figure 20b - Initial α_{TIP} = -4 Degrees

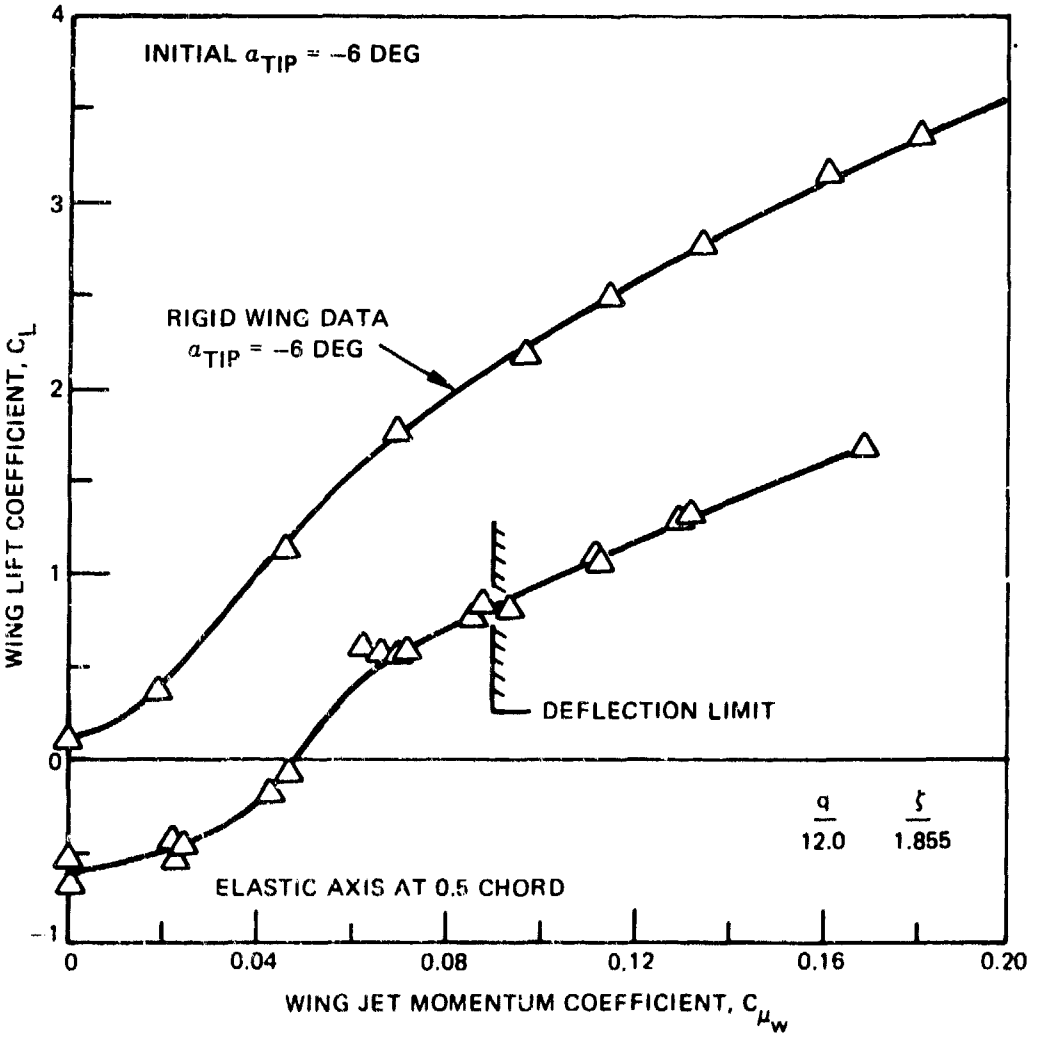

Figure 20c - Initial α_{TIP} = -6 Degrees

further reduced the pitching moment. This resulted in a sudden angle-of-attack change to a new equilibrium position between the aerodynamic moment and the spring restoring moment. Beyond this point of CC reversal, further C_{μ_w} increases were characterized by reduced wing C_L. In this region, increased C_{μ_w} caused larger negative pitching moments which reduced the angle-of-attack. The angle-of-attack change caused a still larger negative pitching moment that affected the new equilibrium position. The result was a net reduction in wing C_L due to the overpowering reduction in angle-of-attack. Figure 20a shows that this region continued until the deflection limit was reached.

The hysteresis effect shown is aerodynamic in nature. On the return, the angle-of-attack is already at a large negative value. As C_{μ_w} is decreased, the pitching moment magnitude is decreased. However, the negative deflection angle tends to support itself by maintaining the large negative pitching moment magnitude. The double dependence of lift and pitching moment on angle-of-attack and jet momentum suggested the possibility of some aeroelastic problems not considered in the study. Specifically, the intentional or inadvertent addition of oscillating C_{μ_w} to the above-mentioned hysteresis could potentially result in a condition similar to stall flutter.

The return points were eliminated from the plot for an initial α_{TIP} of -4 deg (Figure 20b) to show more clearly the effects of stiffness ϵ variations. The onset and full development of CC reversal is evident as ζ decreased. There was a reduction in both lift effectiveness and control effectiveness at the large ζ, but the deflection angle limit was reached before a reversal condition was obtained. A condition of CC reversal was obtained at $\zeta = 1.621$. The wing lift remained nearly constant beyond the reversal point even though C_{μ_w} was increased to three times its value at reversal. This reflects the balance between increasing lift due to jet momentum and decreasing lift due to decreasing angle-of-attack. Finally at $\zeta = 1.471$, the reversal condition occurred at a lower value of C_{μ_w} and was

characterized by significant reductions in lift for further increases in C_{μ_w} ($\partial L_w/\partial \dot{m} V_j < 0$).

The trends changed at an initial wing incidence of -6 deg (Figure 20c). At this low incidence, the pitching moments started off negative, causing a reduction in lift even at $C_{\mu_w} = 0$. The initial deflection angle was observed to be approximately -7 deg, putting the blade tip at a geometric angle of about -13 degrees. As jet momentum was increased, the deflection angle continued to decrease, but lift increased and did not display a CC reversal condition. The deflection limit, approximately -14 deg, was reached at $C_{\mu_w} \simeq 0.09$. Since the elastic wing was against the deflection stops for C_{μ_w} values above this point, the setup prevented finding a CC reversal condition if one did exist. Theoretical calculations predicted a CC reversal at $C_{\mu_w} \simeq 0.16$, with deflection angles beyond the range of the model.

Life effectiveness (L.E.) and control effectiveness (C.E.) were evaluated by comparing the data of Figure 20b to the rigid wing data of Figure 18. The L.E. is a direct ratio of elastic wing to rigid wing lift and was calculated directly. Figure 21 shows the variation of L.E. with C_L for each q value for an initial α_{TIP} of -4 deg. Large initial values of L.E. resulted from the initial nose-up pitch attitude of the wing at $C_{\mu_w} = 0$. As C_{μ_w} was increased, the pitching moments decreased and then became negative, resulting in reduced pitch attitudes, reduced lift, and reduced L.E. It should be noted that the L.E. plot does not provide information on the occurrence of CC reversal. In fact, the elastic wing lift was still greater than the rigid wing lift (L.E. > 1.0) shortly after the reversal condition. Likewise the C.E. parameter, discussed below, gives no information on the large initial lift of the elastic wing as shown by L.E. However the two parameters do provide two different types of information for examining elastic wing behavior.

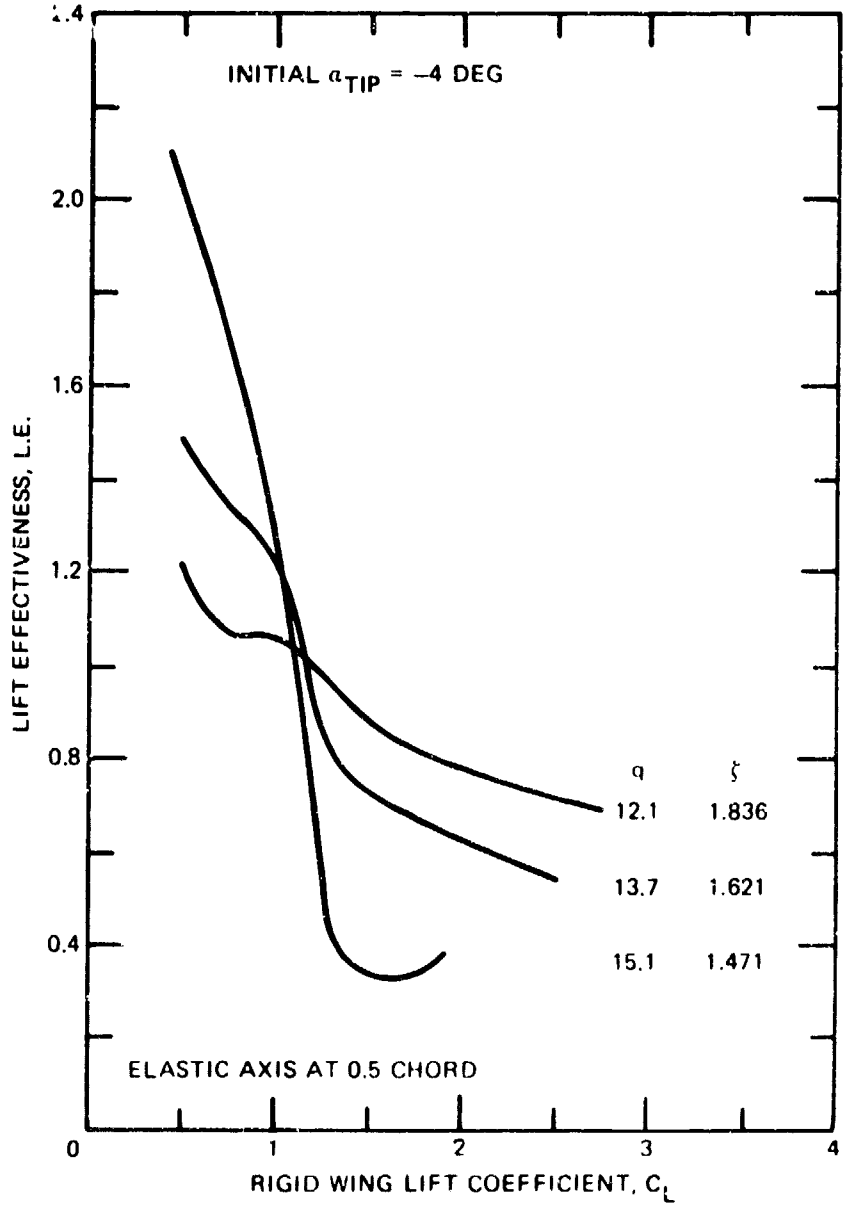

Figure 21 - Variation of Elastic Wing Lift Effectiveness with C_L for Various Values of q and ζ

The C.E. was defined by Equation (24) relative to the jet momentum at some reference station on the wing $\dot{m}V_j)_r$. The C.E. of the model wing data may be evaluated by observing that jet momentum at some reference station bears a fixed relation with the wing total jet momentum, or $\dot{m}V_j)_r = Q\ \dot{m}_T V_j$, where the Q factor depends on distributed slot height and strip width at the reference station. Furthermore, since this relation is unaffected by wing elasticity, it is the same for the elastic wing as for the rigid wing. Therefore C.E. may be easily evaluated from the model wing data by the equivalent equation expressed in coefficient form:

$$C.E. = \frac{\partial C_L/\partial C_{\mu_w}\ \text{(elastic wing)}}{\partial C_L/\partial C_{\mu_w}\ \text{(rigid wing)}}$$

Figure 22 indicates the variation of C.E. with C_L for each value of q and an initial $\alpha_{TIP} = -4$ deg, as evaluated from the data of Figure 20b. CC reversal is indicated by those points where C.E. = 0. Negative values of C.E. denote the condition beyond CC reversal where increases in jet momentum result in decreases in wing lift.

A comparison of Figures 21 and 22 shows some unusual conditions. At the highest q and $C_{\mu_w} = 0$, the L.E. was quite high and C.E. was positive but rather small. This corresponds to a high lift condition (due to a positive deflection angle) but a very low control power condition. The low control power stems from the fact that very high section angles on the inboard position of the wing cause a partial angle-of-attack stall or the formation of a leading edge bubble. The circulation control becomes rather ineffective under these conditions and, for the wing, resulted in a significant loss of control. The C.E. went to zero for the high q curve of Figure 22, denoting CC reversal. However, the value of L.E. was still greater than 1.0 at this point. Again, this was a relatively high lift condition even though control effectiveness had become zero. The region $C_L > 0.80$ showed

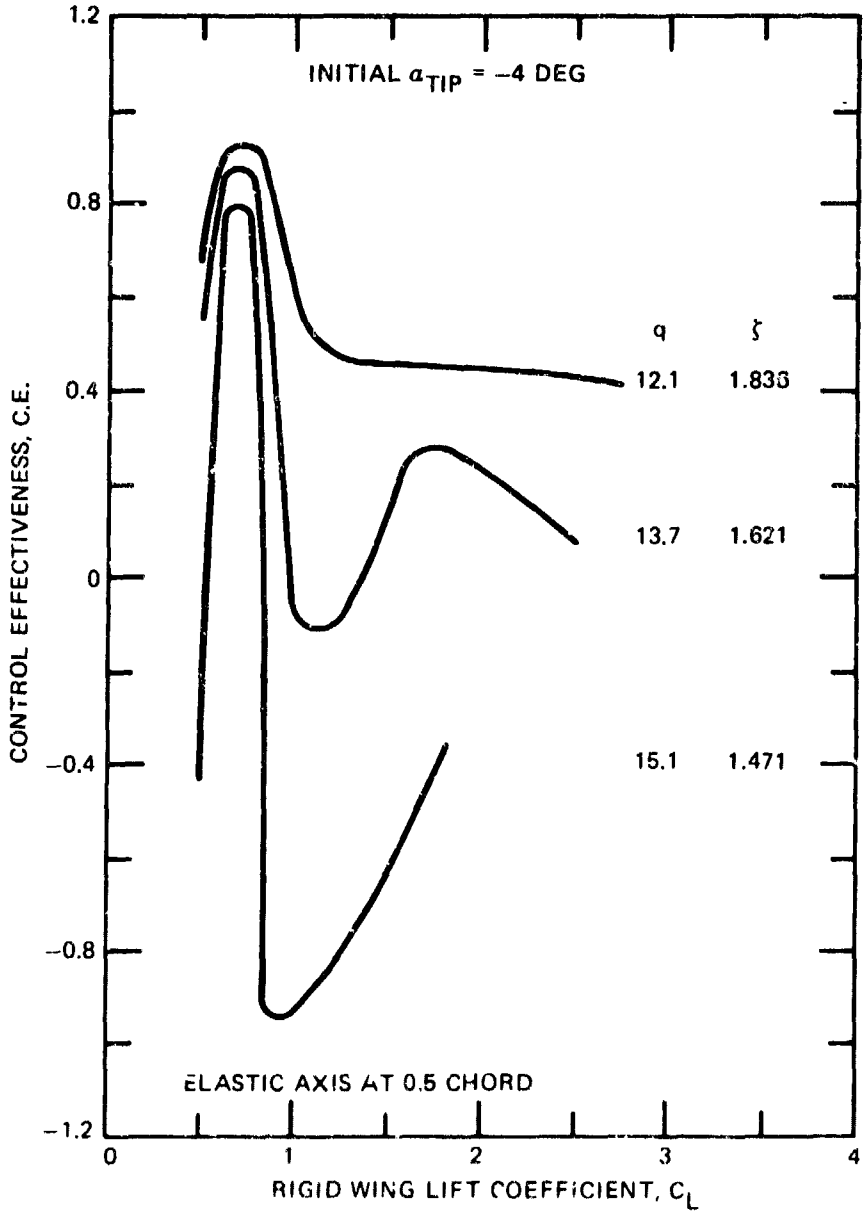

Figure 22 - Variation of Elastic Wing Control Effectiveness with C_L for Various Values of q and ζ

strong control reversal (C.E. < 0) and associated strong reductions in L.E. as lift and angle-of-attack dropped rapidly with further increases in C_{μ_w}.

The L.E. and C.E. values at initial α_{TIP} = -6 deg shown in Figure 23 were calculated from the data of Figure 20c. The L.E. began as a strong negative value at C_{μ_w} = 0 but rapidly increased to become positive for

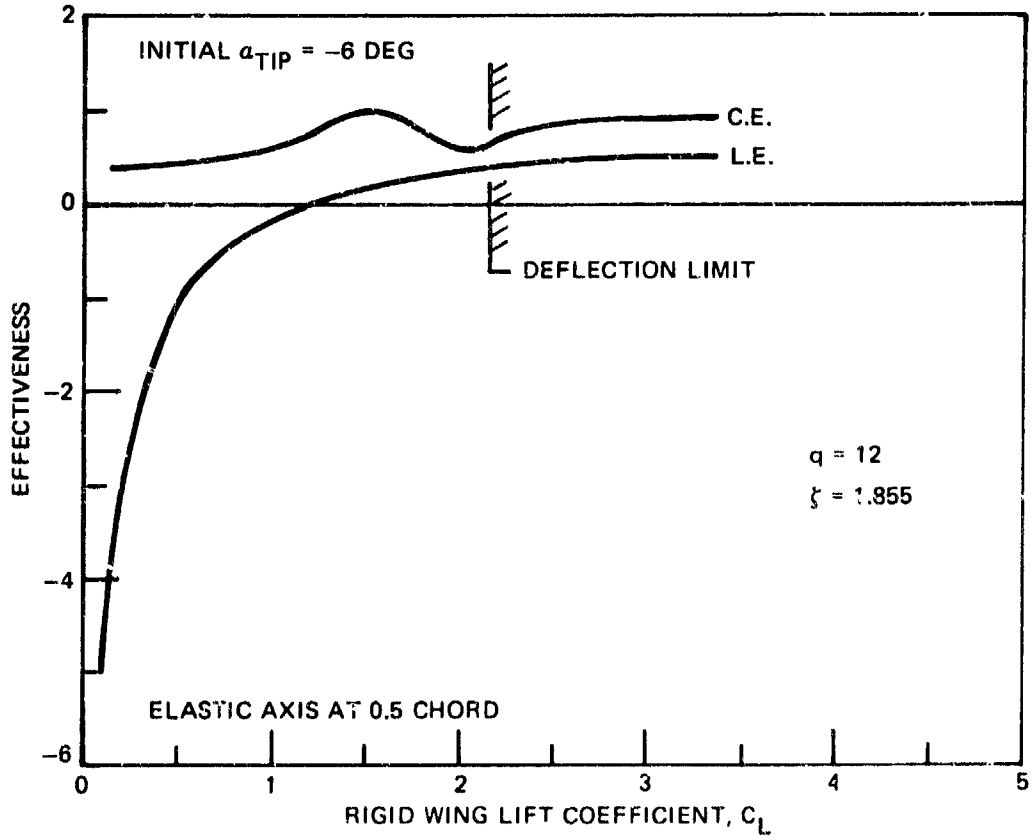

Figure 23 - Variation of Elastic Wing Lift and Control Effectiveness with Wing Jet Momentum Coefficient

$C_L \geq 1.20$. This behavior is quite different from that displayed in Figure 21 which showed high initial values of L.E. and then a drop with increasing C_{μ_w}. The negative initial value of L.E. is attributed to negative initial deflection angle. This drove the elastic wing to negative lift compared to a small positive lift for the rigid wing. The reason for increasing lift of the elastic wing with increasing C_{μ_w} is less clear, especially since the

deflection angle went to larger negative values as C_{μ_w} increased. It is believed that the wing inboard section was at a more favorable operating condition and provided a strong lift response to the increasing jet momentum. Examination of the wing center of lift position (rolling moment/lift) indicates a significant inboard lift in support of this argument. Figure 24

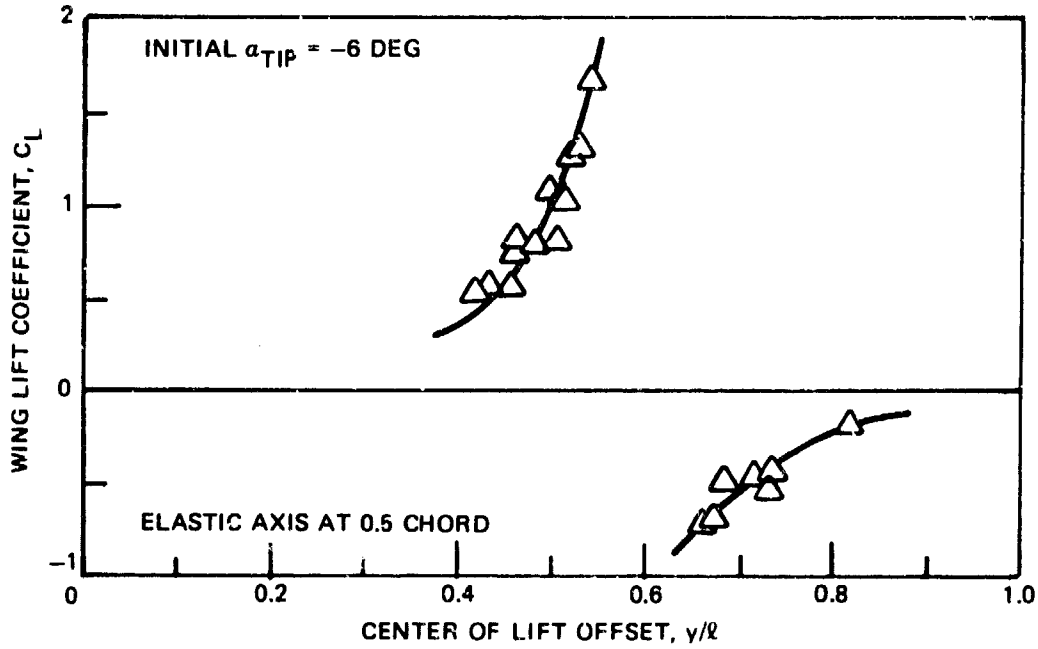

Figure 24 - Elastic CCW Center of Lift Variation with Wing Lift Coefficient

shows that the center of lift was outboard for the negative lift condition on the elastic wing. This suggests that the inboard section may have been developing positive lift because of camber and jet momentum even though the net wing lift was negative. At positive wing lift, the center of lift was around the midspan position, reflecting a nearly uniform distribution across the semispan.

MODEL WING WITH ELASTIC AXIS AT 0.6 CHORD

The root attachment mechanism shown in Figure 15 was repositioned so that the center of rotation of the device corresponded to the 0.60 chord

position of the model wing. This established the elastic axis at 0.6 chord or EA offset of $\epsilon = -0.10$, where $\epsilon = 0.50 - EA/c$. The center of rotation was shifted to have the CCW model in the same position relative to the wind tunnel and thus avoid any need to consider model position in the data reduction program.

Since the model center of gravity position was forward of the elastic axis for this configuration, static moments resulted. These were compensated for by the spring restraint, leaving the model at an equilibrium angle - a balance between static moment and spring restoring moment. Model incidence angles were then set from this condition as previously described. The initial spring deflection required to establish moment equilibrium reduced the usable range of pitch-down deflection and increased the usable range of pitch-up deflection. This did not hinder the results in any way since model deflections were predominantly in the pitch-up direction for the aft EA position.

An EA offset of $\epsilon = -0.10$ results in rather strong pitch-up moments from the wing lift (at 0.50 chord) acting through the 0.10 chord moment arm. This moment contribution from lift increases with C_{μ_w} and α and tends to conceal the decreasing negative pitching moments resolved at the airfoil mid-chord. Figure 6 has previously shown the pitching moment trends as all forces and moments were resolved to different chord locations. Extrapolation of those data to a 0.60 chord resolution point would show that the net pitching moment increases with C_μ. This behavior is opposite to that shown for the 0.50 chord resolution point. It is interesting to note from Figure 6c that pitching moments tend to be independent of C_μ when resolved to a 0.55 chord location.

The above discussion suggests that deflection angles should be positive for the aft EA position. Divergence conditions are also suggested by positive pitching moments which increase with angle-of-attack. The CCW wind tunnel test showed an immediate pitch-up divergence for an initial incidence angle of $\alpha_{TIP} \approx -3$ deg, even for zero blowing. Obviously meaningful data

were unobtainable for this incidence angle. However, data were obtained for α_{TIP} = -8 deg over a broad range of blowing conditions. These reduced angles of attack produced small negative initial pitching moments. As C_{μ_w} was increased, the moments became positive and resulted in pitch-up deflections of the model wing.

Figure 25 presents the elastic wing lift coefficient behavior versus C_{μ_w} for two different initial α_{TIP} values. For α_{TIP} = -6 deg (Figure 25a), the zero blowing deflection angle was estimated to be -3 deg, corresponding to a negative initial pitching moment. As C_{μ_w} was increased, the deflection angle became positive and produced rapid increases in wing lift. The deflection angle reached a maximum of about + 9 deg at $C_{\mu_w} \simeq 0.20$, which corresponds to α_{TIP} of about +3 deg. Inasmuch as this angle is beyond the wing stall condition, further C_{μ_w} increases produced very little change in wing C_L.

Comparison between the C_L characteristics of Figure 20c (ε = 0.0, q = 12.0, ζ = 1.855) and Figure 25a (ε = -0.10, q = 7.69, ζ = 2.895) shows a marked difference in the overall elastic wing response to changes in the elastic axis location. The elastic wing C_L was considerable less than that of the rigid wing for ε = 0.0. However the case for ε = -0.10 showed regions of substantial improvements in elastic wing C_L relative to that of the rigid wing. It should be noted that because of the reduced q, the relative stiffness was higher for Figure 25a than for Figure 20c. An attempt was made to evaluate the wing at ε = -0.10 for q = 12.0. However the reduced relative stiffness resulted in abrupt changes in angle-of-attack, giving the appearance of a divergent condition.

The elastic wing response for ε = -0.10 at an initial angle of α_{TIP} = -8 deg (Figure 25b) was similar to that shown at α_{TIP} = -6 deg (Figure 25a). The initial deflection angle was estimated to be -6 deg at zero blowing. The larger negative deflection angle and reduced wing C_L were expected for α_{TIP} = -8 deg compared to α_{TIP} = -6 deg.

Figure 25 - Elastic Wing Lift Coefficient Behavior versus C_{μ_w} for the 0.60 Chord EA Location at Two Initial α_{TIP} Values

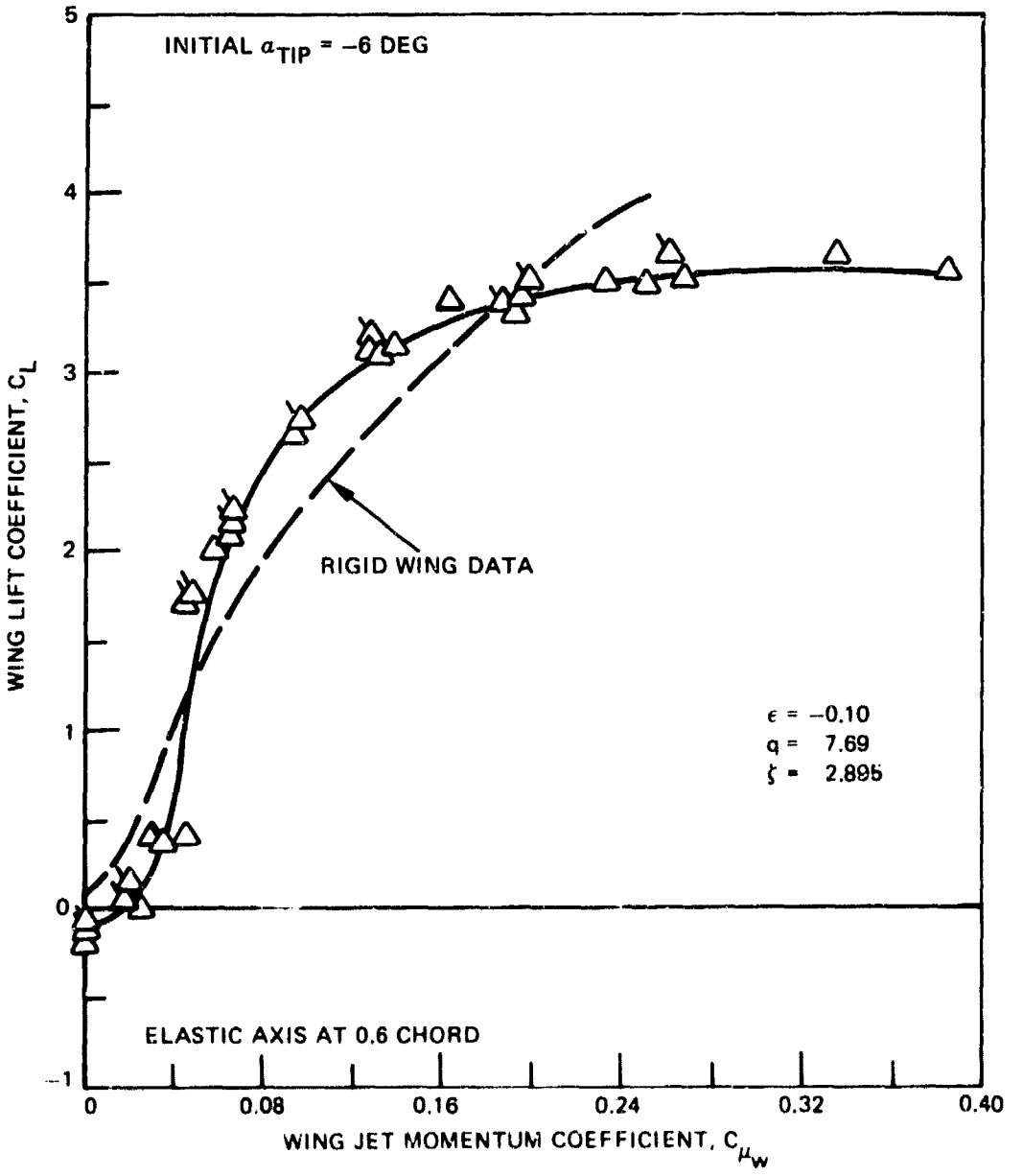

Figure 25a - Initial α_{TIP} = -6 Degrees

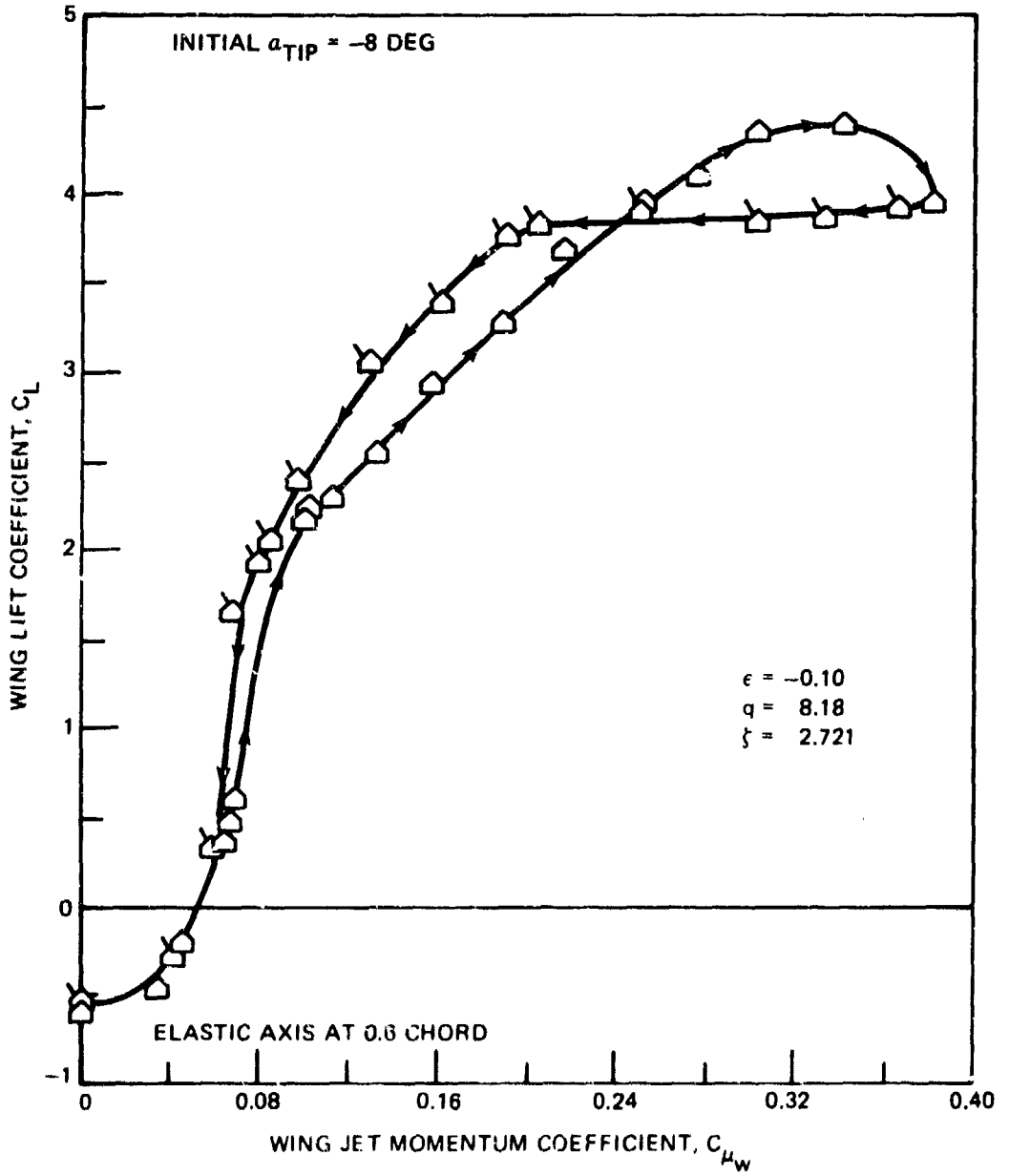

Figure 25b - Initial α_{TIP} = -8 Degrees

The L.E. and C.E. shown in Figure 26 were determined from the data of

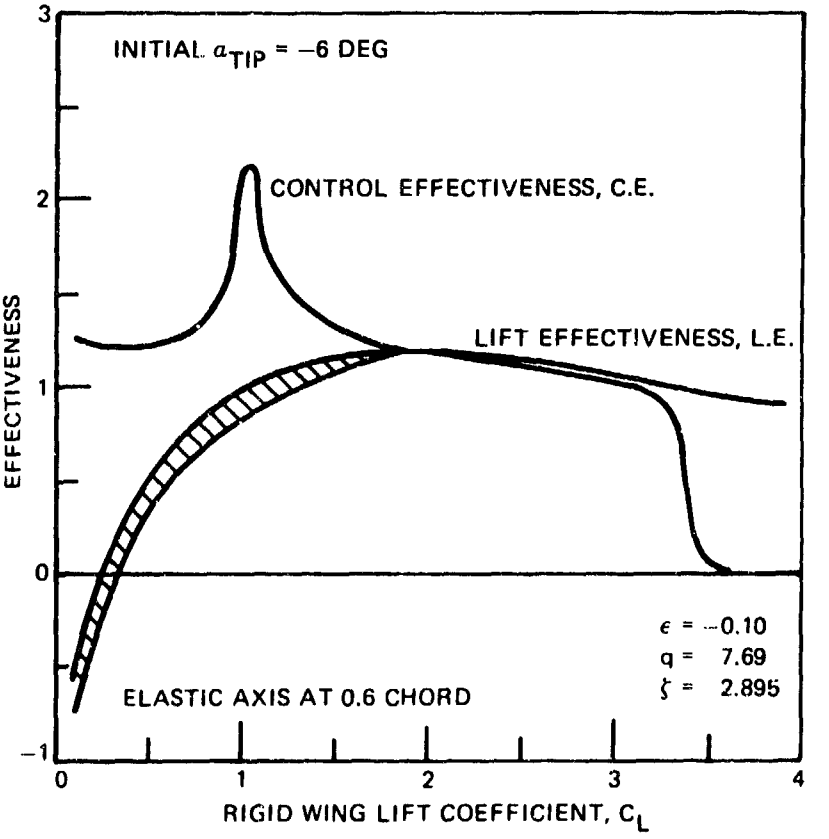

Figure 26 - Elastic Wing Lift and Control Effectiveness for the 0.6 Chord EA Location and Initial α_{TIP} = -6 Degrees

Figure 25a (initial α_{TIP} = -6 deg). Values of L.E. started off negative but quickly approached 1.0 and above as C_{μ_w} was increased. Values of C.E. ranged from about 0.4 to 2.3 in the more important C_{μ_w} region. The values around 2.0 and above indicate a potential for increased control effectiveness by proper EA placement. However the C_{μ_w} range where this occurred was very limited, and any such gains must be traded off against the problems of operation near divergence boundaries.

COMPARISON OF THEORY AND MODEL WING DATA

The previously derived theory is now compared to results from the wind tunnel evaluation of the CCW model. Rigid wing conditions are used as a baseline to establish the relative ability of the theory and two-dimensional data to predict three-dimensional wing behavior. Comparisons include the L.E. and C.E. parameters and the limiting conditions of CC reversal and torsional divergence. First, however, it is necessary to describe the computer-programmed solutions for the theory.

DESCRIPTION OF PROGRAMMED SOLUTION

The equations derived in the section on wing root elasticity were computer programmed in Fortran IV for use on a CDC 6700 digital computer. The program calculations followed the same procedure outlined in the aforementioned section. Specifically, the rigid wing lift distribution was solved first by an iterative method, resulting in reference distributions of C_ℓ, $C_{m_{50}}$, α, C_μ, induced angle, and associated airfoil derivatives. These reference distributions and derivatives were then used in a linear analysis which evaluated L.E. and C.E. as a function of q for a given wing stiffness and jet momentum distribution. Note that this corresponds to decreasing values of dimensionless stiffness ζ and jet momentum coefficient C_μ. Airfoil derivatives evaluated at the reference condition were also used to evaluate CC reversal speed q_R and torsional divergence speed q_D. A flow chart of the program is shown in Figure 27.

The program allows for arbitrary inputs of wing semispan, chord, slot height distribution, root and tip thickness ratio, twist angle distribution, root stiffness, and initial incidence angle. In keeping with the CCW model geometry, the program is currently limited to constant chord and full-span CC airfoils, but modifications to a more general case would not require extensive changes. The N matrix of Equation (11) is internally evaluated by the program from the above input geometry. At least one tabulated set of two-dimensional CC airfoil characteristics is also required. If the program

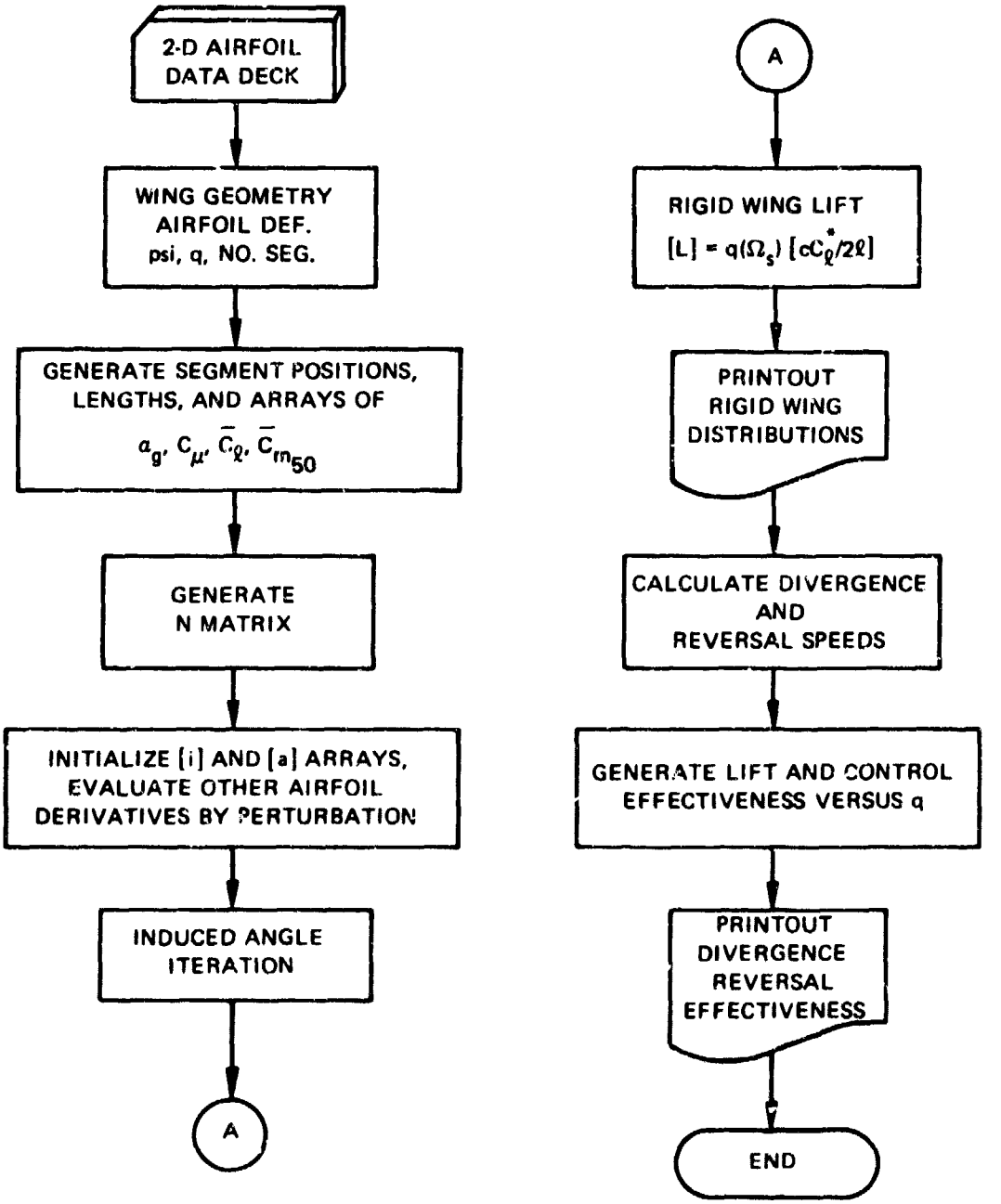

Figure 27 - Flow Chart of CCW Analysis Program

were modified to accommodate partial-span CC airfoils, then an additional table of the appropriate two-dimensional conventional airfoil data would have to be provided also.

Several characteristics of the analysis were noted during use of the program. The first concerned the angle-of-attack stall conditions previously noted. Although this required rearranging the order of solution, it did not solve all the problems of a discrete numerical solution. Any parameter which causes a sudden change in the spanwise lift distribution would physically be expected to cause corresponding local changes in the induced velocity and induced angle distributions. The induced angle change would diminish as distance from the disturbance increased, and the magnitude of the change would depend on the magnitude and distribution of the disturbance. It is a basic advantage of lifting line theory that it can reflect such interactions of one station with another and in quantitative terms.

When this interaction is combined with a discontinuous distribution of even one parameter in a discrete strip analysis, the result becomes dependent on the number of strips into which the wing is divided. This is easily seen if one considers that in a strip analysis a discontinuity can be over no less than the width of one strip. Likewise the effect of the discontinuity on adjacent sections must be over their entire width, and so the minimum impact may be determined by the strip width. Since CC airfoils depend on two independent parameters, α and C_μ, there is ample room for highly nonlinear distributions; these appear as discontinuities in a strip analysis. Each section C_ℓ depends on the local induced angle, and this dependence is not unique for operation in the gradual stall region. The characteristic becomes compounded by the interaction between adjacent wing stations, as provided for by lifting line theory, and results in multistable numerical solutions that lead to erroneous answers or simple nonconvergence.

The missing ingredient in the above analysis which allows multistable conditions is the very one which in nature prevents the problem, namely, viscosity. Viscous effects on the wing prevent sudden changes in adjacent airfoil pressure distributions even if a slot height suddenly changes. The

simplest means of accounting for this in the analysis is to smooth the input slot height distribution and to simultaneously increase the number of strips (decreasing strip width), or to change the distribution of strips. This reduces local variations and also allows a more accurate analysis of their effect. This analysis used 14 wing segments with the following nondimensional end points: 0.0, 0.1, 0.2 0.3, 0.4, 0.5, 0.6, 0.68, 0.75, 0.80, 0.85, 0.90, 0.95, 0.98, 1.00.

Figure 28 shows typical output from the computer program for rigid wing results and for the calculation of q_D, q_R, L.E., and C.E. The top line prints out the more significant input parameters, primarily for identification. The second line contains calculated values of the semispan wing air weight flow in (pounds per second), jet velocity in (feet per second), wing jet momentum coefficient C_{μ_w}, compressor horsepower required, and an equivalent drag term calculated from the compressor power. The next two lines are the net lift and pitching moment of the semispan wing and their respective coefficients. The series of columns then show span distributions of airfoil thickness ratio (T/C), local angle-of-attack (ALPHA) in degrees, induced angle (IND ANG) in degrees, local section C_μ (CMU), local section C_ℓ (CL), wing segment lift (LIFT), and local section $C_{m_{50}}$ (CM50). Divergence and CC reversal predictions are on the next two lines, respectively. The next section of output, headed LIFT AND CONTROL EFFECTIVENESS, shows the variations of these parameters with increasing dynamic pressure.

COMPARATIVE ANALYSIS

Theoretical predictions of the CCW model lift and pitching moment were made by using the basic two-dimensional airfoil data available at DTNSRDC. Airfoil characteristics were corrected in the computation for variations in Reynolds number and slot height-to-chord h/c ratios which differed from that of the basic data.*

*Details of these corrections were reported informally by the author in March 1973 as NSRDC Technical Note AL-290.

C C W I N G A N A L Y S I S

SPAN	CHORD	PSIG	VEL	Q	TIP ALF	RN
3.000	.267	.0	100.0	12.0	-3.0	170000.

WDOT	VJET	CMUW	HPC	EQDRG
.001	10.	.000	.000	.0

RIGID WING LIFT = 5.0 CLWING = .539

RIGID WING MOMENT = .09 CM50WING = .035

STA	T/C	ALPHA	IND ANG	CMU	CL	LIFT	CM50
.15	.248	3.62	1.79	.000	1.195	1.14	.086
.45	.237	3.33	1.19	.000	1.076	1.03	.082
.75	.227	2.79	.85	.000	.929	.89	.070
1.05	.217	2.17	.58	.000	.771	.74	.057
1.35	.207	1.55	.32	.000	.606	.58	.044
1.65	.196	.88	.10	.000	.440	.42	.028
1.92	.187	.28	-.09	.000	.293	.22	.011
2.15	.179	-.17	-.31	.000	.170	.11	-.001
2.33	.173	-.49	-.52	.000	.072	.03	-.010
2.48	.168	-.70	-.75	.000	-.005	-.00	-.016
2.63	.163	-.85	-1.05	.000	-.074	-.04	-.020
2.78	.158	-.87	-1.47	.000	-.127	-.06	-.022
2.90	.154	-.66	-2.03	.000	-.138	-.04	-.017
2.97	.151	-.22	-2.69	.000	-.098	-.02	-.006

DIVERGENCE. C = 16.9 V = 118.8 K/QSCD = 1.32

CC REVERSAL. C = 14.1 V = 108.3 K/QSCR = 1.57

LIFT AND CONTROL EFFECTIVENESS

C	LIFT	L.E.	C.E.	ROOT ANG
12.0	8.23	1.642	.533	3.54
13.0	10.18	1.874	.365	4.81
14.0	13.24	2.263	.081	6.95
15.0	19.17	3.058	-.496	11.32
16.0	37.24	5.569	-2.321	25.14
17.0	-418.21	-58.859	44.501	-329.29

Figure 28 - Typical Program Output

Slot height magnitude affects the h/s correction to airfoil C_ℓ and is the primary term in the pressure-mass flow relationship which determines the C_μ value. Internal duct losses for the model had been measured and found to correspond to an 18-percent loss in the duct gage pressure at the wing tip. This factor was used in the analysis when calculating pressure ratio and jet velocity. Figure 29 indicates good agreement between test data and theoretical values of C_{μ_w} for a range of pressure ratios. This agreement is basic to the prediction of wing $C_L - C_{\mu_w}$ relations.

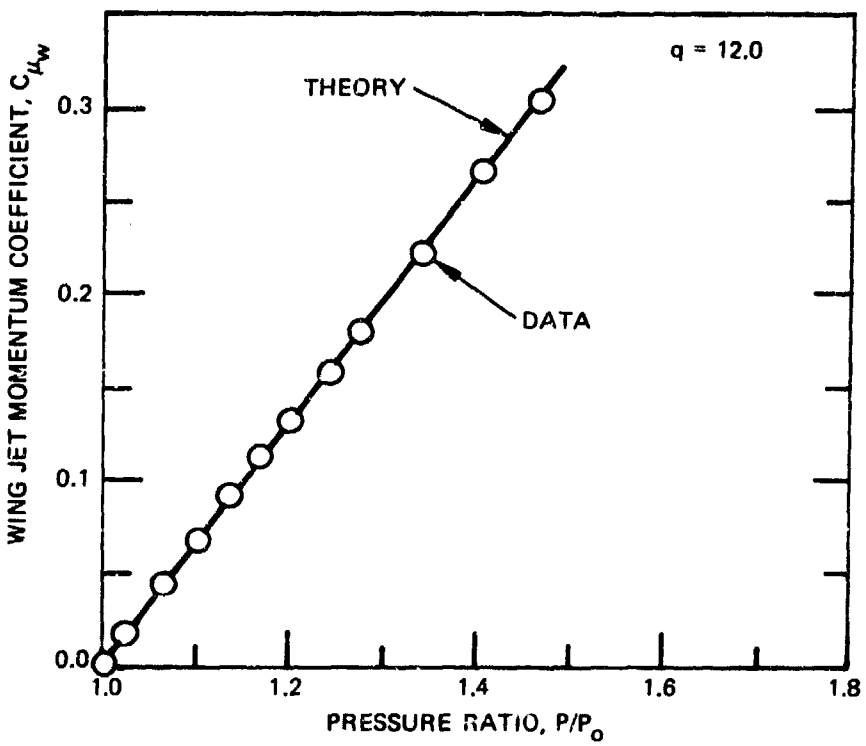

Figure 29 - Comparison of Theoretical and Experimental Values of C_{μ_w} for a Range of Pressure Ratios

The analysis was originally derived and programmed for application to normal full-span wings, but it is applied here to a wing model of one-half span. This difference in geometry is believed to be alleviated somewhat by the sizable hub to which the model wing was attached; see Figure 13. Nevertheless the predicted values of induced velocity at the wing inboard

stations are affected by the inherent assumptions of a full-span wing. Consequently some differences may be expected between the one-half span model data and the theorectical predictions.

Rigid Wing

Figure 30 gives predicted values of wing C_L versus C_{μ_w} for several

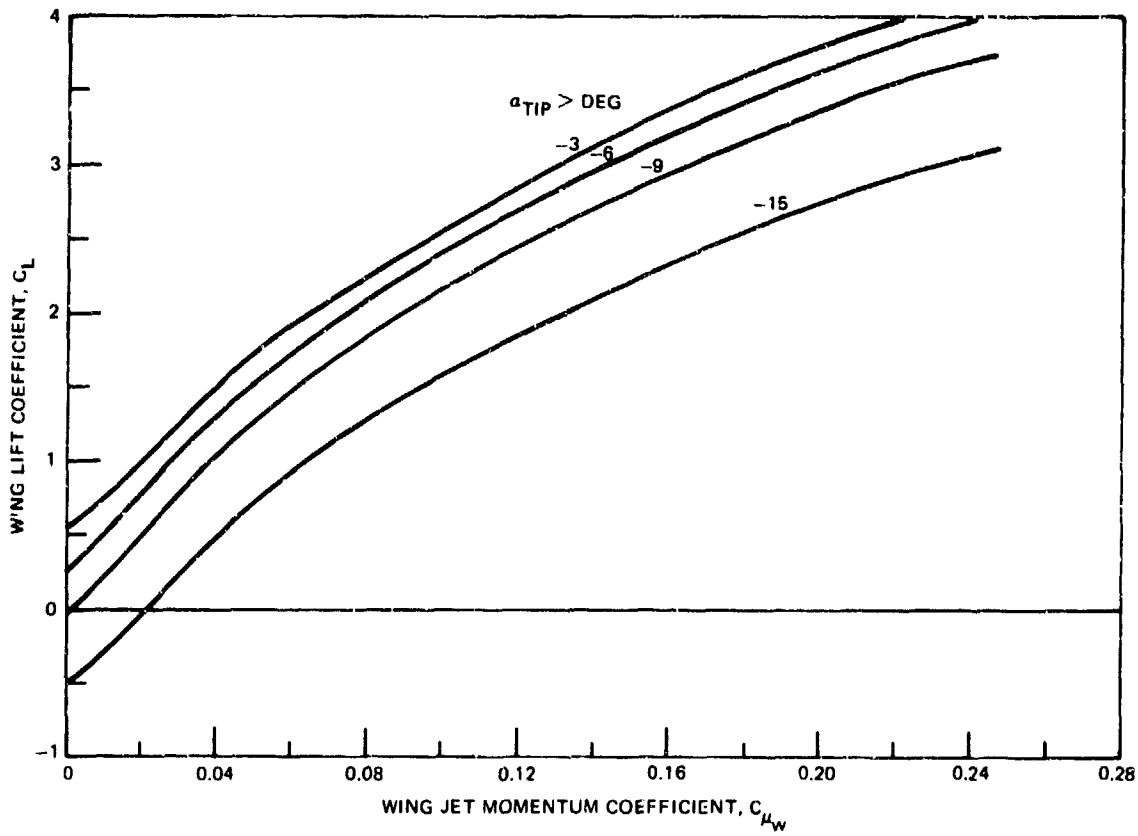

Figure 30 - Predicted Rigid Wing Lift Coefficients for Several Initial α_{TIP} Values

incidence angles. In general the calculated values agreed quite well with those measured in the wind tunnel. There were two notable differences however. First, the model data showed much less initial lift augmentation

than predicted by the program. A comparison of rolling moments for $\alpha = -6$ deg and $C_{\mu_w} \simeq 0.02$ shows that the model wing was still lightly loaded on the outboard sections, with the center of lift at about 12 percent span. Predicted center of lift for the same conditions is more like 35 percent span, representing more outboard loading. This suggests that the outboard regions of the model wing did not attain theoretical values of initial augmentation. Moreover, measured wing lift in this condition was only 4.5 lb and so small differences in section C_ℓ would account for considerable variations in the center of lift.

The second notable difference between model data and predicted C_ℓ concerned behavior at extreme C_{μ_w} values, $C_{\mu_w} > 0.20$. Model data in this region showed that the wing C_L became less sensitive to angle-of-attack setting, but predicted value of C_L at extreme C_{μ_w} retained about the same sensitivity to angle-of-attack. Most of this difference is attributed to the C_μ range of the two-dimensional data. Two-dimensional data are normally limited to the practical range $0 \leq C_\mu \leq 0.24$, which is also the range of data used in current performance prediction programs. Wing lift predictions which require section C_μ greater than this are based on a simple linear extrapolation of two-dimensional data. Accordingly, the general agreement in C_L magnitude is considered very good, and it is not surprising that nonlinear behavior is not predicted in the high C_{μ_w} range.

Typical spanwise distributions of predicted C_ℓ and α are shown in Figure 31. At zero blowing, the program predicts an upwash on the outboard portion of the wing (induced by that portion which develops negative C_ℓ) and a small downwash inboard. These induced angles are algebraically addded to the wing geometric twist angle to give the local effective angle-of-attack distributions shown. At moderate values of C_{μ_w}, a downwash is predicted over most of the wing span corresponding to positive C_ℓ. However, the wing tip station will retain an upwash until extreme magnitudes of C_{μ_w} are reached. Even under these conditions, the tip downwash will be much less than that of the adjacent inboard stations.

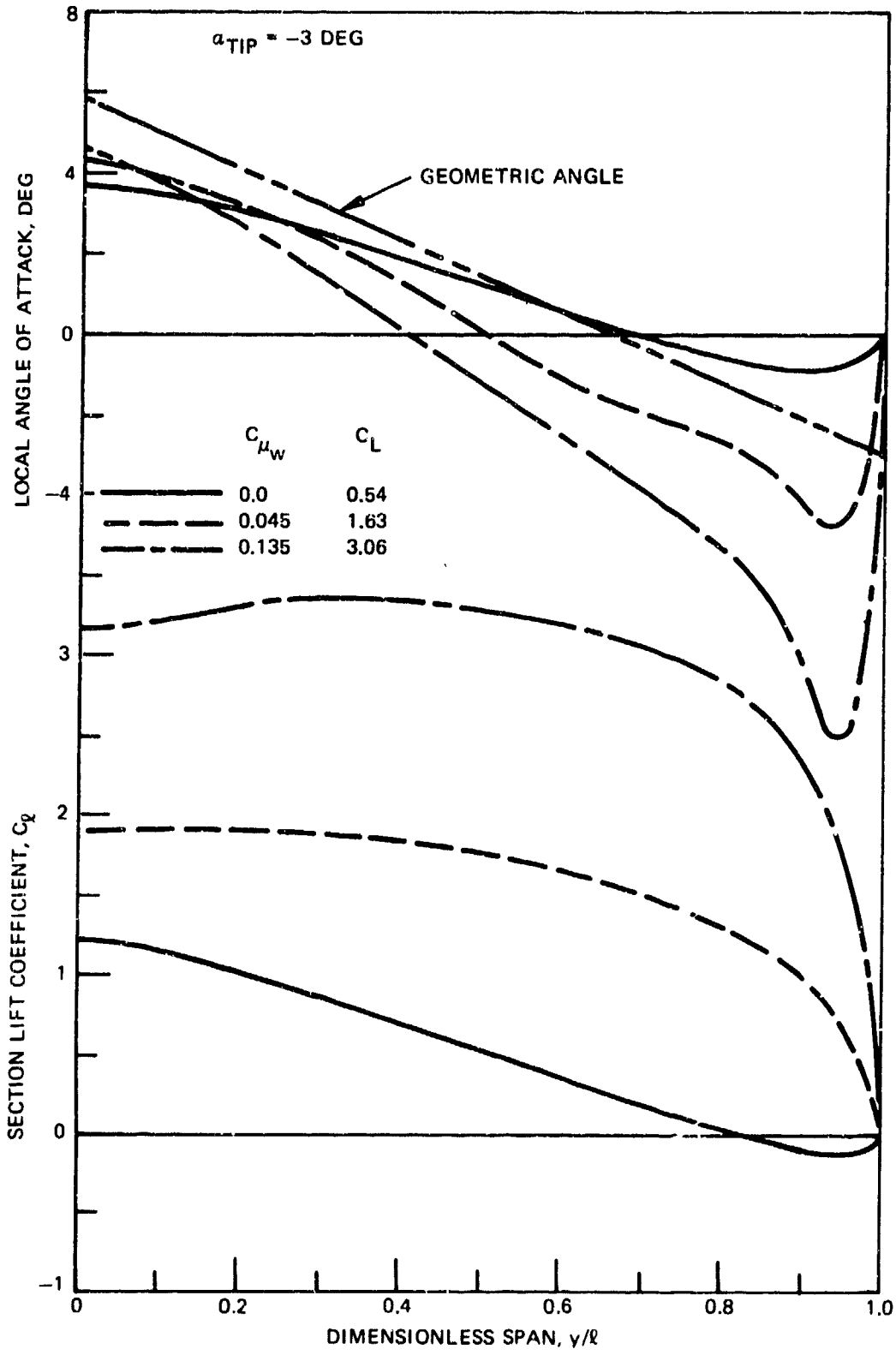

Figure 31 - Predicted Rigid Wing Distributions of Lift Coefficient and Angle of Attack

Predicted values of wing root pitching moment $C_{m_{50}}$ are shown in Figure 32 for a range of C_{μ_w} and α. The predicted trends and magnitudes are in

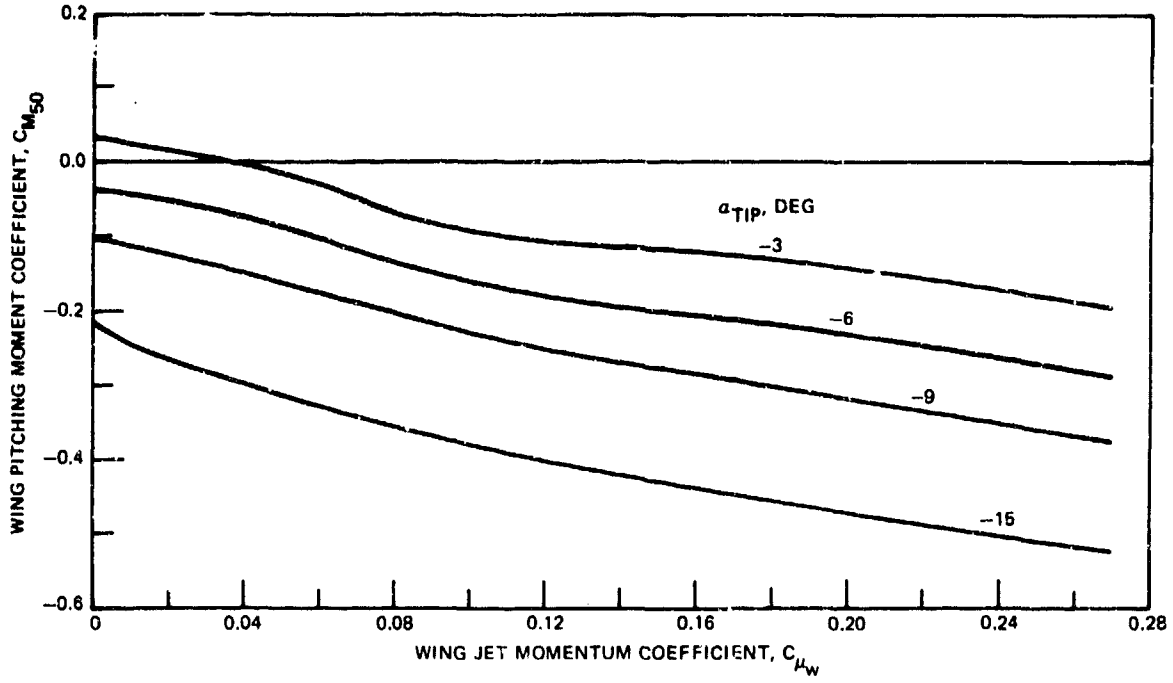

Figure 32 - Predicted Rigid Wing Root Pitching Moment Coefficients

fair agreement with measured data. Model wing data showed generally lower $C_{m_{50}}$ values than those predicted. It is believed, however, that the measured data were low and that the predictions are more representative of those moments developed by the model wing. The elastic wing responses in Figures 20a and 20b support this belief. In those figures, the initial wing response was to pitch up for α_{TIP} of -3 and -4 deg, as indicated by the initial wing increase in lift. This requires a positive pitching moment at $C_{\mu_w} = 0$ for these angles. However, as shown in Figure 19, the pitching

moment measured from rigid wing data was slightly negative for $\alpha_{TIP} = -3$ deg and $C_{\mu_w} = 0$. Linear interpolation across the angles would give even more negative values of pitching moment for $\alpha_{TIP} = -4$ deg. These elastic wing responses suggest that rigid wing pitching moment behaves more like the predicted values of Figure 32 than the measured values of Figures 19.

Overall, the rigid wing is reasonably well represented by theory. This is, of course, a necessary prerequisite to enable predictions of divergence and CC reversal conditions. Calculations of L.E. and C.E. also depend on the basic rigid wing characteristics, as will be shown in the following section.

Elastic Wing with Axis at 0.5 Chord

As shown in Figure 27, elastic wing characteristics are obtained from the converged solution of the rigid wing lift distributions. The elastic wing properties are summarized in the computer output directly after the rigid wing detailed output shown in Figure 28. The predicted elastic wing characteristics will now be shown for selected cases corresponding to previously presented CCW model data. These predicted values were generated with pressure increments of 0.1 psig in order to accurately define the elastic wing C_L, L.E., and C.E. variations with wing C_{μ_w}. This pressure increment corresponds to C_{μ_w} increments of 0.0045, 0.0040, and 0.0036 for the q values of 12.1, 13.7, and 15.1, respectively. Larger increments allow inaccurate fairings which would not represent the intricacy of the analysis.

Increments of C_{μ_w} for the model data were about three times those used for the analysis. This required the L.E. and C.E. parameters to be evaluated from fairings through the data. As such, these parameters evaluated from model data are representative, but they may lack detail in those regions where C_L changes rapidly.

Initial conditions are also different between model data and theory. The model data were obtained by successive increments in pressure. Therefore, as a new value of C_{μ_w} was being set, the model was being perturbed

from its C_L and deflection angle at the old setting. In contrast, the theoretical prediction is based on an initial condition of zero deflection angle for each point (i.e., the analysis is not one of time history and so does not have memory). Figure 20a indicated that the initial condition significantly influences wing behavior, especially at conditions involving larger deflection angles. Thus this difference in intial conditions between theory and experiments can be expected to affect their agreement at any given point, but it does not reflect on the validity of the theory. The difference occurs only when deflection angles are relatively large, and this happens only when the boundaries of CC reversal and torsional divergence are approached. Therefore, the initial condition is significant only to the extent that it affects particular behavior in the proximity of these boundaries. In contrast, the validity of the theory lies in its ability to predict where the boundaries are and to predict the general wing characteristics in the flight regime prior to such boundaries.

Predicted elastic wing lift coefficients are presented in Figure 33 for initial $\alpha_{TIP} = -4$ deg. (Comparative model wing data for this angle was shown in Figure 20b.) At zero blowing, the trend of increasing wing C_L with increasing q is in good agreement with the data. The predicted behavior also shows that the CC reversal condition will occur at zero blowing for q = 15.1 and will reoccur at $C_{\mu_w} \simeq 0.02$. This also agrees well with model data. The intent of the analysis is to predict those operating conditions at which CC reversal will occur and to provide a means of evaluating proximity to those conditions. To this extent, the theory has a good correlation with model data.

Predicted values of lift effectiveness are indicated in Figure 34 for an initial angle of $\alpha_{TIP} = -4$ deg. (Comparative data were shown in Figure 21.) The predicted behavior for q = 12.1 ($\zeta = 1.836$) is very similar to that shown by the data. At zero blowing (minimum C_L), the predicted L.E. was within 3 percent of the data, and for $C_L \simeq 2$, the difference was within 5 percent. The agreement was less satisfactory for intermediate values of

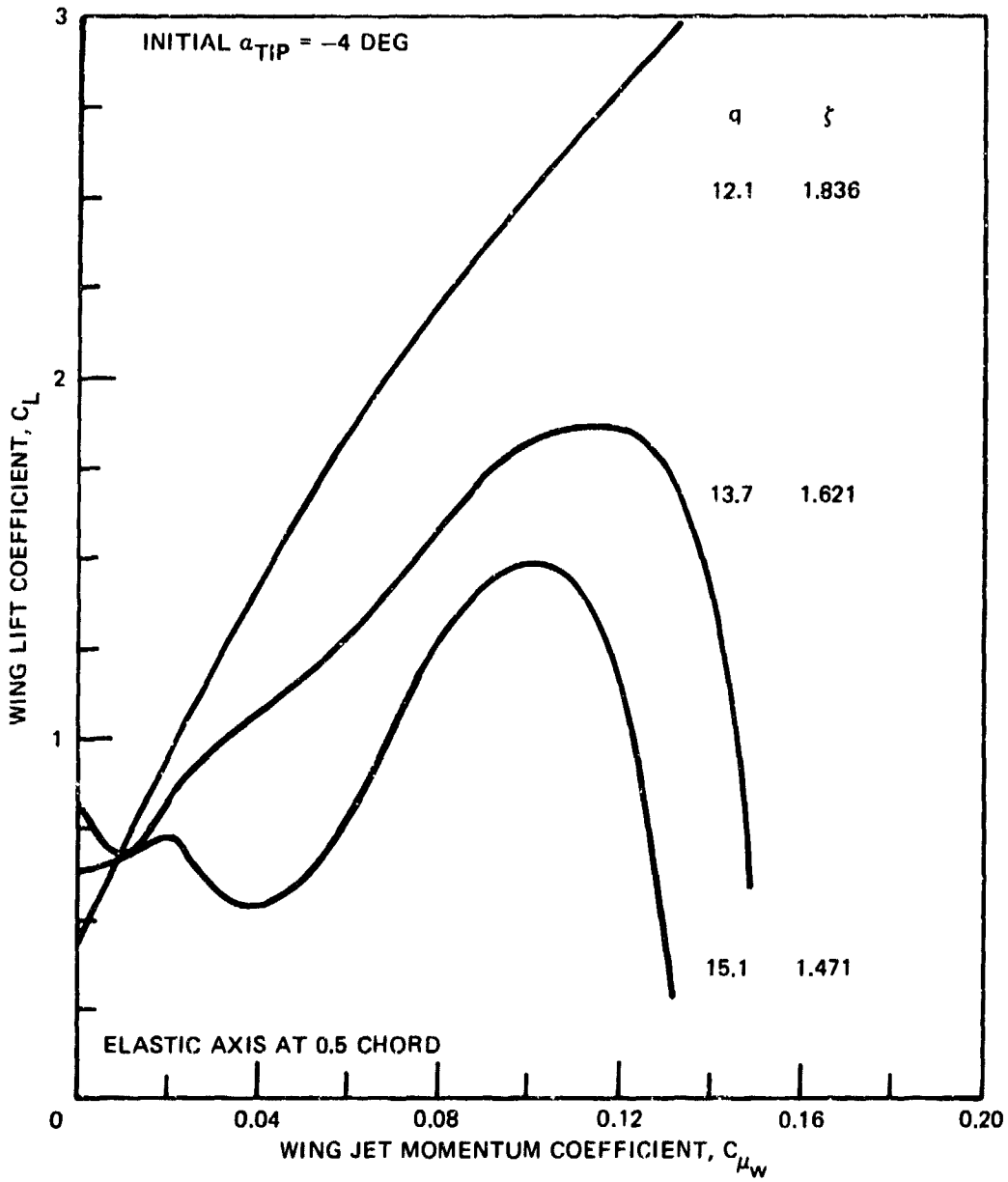

Figure 33 - Predicted Elastic Wing Lift Coefficient at Initial α_{TIP} = -4 Degrees

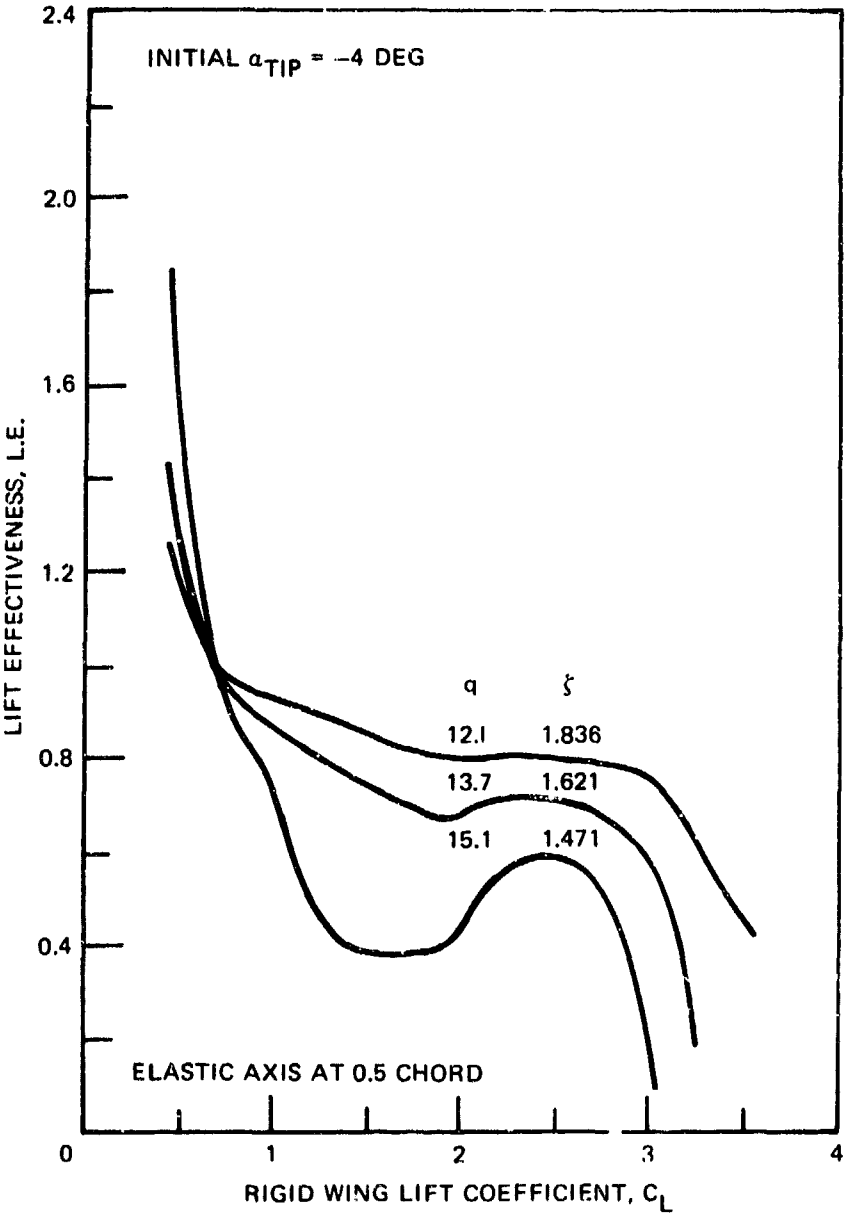

Figure 34 - Predicted Elastic Wing Lift Effectiveness at Initial α_{TIP} = -4 Degrees

C_L. As q is increased, the predicted L.E. also increases for zero blowing conditions. In general the predicted L.E. agreed with the data, showing the strong q effect as CC reversal and torsional divergence boundaries are approached.

Torsional divergence is indicated by the sharp dropoff in predicted L.E. at the higher C_L value in Figure 34. Note that the boundary is predicted to approach rather quickly for q = 13.7 and q = 15.1 as C_{μ_w}, and hence C_L, is increased. In this case the torsional divergence is in the pitch-down direction, as indicated by the reduction of L.E. in this region.

Predicted values of C.E. are given in Figure 35 for an initial angle of α_{TIP} = -4 deg. (Comparative data were shown in Figure 22.) The theory shows a consistent peak in the C.E. for all three q values shown at $C_L \simeq 1.0$. This same characteristic was seen in the model data for each q value, but it occurred at the slightly shifted position of $C_L \simeq 0.70$.

The model data exhibited an unusual behavior of CC reversal at q = 15.1 (see Figure 23). There was an initial condition of CC reversal at C_{μ_w} = 0 (minimum C_L), but a rapid recovery as C_L was increased until it reached the above-mentioned peak in C.E. As C_L was further increased beyond the peak, C.E. dropped as rapidly as it had previously increased, and again plunged deep into the CC reversal condition (C.E. < 0.0) until it reached a minimum C.E. Beyond this point, the curve again changed direction and went back to approach C.E. = 0.0, but was stopped by the model deflection limits. At q = 13.7 and 12.1 the model data exhibited the same general behavior. This very complex behavior reflects a delicate balance between wing aerodynamic moment contributions from angle-of-attack and from jet momentum. The predicted behavior shown in Figure 35 reproduced each of the peaks and valleys demonstrated by the model as it crossed back and forth from CC reversal to nonreversal conditions.

No recovery from the final plunge in C.E. was shown in Figure 35 for q = 13.7 and q = 15.1. This is the same negative torsional divergence shown by the L.E. behavior of Figure 34.

A comparison between model data and theory would be incomplete without mention of the two-dimensional analysis presented earlier. The model wing

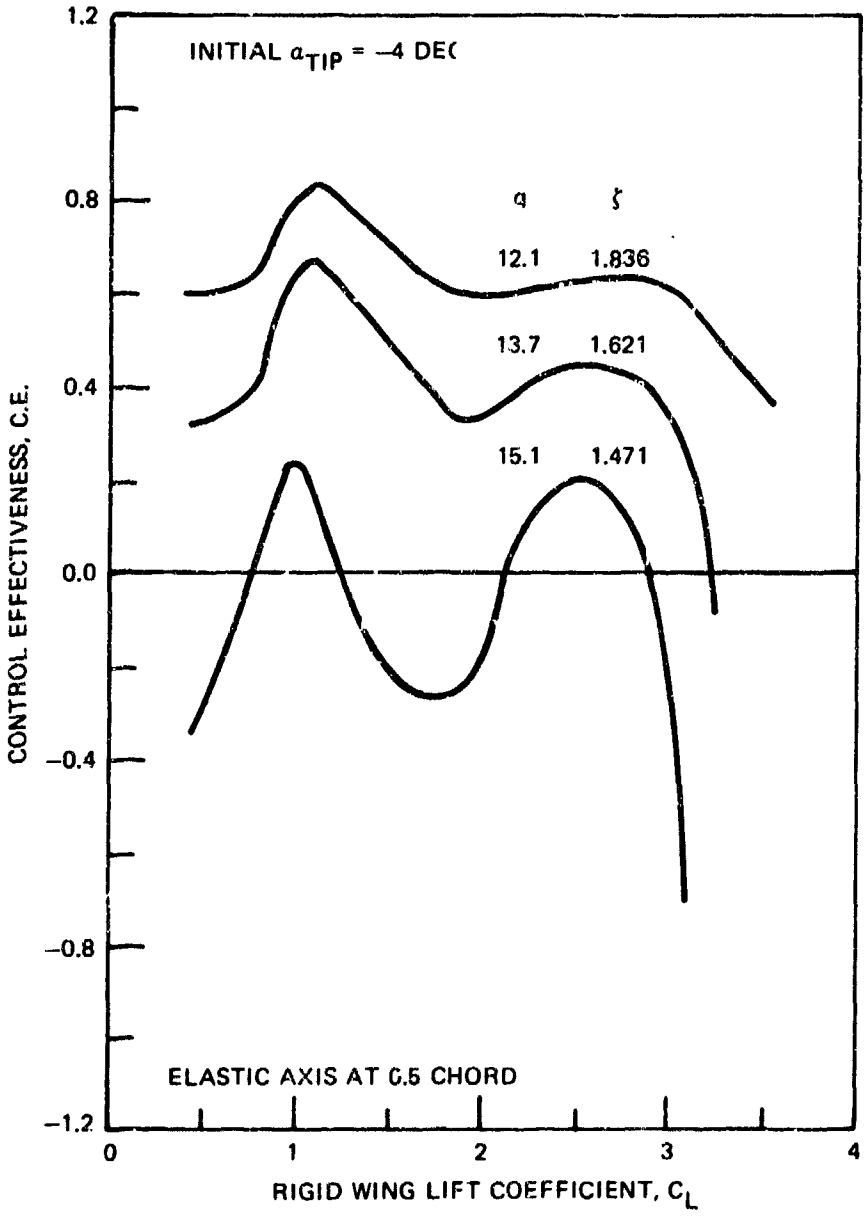

Figure 35 - Predicted Elastic Wing Control Effectiveness at Initial α_{TIP} = -4 Degrees

response is similar to that analysis in that the model allowed only for root torsional elasticity. The CCW data of Figure 20b showed that CC reversal conditions occurred at a C_{μ_w} value of about 0.03 for an initial α_{TIP} of -4 deg. It is interesting to compare the two-dimensional value of ζ_R (dimensionless reversal stiffness) to the experimental values shown. According to Figure 31 the local angle-of-attack at this value of C_{μ_w} and at 90-percent span would be approximately -4 deg. This rough angle-of-attack estimate may be used in Figure 8 to evaluate the ζ_R of the two-dimensional analysis. At α = -4 deg and $C_\mu \simeq 0.03$, the prediction that ζ_R will be about 1.6 agrees quite well with the value of 1.621 (Figure 20b) where the CCW model first experienced CC reversal. According to Figure 11, the operational limit on ζ should be no less than about 4 ζ_R to avoid excessive structural deflections and stay within a 10-percent deviation from rigid wing performance. The use of 4 ζ_R for design purposes gives some latitude so that the two-dimensional estimate of ζ_R may be all that is required to avoid CC reversal conditions.

Elastic Wing with Axis at 0.6 Chord

The elastic wing behavior changes dramatically as the elastic axis is shifted aft of the 50-percent chord. As was shown in Figure 25a for an initial angle of α_{TIP} = -6 deg, the CCW model exhibited pitch-up tendencies for a 60-percent chord elastic axis (ε = -0.10) as C_{μ_w} was increased. Eventually the deflection angle became so great as to cause angle-of-attack stall on the wing, which is shown by the asymtotic C_L characteristic for $C_{\mu_w} > 0.16$. Predicted lift coefficients for the same case are shown in Figure 36. The slightly negative deflection angle predicted at $C_{\mu_w} = 0.0$ results in a lower C_L for the elastic wing than that obtained for the rigid wing; this is in agreement with the data. As C_{μ_w} is increased, the predicted deflection angles become increasingly positive and produce higher elastic wing C_L values. This is also in agreement with model wing data

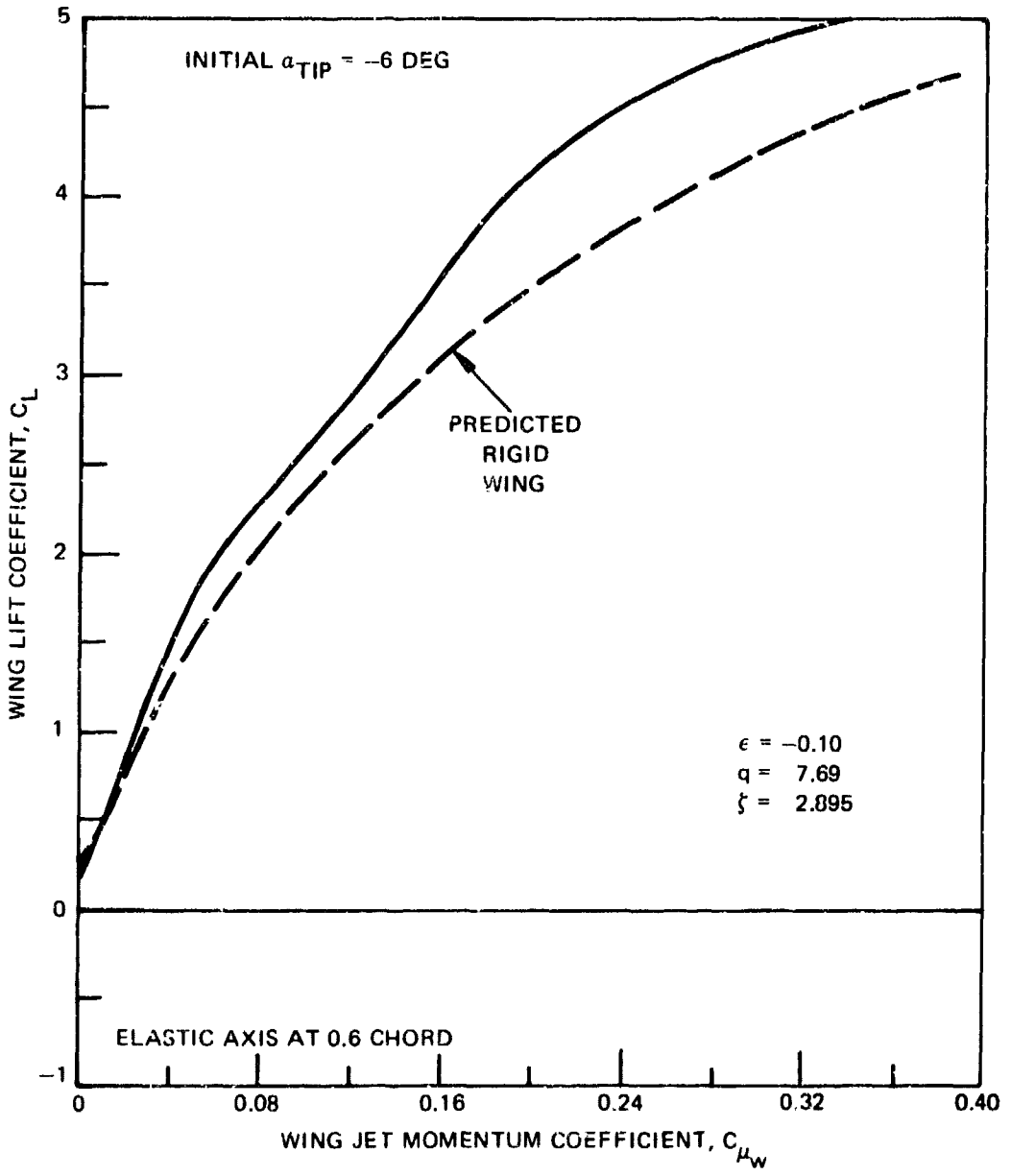

Figure 36 - Predicted Elastic Wing Lift Coefficient for 0.6 Chord EA Location at Initial α_{TIP} = -6 Degrees

until stall occurs. The theoretical analysis of elastic wing behavior is based on linear coefficients from the established rigid wing operating conditions, and it is therefore incapable of predicting a nonlinear stall characteristic created by the elastic deflection. Linearity assumptions are commonly of a conservative nature.

Predicted variations of L.E. and C.E. for the elastic wing are shown in Figure 37 for $\epsilon = -0.10$ and an initial angle of $\alpha_{TIP} = -6$ deg.

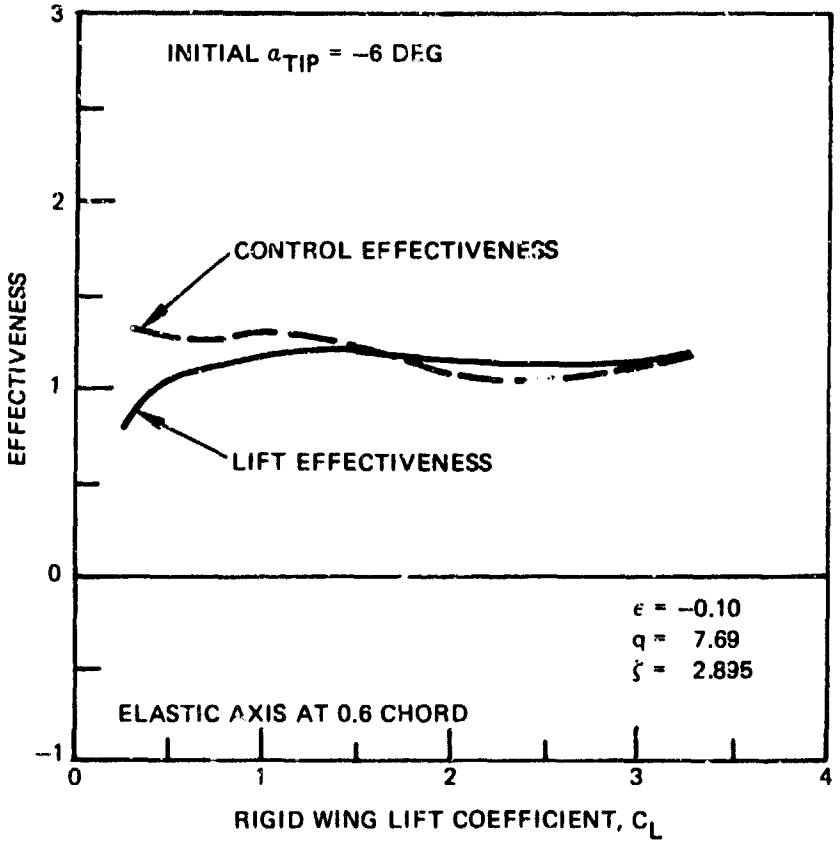

Figure 37 - Predicted Elastic Wing Lift and Control Effectiveness for 0.6 Chord EA Location and Initial $\alpha_{TIP} = -6$ Degrees

(Comparative data were shown in Figure 26 as evaluated from the CCW model data.) The predicted variations have trends similar to those for the model data, but there are also dissimilarities. Because of the aft EA

location, the elastic wing C_L plays a significant role in determining moments about the elastic axis for these cases. This adds a pitch-up moment contribution at low C_{μ_w} conditions in the predicted behavior which did not exist in the CCW model. As a result, the theory predicts more positive deflection angles and correspondingly higher values of elastic wing C_L and L.E. than found for CCW data in the lower C_{μ_w} range.

Figure 37 indicates that predicted C.E. trends drop rather steadily from about 1.3 at zero blowing to about 1.05 at $C_L \approx 2.5$, with a slight rise at $C_L \approx 1.0$. This behavior is very similar to the CCW model data.

Summary

The predicted variations of elastic wing C_L, L.E., and C.E. have been shown for two different EA locations and compared to CCW model data. Figures 33-35 indicated the predicted elastic wing behavior for a 50-percent chord EA location as it varies with dimensionless stiffness ζ. The prediction of strong reductions in wing performance as ζ was decreased agreed well with CCW model data. At the lowest ζ value, the theory predicted repetitive conditions of CC reversal as C_{μ_w} is increased, ending in the prediction of a negative torsional divergence. The repetitive CC reversal was clearly shown in the model data for the same value of ζ, substantiating the theoretical prediction. Figures 36 and 37 showed the predicted elastic wing behavior for a quite different condition where the elastic axis was located at the 60-percent chord. This EA location involves strong pitching moment contributions from the elastic wing C_L and results in predominantly pitch-up tendencies. The predicted variations for this condition are also in general agreement with the model data. The theoretical analysis of both rigid wing and elastic wing behavior has been seen to represent the CCW characteristics over a broad range of conditions. The theory has predicted general trends of L.E. and C.E. as well as particular variations of these parameters with changing jet momentum and changing dimensionless stiffness. Finally, the theory has predicted magnitudes of q and dimensionless stiffness for CC reversal conditions which are in good agreement with the data.

TWO-DIMENSIONAL STALL FLUTTER

The stall flutter characteristics of a wing with CC airfoils may vary considerably from those of wings with conventional airfoils. This difference is attributable to the gradual stall of the typical CC airfoil and to the varying combinations of α and C_μ at which it occurs. A detailed discussion of the phenomenon which creates this stall pattern is beyond the scope of this paper, but it is contributed to by the larger leading edge radius of CC airfoils together with the continued forced circulation due to trailing edge blowing. Figure 2 has presented the angle-of-attack behavior of a typical CC airfoil for constant blowing rates. As shown, the stall angle lowers significantly for increased blowing. This behavior creates a stall flutter condition which involves only the wing bending degree of freedom. The resulting flutter condition occurs basically at the wing first natural frequency in bending. It is not suggested that this type of stall flutter is the only one which may develop. The previous chapters have certainly shown the importance of including torsional moments in any general analysis. Furthermore, the flutter condition may be continued by oscillating values of C_μ in response to oscillating pressures at the blown slot, or by unsteady aerodynamic responses. The coupled bending-torsion wing response is not to be dismissed as a possible mode for stall flutter either. It is observed, however, that stability boundaries are usually lower when they are determined by the lower energy levels of structural response. Specifically, it is suggested that a stall flutter involving only wing bending will be lower, and hence more important, than one involving the higher bending-torsion wing response.

The experimentally observed stall flutter tends to be of limit-cycle nature as the effective angle-of-attack oscillates about that at $C_{\ell_{max}}$. In contrast, on the stalled side of the curve, negative aerodynamic damping extracts energy from the free stream, thus adding energy to the aeroelastic wing system. The limit-cycle behavior is apparently caused by the balance of structural damping and the symmetry of C_ℓ about $C_{\ell_{max}}$ (the gradual stall).

FORMULATION

Consider a section of CC wing acting in two-dimensional flow. The section is torsionally rigid and restrained in heave through a spring mount and damper, as shown in Figure 38. The equation of motion for this system is

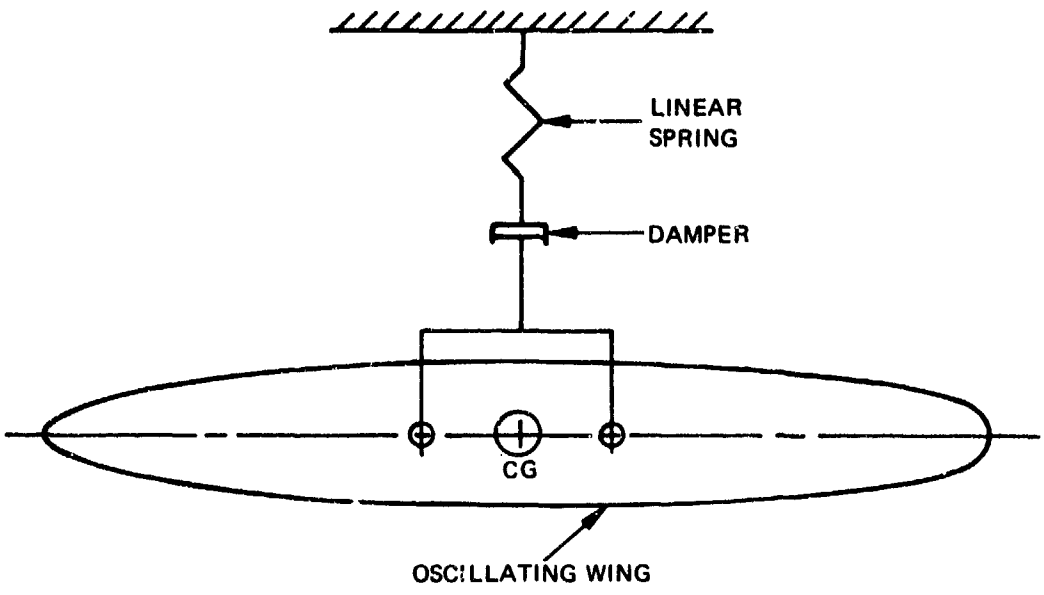

Figure 38 - Wing Representation for Two-Dimensional Stall Flutter

$$\ddot{\delta} + 2\gamma\omega_n\dot{\delta} + \omega_n{}^2\delta = (1/m)\ F(t) \qquad (41)$$

where m = mass per unit length

ω_n = undamped natural frequency

γ = structural damping factor

$F(t)$ = aerodynamic forces = $qc\ C_\ell$

$C_\ell = C_\ell\ (\alpha(t))$

The behavior of C_ℓ at a constant C_μ may be catagorized as linear or non-linear. Linear behavior with angle-of-attack may be represented as

$$C_\ell = C_{\ell_0} + C_{\ell_\alpha} \Delta\alpha$$

where $\Delta\alpha$ is the change in angle-of-attack due to bending oscillations such that $\Delta\alpha = -\dot{\delta}/V_\infty$. Prior to stall, $C_{\ell_\alpha} > 0$; this represents conventional aerodynamic damping and it adds to the structural damping. For some region beyond stall, the lift curve slope remains negative over a significant α range for CC airfoils. This tends to cancel structural damping and may or may not cause divergent oscillations. Stability for this case is simply defined by:

$$2\gamma\omega_n + (1/m)\ q\ c\ C_{\ell_\alpha}/V_\infty > 0 \quad .$$

Nonlinear behavior with angle-of-attack occurs near the stall condition. In order to evaluate the system characteristics in a closed form, it is necessary to approximate the nonlinear $C_\ell - \alpha$ relationship in this region by some continuous function. A parabolic function was chosen for its convenience and the ease with which it is fitted to data. Admittedly, the function will not precisely represent a given data set, but it is sufficient to model the more important overall trends. Appendix A shows that the basic parabolic equation of $X^2 = 2PY$ provides a good representation of two-dimensional data. The resulting expression for the lift coefficient is shown below in terms of the mean effective angle $\bar{\alpha}$, the angle for maximum lift coefficient α_m, and the oscillatory angle - $\dot{\delta}/V$.

$$C_\ell = \frac{1}{2P}\left[(\bar{\alpha} - \alpha_m)^2 - 2\left(\frac{180}{\pi}\right)\frac{\dot{\delta}}{V}(\bar{\alpha} - \alpha_m) + \left(\frac{180}{\pi}\ \frac{\dot{\delta}}{V}\right)^2\right] + C_{\ell_m} \qquad (42)$$

Terms in the above equation which have not been previously defined may be found in Appendix A.

The nonlinear angle-of-attack behavior is of primary interest since it is encountered prior to the oscillatory divergence associated with constant negative C_{ℓ_α}. Equation (42) is seen to consist of constant terms and time-dependent terms. Substitutions into Equation (41) would yield a differential equation that describes a damped oscillatory motion of the wing section. The constant portion of the forcing function contributes only to the steady-state solution and is of no particular interest here. The time-dependent portion of the forcing function is the aerodynamic damping contribution, and it determines the system stability in forced vibrations. It is this portion which determines the existence and sustainment of the stall flutter condition.

Substituting Equation (42) into Equation (41) and rearranging terms give an equivalent damping coefficient of

$$2\gamma\omega_n + \frac{1}{m}\left(\frac{qc}{2P}\right) 2\left(\frac{180}{\pi}\right) (\bar{\alpha} - \alpha_m)\left(\frac{1}{V}\right) - \left(\frac{180}{\pi V}\right)^2 \dot{\delta} \qquad (43)$$

An interpretation of the aerodynamic damping terms may be found by examining their source in Equation (42). The term containing $(\bar{\alpha} - \alpha_m)$ is the mean aerodynamic damping and is linear with $\dot{\delta}$. Its magnitude and sign depends on the value of the mean effective angle $\bar{\alpha}$ relative to the angle for maximum lift α_m. When the mean effective angle is on the back side of the lift curve ($\bar{\alpha} > \alpha_m$), the mean aerodynamic damping contribution is negative, or destabilizing. This term is the predominant of the two in establishing system stability for small oscillations.

The other aerodynamic damping contribution is a function of $\dot{\delta}^2$ in Equation (42), or $\dot{\delta}$ in Equation (43). This term reduces the section C_ℓ for both positive $\dot{\delta}$ and negative $\dot{\delta}$, thus contributing both positive and negative aerodynamic damping respectively. As the wing section plunges down during its oscillations, this term contributes negative damping by reducing C_ℓ. The reduced C_ℓ effectively adds energy to the system, allowing the wing to plunge further down than it would otherwise. This energy is conserved in

the spring as a pontential energy of deflection and is then converted to wing kinetic energy as the cycle progresses and the wing heaves up. However, as the wing heaves upward (positive δ), the same damping term still reduces the C_ℓ, which now contributes a positive aerodynamic damping. The positive damping now extracts from the system that energy which had previously been added during the downward plunge. Thus, the net energy gain per cycle is essentially zero even though the motion tends to be sustained.* It is this process which is believed to be responsible for the limit-cycle behavior observed during stall flutter tests of the CCW model.

The first term discussed above has a greater relative magnitude than the second for small amplitudes of motion. As such, it determines the initial stability of the system. As amplitude increases, the second term becomes predominant and tends to develop the limit-cycle response. For the purpose of establishing stall flutter boundaries then, the $\dot{\delta}^2$ term will be dropped and only the first term will be retained. This gives the following equation as the stability criterion for the modified equivalent damping:

$$2\gamma\omega_n + \frac{1}{m}\ \frac{qc}{2P}\ \frac{2}{V}\ \frac{180}{\pi}\ (\bar{\alpha} - \alpha_m) > 0 \qquad (44)$$

This may be solved as an expression for the limit on the mean effective angle-of-attack to avoid stall flutter:

$$(\bar{\alpha} - \alpha_m) \leq -\frac{\pi}{90}\ \frac{\gamma\omega_n (2P)\ m}{\rho\ Vc}$$

where $(\bar{\alpha} - \alpha_m)$ is in degrees. Since the quantity (2P) is always negative and the other terms on the right-hand side are all positive, the equation states that in order for stall flutter to occur, the mean effective angle $\bar{\alpha}$

---

*This explanation does not violate the First Law of Thermodynamics since the energy source is provided by the free-stream velocity.

must be greater than the value of α_m. This is especially interesting since oscillatory motion could carry the maximum angle even further into stall, or further beyond α_m.

An alternate solution of Equation (44) gives the boundary on free-stream velocity for the avoidance of stall flutter:

$$V_{SF} = -\frac{\pi}{90} \frac{\gamma \omega_n (2P) m}{\rho c (\bar{\alpha} - \alpha_m)} \tag{45}$$

The stall flutter velocity V_{SF} is seen to decrease as the reciprocal of the quantity $(\bar{\alpha} - \alpha_m)$. As $\bar{\alpha}$ becomes much greater than α_m, the section moves further into stall and provides more negative aerodynamic damping, decreasing the stall flutter boundary. In general the level of free-stream velocity for stall flutter must be great enough to amplify the negative aerodynamic damping to the extent that it equals or exceeds the structural damping of $\delta\omega_n$. As structural damping $\delta\omega_n$ is increased, the stall flutter boundary also increases.

The values of α_m and (2P) in Equation (45) are quite dependent on the magnitude of C_μ. Therefore the calculation of V_{SF}, which is for constant C_μ, does not correspond to constant jet momentum conditions. This is not restrictive, but it could lead to misinterpretation of the results. For example, if C_μ is initially evaluated for a reference jet momentum $\dot{m}V_j)_o$ and dynamic pressure q_o, then the jet momentum at the stall flutter velocity $\dot{m}V_j)_{SF}$ would have to be

$$\dot{m}V_j)_{SF} = \frac{q_{SF}}{q_o} \dot{m}V_j)_o$$

for the same C_μ. The use of Equation (45) will be shown later in comparing theoretical stall flutter boundaries to the CCW model data.

The unusual point of this stall flutter is the manner in which it is approached with CC airfoils. The angle-of-attack at C_{ℓ_m} may decrease by as much as 10 deg as jet momentum is increased. So although the system may be stable at low blowing rates (low C_μ and high α_m), it may pass into stall flutter and even divergent oscillations at high blowing rates (high C_μ and lower α_m) while at the same $\bar{\alpha}$ and flight speed. Even more interesting is the lift behavior in this transition. Generally the C_ℓ - C_μ relationship shows continued positive augmentation beyond the α stall. Thus greater magnitudes of lift may be developed by increasing C_μ while going deeper into stall flutter conditions, even neglecting the effects of dynamic stall overshoot commonly developed by conventional airfoils. This is apparent from Equation (42) which shows that the time average C_ℓ, and hence lift, is primarily dependent on the steady-state conditions of C_μ and $\bar{\alpha}$ and that $\dot{\delta}$ terms contribute only to the high frequency oscillatory forces of flutter.

This predictable and gradual behavior may prove to be very important and useful in application. It has several implications. First, stall flutter for a CC airfoil does not mean an attendant sudden loss of lift. Second, increased blowing alone at flutter conditions will worsen the condition by driving the α_m to still lower values. Third, recovery is obtainable by a sharp decrease in angle-of-attack along with increased blowing rates. Fourth and finally, this recovery process may actually increase lift, resulting in no loss of altitude.

MODEL WING DATA AND COMPARATIVE ANALYSIS

The experimentally observed stall flutter appeared as a simple harmonic motion involving only the wing bending mode. At an incidence angle of α_{TIP} = 0 deg and above, the flutter began to occur only as C_{μ_w} was increased beyond a value of about 0.20. The frequency and character of motion was examined by a strobe light aimed at the wing tip. This showed that the frequency of oscillation was that of the first cantilevered natural bending frequency of the wing. Strobing the tip at multiples of this frequency

produced a multiple exposure during oscillation and showed that no torsional deflection occurred. The wing chordwise position of center of gravity and elastic axis are nearly coincident on the model so that such uncoupled motion is possible. The amplitude of oscillation was observed to be about 0.5 to 1 in. peak to peak, which increased as C_{μ_w} was increased. For a 1-in. oscillation to occur at the wing first bending frequency (19.3 Hz), the wing tip must have experienced an oscillating angle-of-attack of ± 2.9 deg.

The previous formulation for the two-dimensional case cannot be applied directly to data for the three-dimensional model wing. Distributed elasticity is one of the primary differences since it produces a distributed deflection for the wing. It is the corresponding distribution of aerodynamic response which then creates the driving bending moments to cause the wing stall flutter condition. However, an equivalence may be drawn between the two systems such that the terms of Equation (41) for the two-dimensional case are scaled to represent the characteristics of the three-dimensional wing. Appendix B shows the details of this equivalence and the numerical values corresponding to the CCW model. The numerical values are valid only for the case of $\alpha_{TIP} = 0$ deg, corresponding to the incidence angle at which stall flutter was observed on the CCW model. The scaling is sensitive to wing incidence since it depends on establishing a position for the wing center of oscillating lift.

The theoretical stall flutter velocity for the CCW model is evaluated by substituting the numerical values of Appendix B into Equation (45) for the two-dimensional wing. This equation is shown below in terms of the aerodynamic operating conditions.

$$V_{SF} = -1.4124 \frac{2P}{(\bar{\alpha} - \alpha_m)}$$

Since the above equation is intended to represent the CCW model, the aerodynamic terms (2P), $\bar{\alpha}$, and α_m must be evaluated at the appropriate model

wing operating conditions. More specifically, these terms must be evaluated from two-dimensional airfoil data by using local values of C_μ and effective angle-of-attack at the representative wing location. They can then be related to the corresponding wing values of C_{μ_w} and α_{TIP} for comparison to the model data.

Appendix B gives the center of oscillating lift for the model wing as 2.467 ft (0.752 m) from the wing root, or at 82.3 percent span. Theoretical values of the wing local C_μ and α for this station were obtained from the rigid wing predictions at an incidence angle of α_{TIP} = 0 deg. The wing root is stalled for this incidence, even at zero jet momentum. As jet momentum is increased, the stall region extends further outboard, approaching the wing tip. Figure 39 presents these values of C_μ and α at the center of

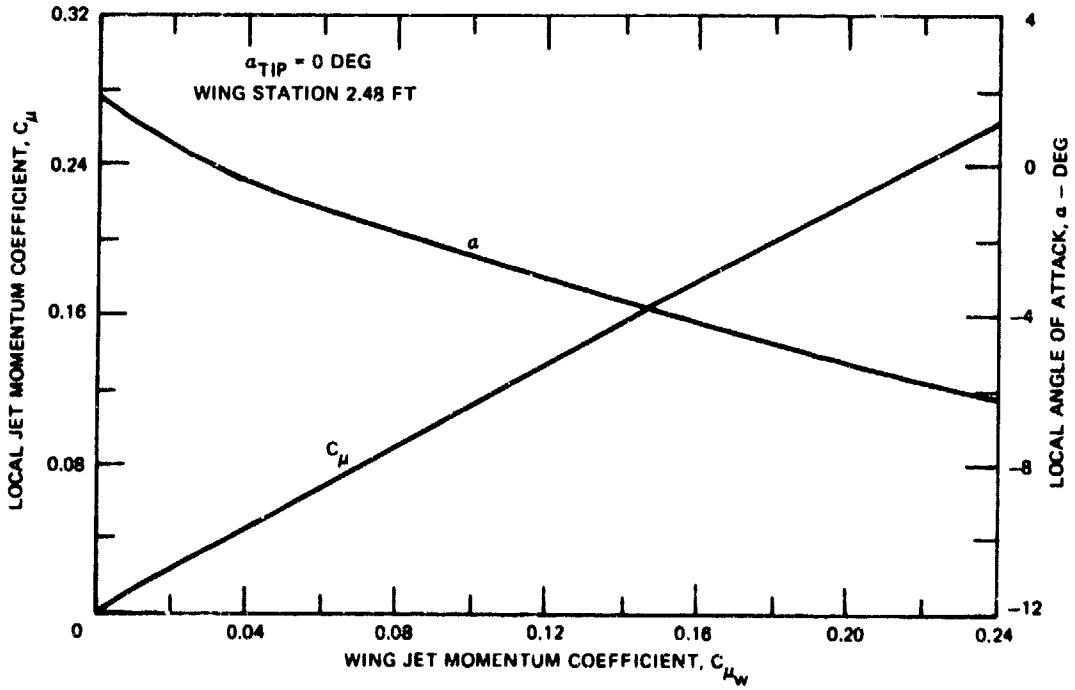

Figure 39 - Theoretical Variation of Local Jet Momentum Coefficient and Angle of Attack

oscillating lift as they vary with the wing C_{μ_w}. Although these values are at the 82.3 percent span, they may be compared to the two-dimensional data which are available for the wing tip airfoil. Figure 40 shows this cross-plot and allows an evaluation of the operational proximity to the stall condition. As previously discussed, the mean operational angle $\bar{\alpha}$ must be greater than the stall angle α_m for stall flutter to occur. This condition is initially satisified at $C_\mu = 0.12$ in Figure 40, suggesting the possibility of stall flutter for $C_\mu \geq 0.12$.

The stall flutter velocity V_{SF} may be evaluated from Equation (46) and the information in Figure 40. The value of the term 2P is a measure of the stall rate (i.e., sharp or gradual). This term was evaluated from the stall region of the two-dimensional data for C_μ values of 0.12, 0.16, and 0.20. A single value gave good agreement with all three C_μ curves. Figure 41 indicates the resulting sensitivity of V_{SF} to the angular difference $(\bar{\alpha} - \alpha_m)$. Plotted this way, the stall flutter boundary is examined independently of any particular value of $\bar{\alpha}$ or α_m. The boundary is seen to drop rapidly as $\bar{\alpha}$ exceeds α_m by just 1 deg. This behavior should be expected with the very low damping factor for the CCW model. Operational conditions for C_μ values of 0.12, 0.16, and 0.20 are superimposed on Figure 41 to give the specific V_{SF} value for each condition. The values of V_{SF} may be related back to the corresponding wing C_{μ_w} values by the curve of Figure 39.

The theoretical stall flutter boundary for the CCW model is shown more meaningfully in Figure 42 as it varies with the wing parameter C_{μ_w}. Experimentally observed stall flutter conditions from the CCW model data are also shown for comparison. In general the agreement is quite good between theory and experiment. To put this in perspective, two important points should be noted. First, the theoretical boundary is based on a single-degree-of-freedom model, using two-dimensional airfoil characteristics and mass scaling, to represent the wing flutter. By contrast, the wing flutter condition actually depends on the span distribution of structural elasticity, aerodynamic properties, induced angles, and wing mode shape. More specifically, the local

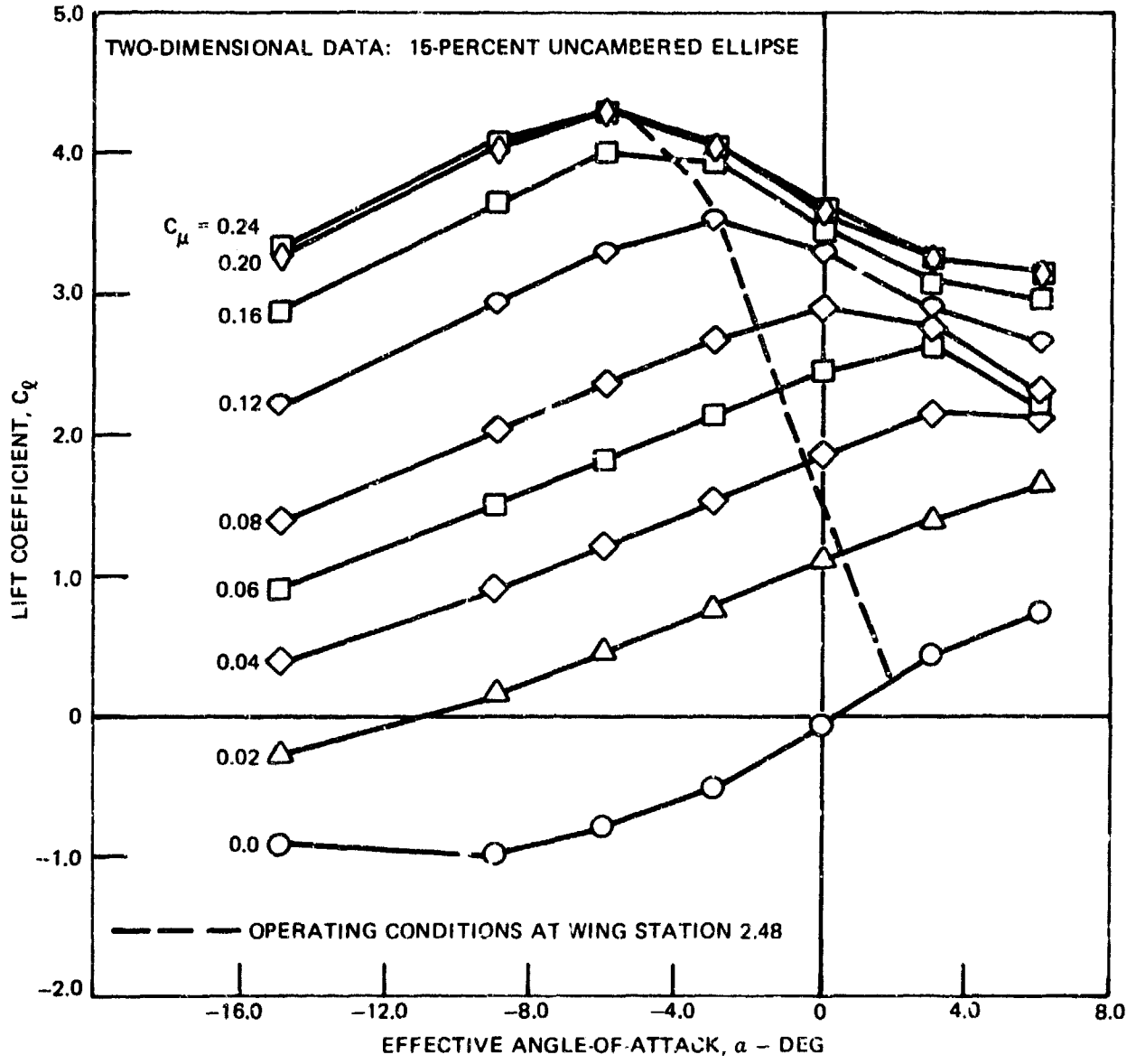

Figure 40 - Theoretical Wing Operating Conditions

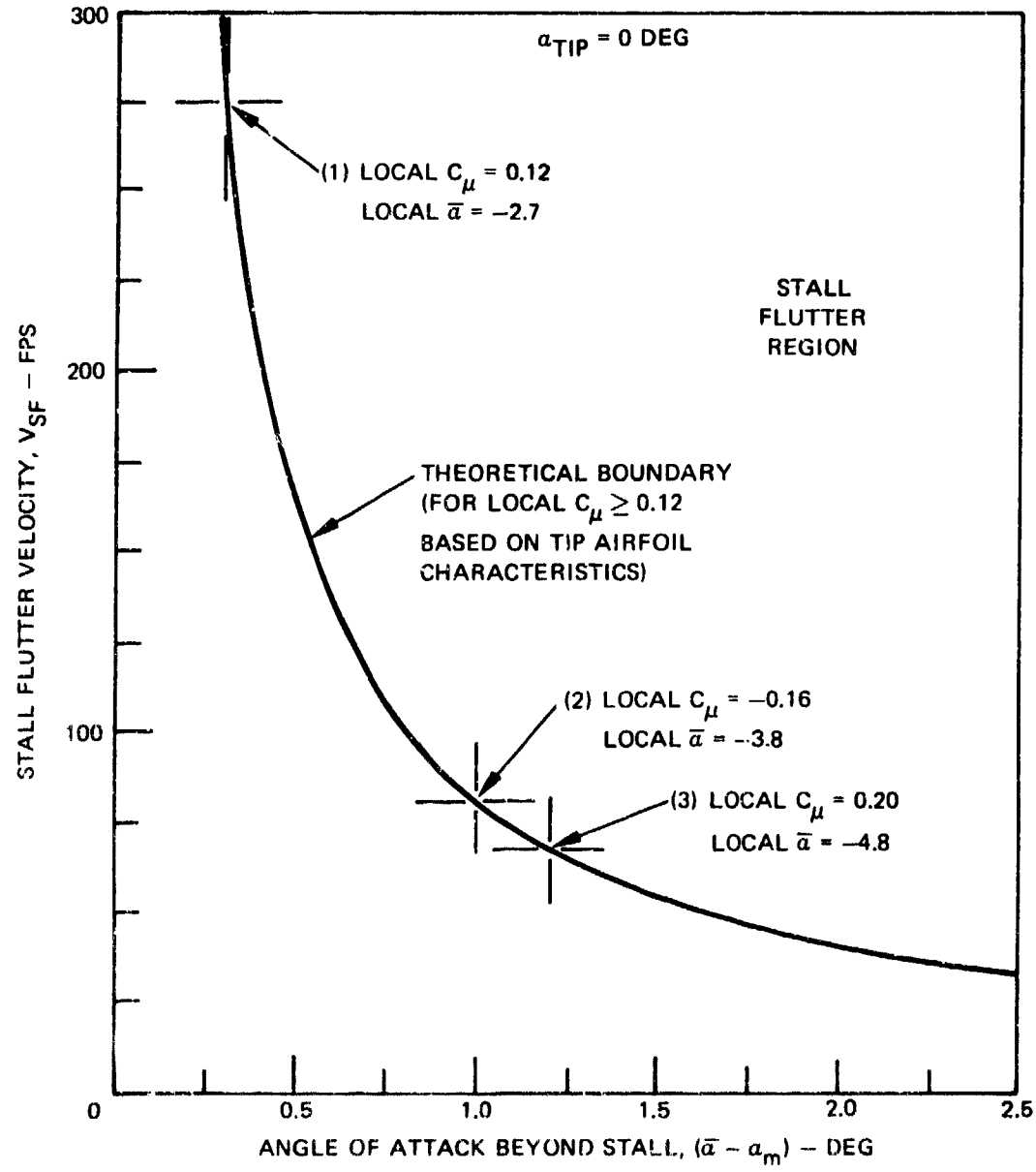

Figure 41 - Variation of Stall Flutter Boundary with Angle of Attack

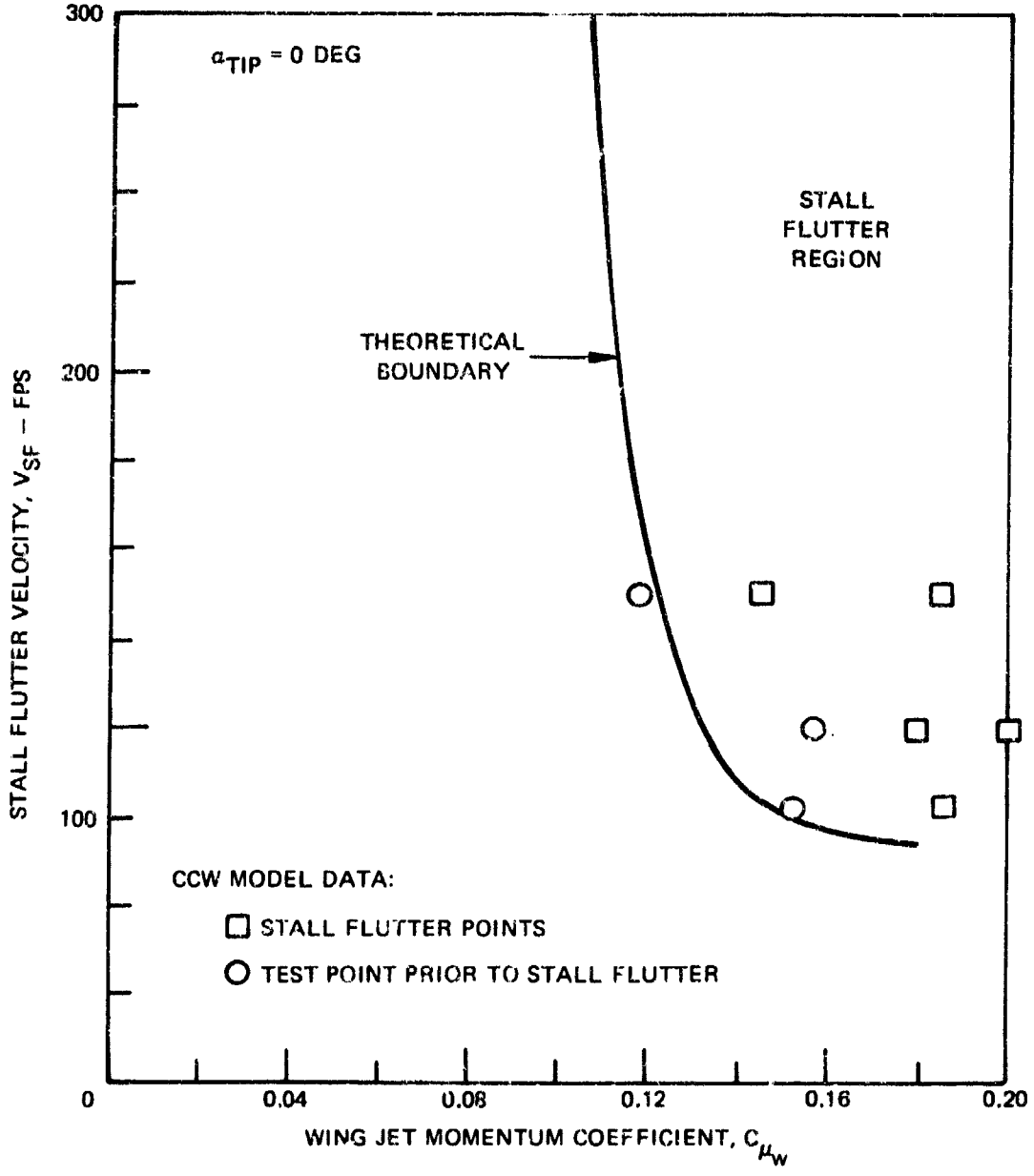

Figure 42 - Comparison of Theoretical Stall Flutter Boundary with CCW Model Data

angle-of-attack changes drastically with the wing span, and it is the spanwise integration of this quantity which creates the negative aerodynamic damping to produce flutter conditions. The simple theory, however, uses representative terms at only a single point along the wing span to predict the stall flutter boundary. The second point to be noted concerns the experimentally observed stall flutter conditions. The model wing was not equipped with an "exciter" of any kind, and so the stall flutter condition was solely dependent on wind tunnel turbulence to initialize the motion. This is certainly sufficient for unstable conditions, but it does not allow an accurate measurement of the neutrally stable flutter boundary. The experimentally observed stall flutter conditions shown in Figure 42 were in a state of steady oscillatory motion and their amplitudes were most certainly beyond the neutrally stable stall flutter boundary. Accordingly, the experimental boundary must lie to the left of the data points marked as being in stall flutter, or at lower C_{μ_w} for a given velocity. This suggests even better agreement between theory and experimental data than shown in Figure 42.

To summarize, the necessary condition for stall flutter is that the effective angle-of-attack must be greater than the stall angle at the appropriate C_μ. If this condition is satisfied, then the stall flutter velocity depends on the relative magnitudes of structural and aerodynamic damping, as given in Equation (45). An equivalence may be established between the three-dimensional wing stall flutter and the single-degree-of-freedom two-dimensional stall flutter boundaries. This equivalence is based on a linear approximation of the wing mode shape, and use of a representative wing station at the center of oscillating lift suggests that only a portion of the wing need be operating in stall conditions for stall flutter to occur. Theoretical calculations of a stall flutter boundary for the CCW model obtained by using the above equivalence are in good agreement with the observed stall flutter condition from CCW model data.

CONCLUSIONS

The static aeroelastic characteristics of a wing with CC airfoils has been examined both by a two-dimensional approach and by a three-dimensional wing approach that utilizes a modification of lifting line theory. The theory has shown good correlation with experimental data from a CCW model, verifying the ability to predict rigid wing performance and the boundaries of torsional divergence and CC reversal. The parameters of lift effectiveness and control effectiveness provide a quantitative assessment of the elastic wing behavior at dynamic pressures below the boundaries, and may serve to establish acceptable limits of operation.

The simple two-dimensional analysis has shown that divergence stiffness ζ is strongly affected by EA placement. More forward EA locations, approaching the quarter-chord, are preferable to improve the boundary of torsional divergence. However this results in larger pitching moment magnitudes about the EA for the rigid wing. The reversal stiffness ζ_R was shown to depend primarily on the airfoil lift and moment coefficient derivatives with respect to C_μ and α. A value of $4\zeta_R$ is suggested as a minimum design stiffness, corresponding to about ± 10-percent deviation from the rigid wing behavior. This stiffness level should provide satisfactory avoidance of torsional divergence as well.

The three-dimensional wing analysis was derived for the general case of distributed elasticity and then modified to allow only wing root elasticity for comparison to the CCW model data. This comparison demonstrated the ability of the theory to predict specific variations of L.E. and C.E. for the elastic wing as a function of C_{μ_w} and incidence angle. The correlation maintained agreement even as CC reversal conditions were encountered.

The wing root elasticity analysis may also be applied to certain trim and stability problems of the aircraft as a whole. The advantage of this application is that specific lift and moment variations can be included along with angle-of-attack in the trim attitude solution. Wing lift may be obtained from many combinations of α and C_{μ_w}; each has different net pitching

moments and so the trim attitude for a specified lift is not unique. It is to be expected that the relative stability will also change with the α C_{μ_w} combination at trim.

Stall flutter conditions encountered with the CCW model may be predicted by a two-dimensional analysis when proper scaling and aerodynamic equivalence are used. This stall flutter condition involves only the wing bending mode and falls in a class of relatively few single-degree-of-freedom flutter problems. The stall flutter condition may occur at a number of α and C_μ combinations since each C_μ level has a different associated stall angle. Wing lift tends to be maintained at stall flutter due to the gradual stall characteristic of CC airfoils. Once stall flutter has occurred, an increase in C_{μ_w} will aggravate the condition by effectively lowering the stall angle. Recovery is obtained by a sharp decrease in angle-of-attack along with an increase in C_{μ_w}. Properly executed, this process should eliminate the condition with no loss in lift or altitude.

It is recommended that further analysis be performed to evaluate the classical flutter problem for CC airfoils. Since the trailing edge stagnation point is variable on this type of airfoil, conventional unsteady aerodynamics do not apply. This requires that wind tunnel data be obtained for CC airfoils during both oscillating α and oscillating C_μ conditions to establish dynamic characteristics for lift and pitching moment.

APPENDIX A

REPRESENTATION OF THE LIFT COEFFICIENT NEAR STALL

The general behavior of CC airfoils near the angle of attack stall condition is gradual and almost symmetric. Therefore, a simple parabolic fit is sufficient to describe first order behavior. The curve shown in Figure A.1 at a constant blowing rate may be represented about the stall condition

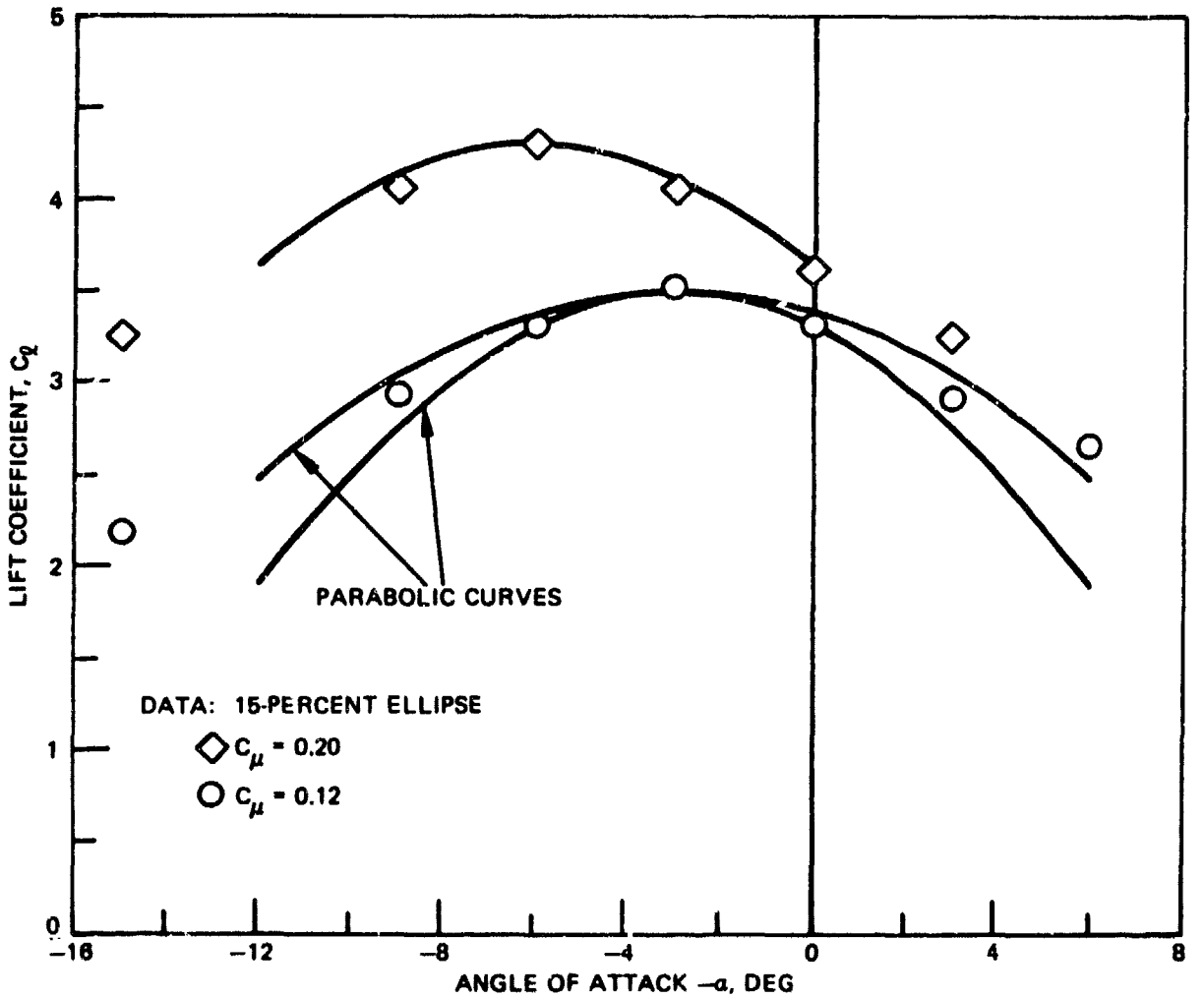

Figure A.1 - Parabolic Representation of Lift Coefficient in the Stall Region

by the following parablolic equation:

$$(\alpha-\alpha_m)^2 = 2P\ (C_\ell - C_{\ell_m}) \tag{A.1}$$

where $2P = (\alpha_1-\alpha_m)^2/(C_{\ell_1} - C_{\ell_m})$. The point (C_{ℓ_m}, α_m) is taken at the maximum C_ℓ condition and the point (C_{ℓ_1}, α_1) is chosen to yield the most reasonable curve fit. Solving the above for C_ℓ yields the more convenient form

$$C_\ell = \frac{1}{2P}\ (\alpha - \alpha_m)^2 + C_{\ell_m} \tag{A.2}$$

Figure A.1 shows that this gives a good approximation of the C_ℓ variation over about a 12-deg range of angle of attack. Two parabolic curves are shown for $C_\mu = 0.12$ to indicate the quality of curve fit which may be obtained. The quality may be improved over a narrow angle-of-attack range ($|\alpha-\alpha_m| \leq 3$ deg) by sacrificing the agreement over the broad angle-of-attack range.

In representing the oscillating airfoil, the angle of attack is separated into a mean value $\bar{\alpha}$ and a time-varying term due to heave. For small angles this may be described as

$$\alpha = \bar{\alpha} - \left(\frac{180}{\pi}\right) \dot{\delta}/V \tag{A.3}$$

where the angles are expressed in degrees. Substituting Equation (A.3) into Equation (A.2) and expanding gives the following equation for the lift coefficient in terms of the mean angle and the heave velocity:

$$C_\ell = \frac{1}{2P}\ \left[(\bar{\alpha} - \alpha_m)^2 - 2(\bar{\alpha} - \alpha_m)\ \left(\frac{180}{\pi}\right)\left(\frac{\dot{\delta}}{V}\right) + \left(\frac{180\ \dot{\delta}}{\delta V}\right)^2\right] + C_{\ell_m} \tag{A.4}$$

The quantity $(\bar{\alpha} - \alpha_m)$ signifies the relative proximity of the mean angle of attack $\bar{\alpha}$ to the angle of attack for maximum lift coefficient C_{ℓ_m}. The sign of this quantity is seen to determine the sign of the first order aerodynamic damping term.

APPENDIX B

EQUIVALENCE BETWEEN THE TWO-DIMENSIONAL STALL FLUTTER EQUATION AND A THREE-DIMENSIONAL WING

The distributed structural properties of a three-dimensional wing yield a frequency and mode shape for the first natural bending mode. This frequency for the CCW model was measured as 19.3 Hz, or 121 radians/second. The calculated mode shape for the CCW model is shown in Figure B.1. In general

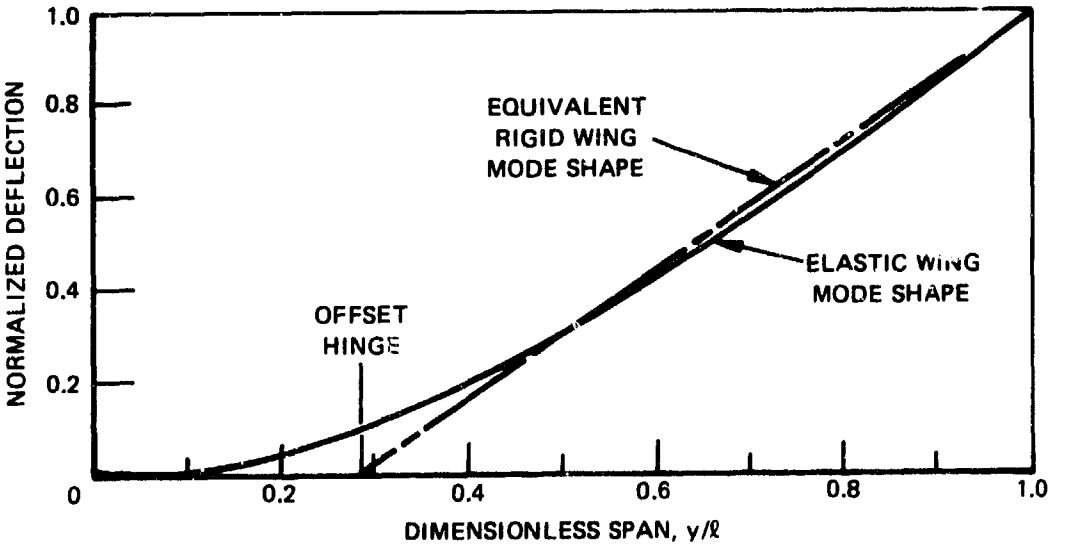

Figure B.1 - Bending Mode Shape and Equivalent Representation of CCW Model

the wing mode shape and frequency may be adequately represented by the rigid body response of an outboard portion of the wing acting about an offset hinge with spring restraint. This equivalent system is also shown in Figure B.1 for the CCW model. The hinge position was chosen to represent the wing mode shape. The equation of motion of this single degree-of-freedom system is

$$\ddot{\theta} + 2\gamma\omega_n\dot{\theta} + \omega_n^2\,\theta = \frac{1}{I_h} M_h(t) \qquad \text{(B.1)}$$

Here I_h is the wing moment of inertia about the hinge, $M_h(t)$ is the time-dependent aerodynamic bending moment about the hinge, and ω_n is the natural frequency (which is set equal to that of the actual wing). The above equation has only a single degree of freedom and its form is similar to the equation which describes two-dimensional stall flutter.

The deflection angle variable θ of Equation (B.1) may be replaced by the linear displacement δ at a distance $\bar{r}$ from the hinge. The substitution of $\delta = \bar{r}\theta$ and its derivatives into Equation (B.1) gives the following equation in terms of the linear displacement at a point $y = h + \bar{r}$ from the wing root:

$$\ddot{\delta} + 2\gamma\omega_n\dot{\delta} + \omega_n^2\delta = \frac{\bar{r}}{I_h} M_h(t) \qquad \text{(B.2)}$$

The equation for two-dimensional stall flutter was previously given as

$$\ddot{\delta} + 2\gamma\omega_n\dot{\delta} + \omega_n^2\delta = \frac{1}{m} L(t) \qquad \text{(B.3)}$$

and it is the equivalence between this equation and Equation (B.2) for the wing which is to be established. These two equations already have the same form. Obviously the frequency ω_n and damping factor γ used in Equation (B.3) should be numerically equal to those of Equation (B.2) for the wing. Furthermore the forcing functions of the two equations should be aerodynamically equivalent and of equal magnitude.

The forcing functions of Equations (B.2) and (B.3) each consist of steady-state and time-varying components. The latter contribute to the system stability and are the components of interest here. Consequently it is the time-varying portions of the two forcing functions which must be equivalent. The induced angle distribution of the wing may be assumed constant in time for quasi-steady-state conditions. Geometric angles are also fixed since no torsional deflections are allowed. This leaves only the

angle of attack change due to δ motion as contributing to the time-varying forcing function. The wing lift and hinge moment may be expressed as

$$L_{w_h} = \int_o^{(\ell-h)} dZ$$

$$M_h = \int_o^{(\ell-h)} rdZ$$

Here $dZ = a\,\Delta\alpha qcdr$, $\Delta\alpha = -r\theta/V$, and r is measured from the hinge. It is more convenient to express the hinge moment in terms of the integrated lift and an offset for the center of oscillating lift as

$$M_h = r_a\, L_{w_h} \tag{B.4}$$

where $r_a = M_h/L_{w_h}$ is the spanwise center of lift offset from the hinge. The value of r_a may be evaluated directly from the above equation as

$$r_a = \frac{\int_o^{(\ell-h)} acr^2 dr}{\int_o^{(\ell-h)} acrdr} \tag{B.5}$$

and is seen to be independent of time. It should be noted that because of similarity of terms in the numerator and denominator, it is necessary to prescribe only the basic distributions of a and c in order to evaluate r_a.

Equation (B.5) may be evaluated from the rigid wing distribution of a, if this is available, and from the known chord distribution. The distribution of a depends on the wing operating conditions of C_μ and angle-of-attack. The conditions of interest are those near the wing stall where the analysis is subject to multistable solutions and cannot provide accurate distributions of the local angle of attack or of the lift curve slope. However, the value of r_a may be approximated by assumed distributions of the a term.

Uniform distributions of a and c place r_a at two-thirds of the hinged wing length. A triangular distribution of a($a = a_o\ r$) and a constant chord place r_a at three-fourths of the hinged wing length. Note that these r_a offsets are measured from the hinge location and must be added to the hinge position h to obtain center of oscillating lift position relative to the wing root.

Geometric twist in the CCW model produces a nearly trapezoidal angle of attack distribution. At $\alpha_{TIP} = 0$ deg and high magnitudes of C_{μ_w}, this gives a basically triangular distribution of the a term over the hinged wing length. This basic distribution of the a term and a constant chord place r_a at three-fourths of the hinged wing length for the CCW model.

Aerodynamic equivalence between the time-varying portion of the forcing functions of Equations (B.2) and (B.3) can now be established by using r_a in Equation (B.2) in place of the arbitrary span location $\bar{r}$. The equation then describes the motion of the center of oscillating lift. Substitution of Equation (B.4) gives the wing forcing function in terms of the oscillating (time-varying) wing lift as

$$\frac{r_a^{\,2} L_{w_h}}{I_h} \tag{B.6}$$

The two-dimensional lift per unit span is assumed to be equal to the average wing lift per unit span as

$$L(t) = L_{w_h}/(\ell-h) \tag{B.7}$$

A solution for the equivalent mass per unit span of the two-dimensional wing is obtained by using the above relation and equating the wing and two-dimensional forcing functions. This equivalent mass per unit span provides the proper magnitude scaling of the two-dimensional aerodynamic forcing function in relation to that of the wing. It is given by

$$m = \frac{I_h}{r_a^2 (\ell - h)} \qquad (B.8)$$

The equivalence between Equation (B.2) for the wing and Equation (B.3) for the two-dimensional stall flutter is now complete. It requires that the two equations have the same natural frequency ω_n and the same damping factor γ and also that the time-varying portion of the aerodynamic forcing functions be scaled. The scaling is based on finding the center of oscillating lift for the wing, Equation (B.5), which is taken as the representative point for the equivalent two-dimensional lift. The magnitude of the two-dimensional forcing function is made equal to that of the wing forcing function by scaling the two-dimensional mass per unit span as shown in Equation (B.8).

The above parameters are tabulated below as calculated for the geometry of the CCW model. The center of oscillating lift was calculated from the triangular distribution of the lift curve slope. The damping factor was evaluated from an oscillograph recording of the blade bending moment variation during free vibrations.

First natural frequency in bending ω_n	121 rad/sec
Damping factor γ	0.00899
Hinge offset h	0.8667 ft
Wing moment of inertia about hinge I_h	0.1295 slug/ft^2
Center of oscillating lift r_a (from hinge)	1.600 ft
Center of oscillating lift r_a + h (from root)	2.467 ft
Equivalent mass m per unit length	0.02371 slug/ft

DTNSRDC ISSUES THREE TYPES OF REPORTS

(1) DTNSRDC REPORTS, A FORMAL SERIES PUBLISHING INFORMATION OF PERMANENT TECHNICAL VALUE, DESIGNATED BY A SERIAL REPORT NUMBER.

(2) DEPARTMENTAL REPORTS, A SEMIFORMAL SERIES, RECORDING INFORMATION OF A PRELIMINARY OR TEMPORARY NATURE, OR OF LIMITED INTEREST OR SIGNIFICANCE, CARRYING A DEPARTMENTAL ALPHANUMERIC IDENTIFICATION.

(3) TECHNICAL MEMORANDA, AN INFORMAL SERIES, USUALLY INTERNAL WORKING PAPERS OR DIRECT REPORTS TO SPONSORS, NUMBERED AS TM SERIES REPORTS; NOT FOR GENERAL DISTRIBUTION.